Assessment of the Onset Condition of Upward Streamers from Energized Franklin Rods

by

Umar Saleh Al-Abdullatif

A Thesis Presented to the

FACULTY OF THE COLLEGE OF GRADUATE STUDIES

KING FAHD UNIVERSITY OF PETROLEUM & MINERALS

DHAHRAN, SAUDI ARABIA

In Partial Fulfillment of the
Requirements for the Degree of

MASTER OF SCIENCE

In

ELECTRICAL ENGINEERING

November, 1994

ASSESSMENT OF THE ONSET CONDITION OF UPWARD STREAMERS FROM ENERGIZED FRANKLIN RODS

BY

UMAR SALEH AL-ABDULLATIF

A Thesis Presented to the

FACULTY OF THE COLLEGE OF GRADUATE STUDIES

KING FAHD UNIVERSITY OF PETROLEUM & MINERALS

DHAHRAN, SAUDI ARABIA

In Partial Fulfillment of the
Requirements for the Degree of

MASTER OF SCIENCE

In

ELECTRICAL ENGINEERING

NOVEMBER 1994

UMI Number: 1360836

UMI

300 North Zeeb Road
Ann Arbor, MI 48103

KING FAHD UNIVERSITY OF PETROLEUM AND MINERALS
DHAHRAN 31261, SAUDI ARABIA

COLLEGE OF GRADUATE STUDIES

This thesis, written by Umar Saleh Al-Abdullatif under the direction of his Thesis Advisor and approved by his Thesis Committee, has been presented to and accepted by the Dean of the College of Graduate Studies, in partial fulfillment of the requirements for the degree of MASTER OF SCIENCE. IN ELECTRICAL ENGINEERING.

Thesis Committee

Abdel-Salam

DR. MAZEN ABDEL-SALAM
Thesis Advisor

DR. FAREED ZEDAN
Member

DR. YOUSSEF ABDEL-MAGID
Member

DR. IBRAHIM EL-AMIN
Member

Department Chairman

Dean, College of Graduate Studies

4-12-94
Date

شكر وعرفان

في ذكرى والدي رحمه الله وإلى والدتي التي لم تألو جهداً في مساندتي وحثي على إتمام هذه الدراسة، وإلى أخي عبدالعزيز الذي كان عضدي ومعيني بعد الله على التفرغ للدراسة، وإلى زوجتي التي هيأت لي الجو المناسب للتحصيل العلمي، وإلى إبنى صالح أمل المستقبل، وإلى جميع إخوتي وزملائي الذين وقفوا معي وشجعنوني على إتمام هذه الدراسة.

ACKNOWLEDGMENT

Acknowledgment is due to King Fahd University of Petroleum and Minerals for support of this research.

I wish to express my appreciation to Professor Mazen Abdel-Salam who served as my major advisor. I also wish to thank the other members of my Thesis Committee Dr. Fareed Zedan, Dr. Youssef Abdel-Magid and Dr. Ibrahim Al-Amin.

Finally, I would like to acknowledge the support provided by Saudi Consolidated Electrical Company in the Eastern Province to accomplish this research.

TABLE OF CONTENTS

LIST OF TABLES

LIST OF FIGURES

Figure		Page
3.7	Electric field distribution along the axis of the Franklin rod versus the normalized distance s/h for h/R=6.	62
3.8	Electric field distribution along the axis of the Franklin rod versus the normalized distance s/h for h/R=4.	62
3.9	Electric field distribution along the axis of the Franklin rod versus the normalized distance s/h for h/R=3.	63
3.10	Electric field distribution along the axis of the Franklin rod versus the normalized distance s/h for h/R=2.	63
4.1	Axial distribution of the ionization α and attachment η coefficients avove the rod.	67
4.2	Emitted photons from the primary avalanche.	68
4.3	Secondary avalanches feeding into the primary avalanche.	70
4.4	Growth of the streamer from Franklin rod.	72
4.5	Division the ionization-zone into small segments.	75
4.6	Division the ionization-zone into small rings if the downward leader extends along the rod axis.	80
4.7	Flow chart for determining the ionization-zone boundary.	83
4.8	Determining the ionization-zone boundary.	84
4.9	Flow chart for calculating the number of photoelectrons created in each segment.	86
4.10	Growth of the primary avalanche and the associated photon emission.	88
4.11	Flow chart for computing the number of positive ions produced by the secondary avalanches.	90

Figure		Page
4.12	Comparison between the experimental data and different empirical equations reported for the ionization coefficient in the range 25≤E≤60.	93
4.13	Comparison between the experimental data and different empirical equations reported for the ionization coefficient in the range 60≤E≤240.	93
4.14	Comparison between the experimental data and empirical equation reported for ionization coefficient.	95
4.15	Present geometry against the one used for the formula.	103
5.1	Downward leader height versus leader current for different radii of the lightning rod.	106
5.2	Downward leader height versus leader current for different heights of the lightning rod.	108
5.3	Downward leader height versus leader current for different lateral distances measured from the rod.	109
5.4	Downward leader height versus leader current for different values of the applied pulse voltage (d=50 m and h=0.5 m).	111
5.5	Downward leader height versus leader current for different values of the applied pulse voltage (d=150 m and h=0.5 m).	112
5.6	Downward leader height versus leader current for different values of the applied pulse voltage (d=250 m and h=0.5 m).	113
5.7	Downward leader height versus leader current for different values of the applied pulse voltage (d=50 m and h=1 m).	114

Figure		Page

Figure		Page
5.20	Virtual increase in rod height due to the pulse voltage applied to the rod.	132
5.21	Radius of protection versus rod height for various types of Helita product.	134
5.22	Radius of protection versus rod height for various types of Helita product after being extrapolated to h=1 m.	134

خلاصة الرسالة

اسم الطالب الكامل: عمر صالح العبد اللطيف

عنوان الدراسة: مدى تأثر كفاءة قضيب ماصة الصواعق بالجهد المفروض عليه

التخصص : هندسة كهربائية

تاريخ الشهادة : ١٤١٥/٦ (١٩٩٤/١١)

تتعرض المنشآت غير المحمية للصواعق مما ينجم عن ذلك خسائر بشرية ومادية فادحة، ومع تطور المعرفة في خواص البرق والصواعق جرت محاولات عدة لتطوير كفاءة قضيب ماصة الصواعق التقليدي المعروف بقضيب فرانكلن. وكان من أحدها فرض جهد كهربائي على قضيب ماصة الصواعق التقليدي، وفي هذه الرسالة تمت أول دراسة نظرية لمدى تأثير الجهد المفروض في القضيب على بداية الإشعاع الصاعد إلى أعلى وذلك بمحاكاة هذا النظام في الكمبيوتر. وفي حالة تكون بداية الإشعاع الصاعد الى أعلى يدل ذلك على أن القضيب قادر على إمتصاص الصاعقة.

تمت أيضاً دراسة العلاقة بين بداية الإشعاع الصاعد إلى أعلى من القضيب وخواص الإشعاع النازل من السحب إلى الأسفل (التيار والإرتفاع). كما تمت دراسة العلاقة بين الإشعاع الصاعد إلى أعلى من القضيب وأبعاد القضيب والجهد المفروض على القضيب.

درجة الماجستير في العلوم

جامعة الملك فهد للبترول والمعادن

الظهران، المملكة العربية السعودية

١٤١٥/٦ (١٩٩٤/١١)

THESIS ABSTRACT

Student name: Umar Saleh Al-Abdullatif

Title of study: Assessment of Onset Condition of Upward Streamer from Energized Franklin rods

Major field: Electrical Engineering

Date of degree: November 1994

If the lightning strikes unprotected structure, a hazard in the human live and damage to the structure's materials could occur. With the increase in the knowledge of the lightning behavior, one of the methods to improve the effectiveness of the classical Franklin rod is to apply a pulse voltage to the rod. In this thesis a theoretical study using computer simulation to investigate the effect of energizing Franklin rod on the onset condition of upward streamers is developed for the first time. The onset condition of the upward streamers from the rod is the condition for these streamers to materialize and become self-propagating.

Moreover, the onset condition of the upward streamers from an energized Franklin rod is correlated to the downward leader current and height as well as the rod dimensions. In addition, the onset condition is also correlated to the amplitude of the pulse voltage applied to the rod.

MASTER OF SCIENCE DEGREE
KING FAHD UNIVERSITY OF PETROLEUM AND MINERALS
Dhahran, Saudi Arabia
November 1994

CHAPTER 1

INTRODUCTION

Since the time of Benjamin Franklin and his invention concerning the development of the lightning rod in the 17th century, the application of his lightning rod extends over almost two centuries during which little progress was made. The serious research on lightning and thunderclouds started late. With the birth of electric power early in the 20th century and many power failures due to lightning, a better understanding of the lightning and the thundercloud charging was necessary. Detailed investigations supported by experiments have been performed to understand this phenomena which will aid in the design of the lightning protection system. One of the pioneer components of this protection system is the lightning arrestors.

With a better understanding of the lightning phenomenon, several trials have been attempted to improve the classical Franklin rod. Researchers in this regard followed two approaches. The first approach is to protect the structure from being struck by the lightning stroke. This approach was achieved by using Faraday cage [1] and Spline Ball Ionizer [2]. The other approach is to develop a methodology to attract the

lightning stroke toward the lightning rod and provide a safe path to dissipate the lightning stored energy. This approach was achieved by using the following methods; laser-triggered ionizer [3,4], radioactive Franklin rod [1] and energized Franklin rod [5,6,7].

The energized Franklin rod has been designed and manufactured by Helita Company in France. High voltage experiments have been performed to confirm an increase in the protection efficiency of an energized rod compared with classical Franklin rod. They argue that a voltage pulse applied to the lightning rod will enhance the corona discharge at the tip of the rod and eventually will result in faster launching of the upward leader which will result in a more efficient lightning rod.

To the author's knowledge, this is the first study using computer simulation to investigate the effect of energizing the Franklin rod on the efficiency of protection against lightning strokes. In this thesis, the Charge Simulation Method [8-13] was used to calculate the electric field in the vicinity of the energized Franklin rod. This is a pre-requisite for assessing the onset condition of upward streamers from the rod i.e. the condition for these streamers to materialize and become self-propagating.

Moreover, the onset condition of the upward streamers from the energized Franklin rod was correlated to the downward leader current and height as well as the rod dimensions and the amplitude of the pulse voltage applied to the rod.

This thesis consists of six chapters and two appendices. In the second chapter, the charging mechanism of cloud and the lightning discharge phenomenon is discussed. A survey on the lightning protection schemes has been presented. To understand the onset criteria of the upward streamer, corona under impulse voltage is explained. Chapter three explains how the electric field in the vicinity of energized Franklin rod is calculated using the Charge Simulation technique. The reasons for adopting this technique and its mathematical formulation is discussed also in chapter three. The electric field along the axis of the Franklin rod is calculated and compared with the previous published results. The criterion of the onset streamer at the tip of the energized Franklin rod are described in chapter four. The mathematical formulation and the iterative digital computer algorithm for assessing the steamer onset condition is also explained. The positive onset condition is checked against an empirical equation widely-used in the literature. In chapter five, the results of the proposed onset criterion are presented. The effect of different parameters of the protection system (including those of the downward leader and the rod dimensions) is discussed. The gain in the radius of protection due to energizing the Franklin rod is compared with the experimental data reported by Helita [5,6,7]. It has been shown that there is a good correlation between the experimental data and the computed values by the present method. Conclusions and suggestions for further work of study are reported in chapter six. The FORTRAN program prepared for this simulation study is given in Appendix-A. Appendix-B reports several

samples of the output results obtained for different parameters of the protection system.

CHAPTER 2

PHYSICS OF LIGHTNING

2.1 Introduction

Physical appearance of lightning has been noted in ancient times, but the understanding of lightning is relatively recent. Franklin carried out experiments on lightning in 6 years only, but most of the knowledge has been obtained over the last 50 years. The real incentive to study lightning is the need for protection of electric power system against lightning [14].

During thunderstorms, positive and negative charges are separated by the movement of air currents forming ice crystals in the upper layer of a cloud and rain in the lower parts of the cloud. The ice crystals would carry only positive charge. This can be explained in the light of the fact that water is ionic in nature and has concentration of H^+ and OH^- ions. The ion density increases with temperature, thus, there will be higher concentration of ions in the lower part of the cloud. Since H^+ ions are much lighter than OH^-, they will diffuse upwards much faster. Therefore, the lower portion of the cloud which is warmer will have a net negative charge density, and

hence the upper portion, i.e. cooler region will have a net positive charge density [15]. Thus, the cloud looks like an electric dipole [1,15,16]. As the separation of charge proceeds in the cloud, the potential difference between the positive and negative concentrations of charges increases with subsequent increase of a vertical electric field along the cloud. The total potential difference between the two main charges may vary from 100 to 1000 MV. Only a part of the total charge (several hundreds of coulombs) is released to the earth by lightning; the rest is consumed in intercloud discharges. The height of the thundercloud dipole above the earth may reach 5 km in tropical regions [15,17].

2.2 Lightning Mechanism

Under normal condition, the electric field at the ground level remains at a value of several hundreds of volts per meter. Under thunder storm conditions, the electric field could reach as high as several thousands of volts per meter. This increase in the electric field is attributed to the charge separation in the cloud, where the negative charge of the cloud becomes closer to the ground surface than the positive charge which is located in the upper portion of the cloud. Fig. 2.1 depicts the development stages of lightning strokes [1,15].

Lightning discharges are classified into cloud-to-ground lightning and intercloud lightning or cloud-to-cloud discharges. There are about

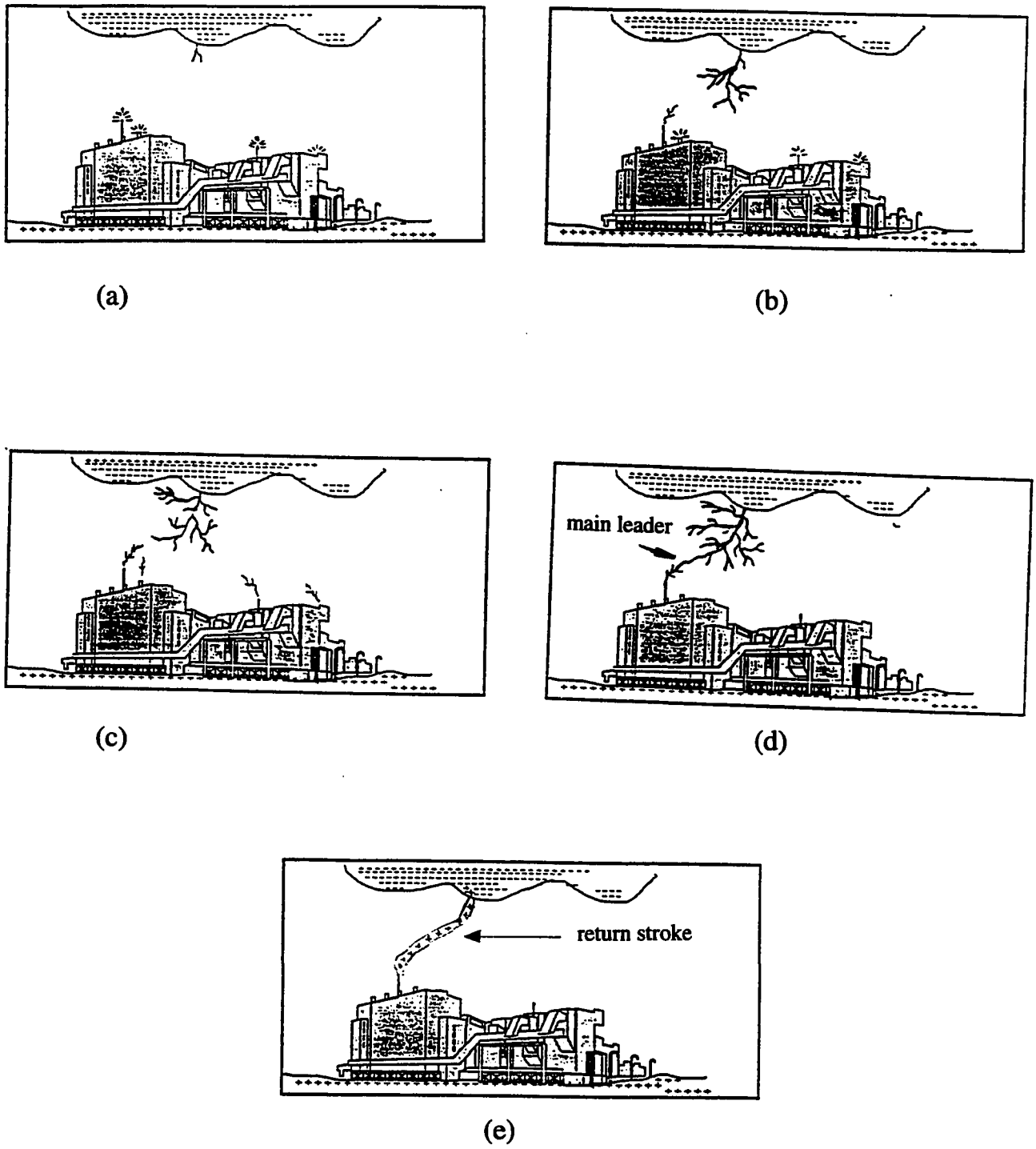

Fig. 2.1 The development of a lightning stroke.

three times as many intercloud discharges as cloud-to-ground flashes, a ratio which seems to vary somewhat with geographical location. For cloud-to-ground lightning, air ionization near the cloud will lead to faint pilot streamers which provide the initial ionized path from cloud to ground.

The pilot streamers is usually followed by a stepped leader which can be described as small steps averaging 50 m in length, Fig. 2.1a. As the pilot streamers works its way down to ground, followed by the stepped leader, the space charge at the head of the downward leader will cause a rapid increase in the electric field at the ground. Due to the increase in the electric field at the ground, a corona discharge appears on protruding structures above the ground level. When the negative downward leader reaches certain height above the ground, an onset streamer at the coronated structures will lead to several positive upward leaders, Fig. 2.1b&c.

As soon as the stepped downward leader (with the pilot streamer at its head) reaches the upward leader, a conducting path between the cloud and the earth is established and the main stroke starts, Fig. 2.1d. The main stroke will transfer charge between the cloud and earth at a rate of 10 kA to 150 kA [2]. Although the main stroke only lasts for a thousandth of a second, it is visible to the naked eye and the sound or acoustic shock wave that follows is obviously that of a lightning bolt. The main stroke often breaks up into several subsequent strokes (multiple flashes), usually three or four per lightning flash. Lightning flashes having as many as 42

subsequent strokes have been reported, Fig. 2.2 [15,18]. There are usually no pilot streamers or stepped leader presented between ensuing strokes in multiple-stroke flash since an ionized bath has already been established after the first stroke. The stepped leader is replaced by a so-called dart leader which works its way down from the cloud in one single jump.

One of the most challenging problems in lightning research is how the lightning bolts drain the large amount of charges from the cloud in small fraction of a second. There are some believes, as reported in [15], that the mechanism involves the following. When the downward leader reaches the ground starting from the negative charge in the lower portion of the cloud, not much charge will be brought down because the negative charge in the cloud is bounded. On the other hand, the earth's surface, which is a good conductor, can easily supply positive charge up to the cloud through the ionized channel provided by the junction between the stepped leader and the upward leader. When the positive charge in the return strokes reaches the cloud it will cause the cloud potential to drop drastically, Fig. 2.1e.[15]

2.3 Lightning Protection

The lightning stroke may strike a structure directly with considerable damage in case there is no protection against lightning, Fig. 2.3a. Lightning protection system can attract the downward lightning

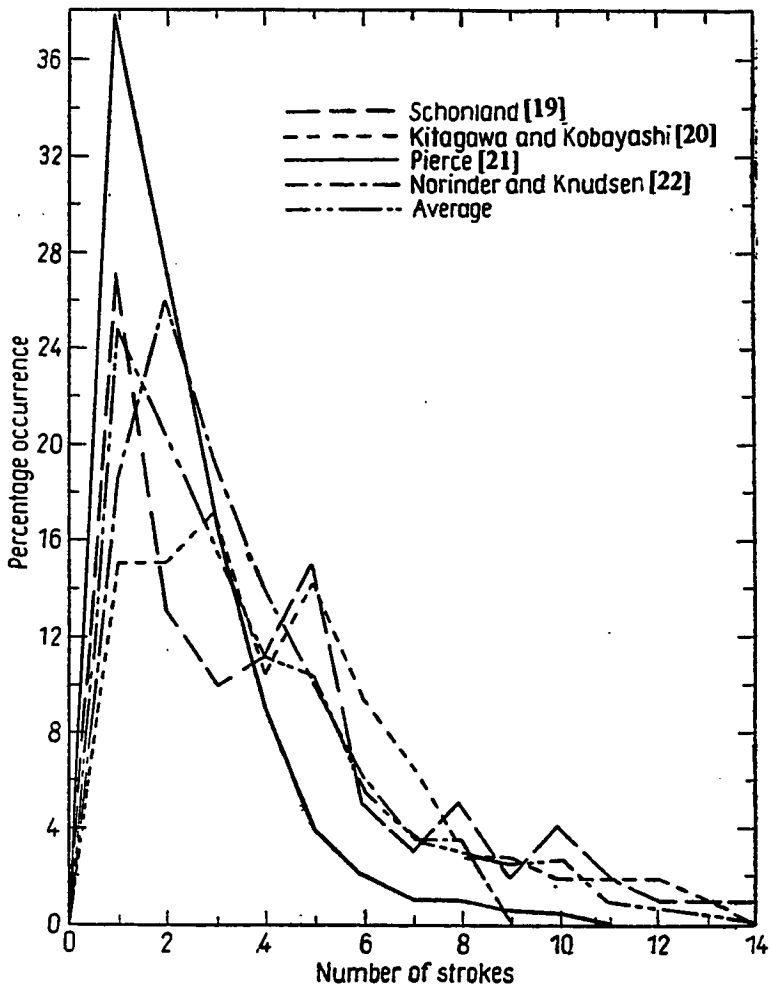

Fig. 2.2 Distribution of multiple lightning flashes [18].

leader and provide a safe path for the lightning stroke to be discharged to the ground, Fig. 2.3b. Thus, the structure is protected from being struck by the lightning stroke. Lightning protection could be implemented using one of the following schemes:

1- Franklin rod [8,15].
2- Faraday cage [1].
3- Spline Ball Ionizer [2].
4- Laser-triggered Ionizer [3,4].
5- Radioactived Ionizer [1].
6- Energized Franklin rod [5,6,7].

The last three schemes for lightning protection have common mechanism to increase the effectiveness of protection using classical Franklin rods by enhancing the air ionization at the rod tip. This is achieved by using laser beam in the fourth scheme, radioactive material in the fifth scheme and voltage pulse in the last scheme.

It has been proven that the function of a lightning rod is not necessarily to attract lightning and lead it to ground in order to dissipate its power. Careful studies show that large amount of corona discharges occur at the points of a lightning rod, Fig. 2.4, before lightning strikes. The corona discharges produce numerous ions which often develop a protective dome around structures fitted with lightning rods. A large conductive dome has a smoothing effect over protruding surfaces and will

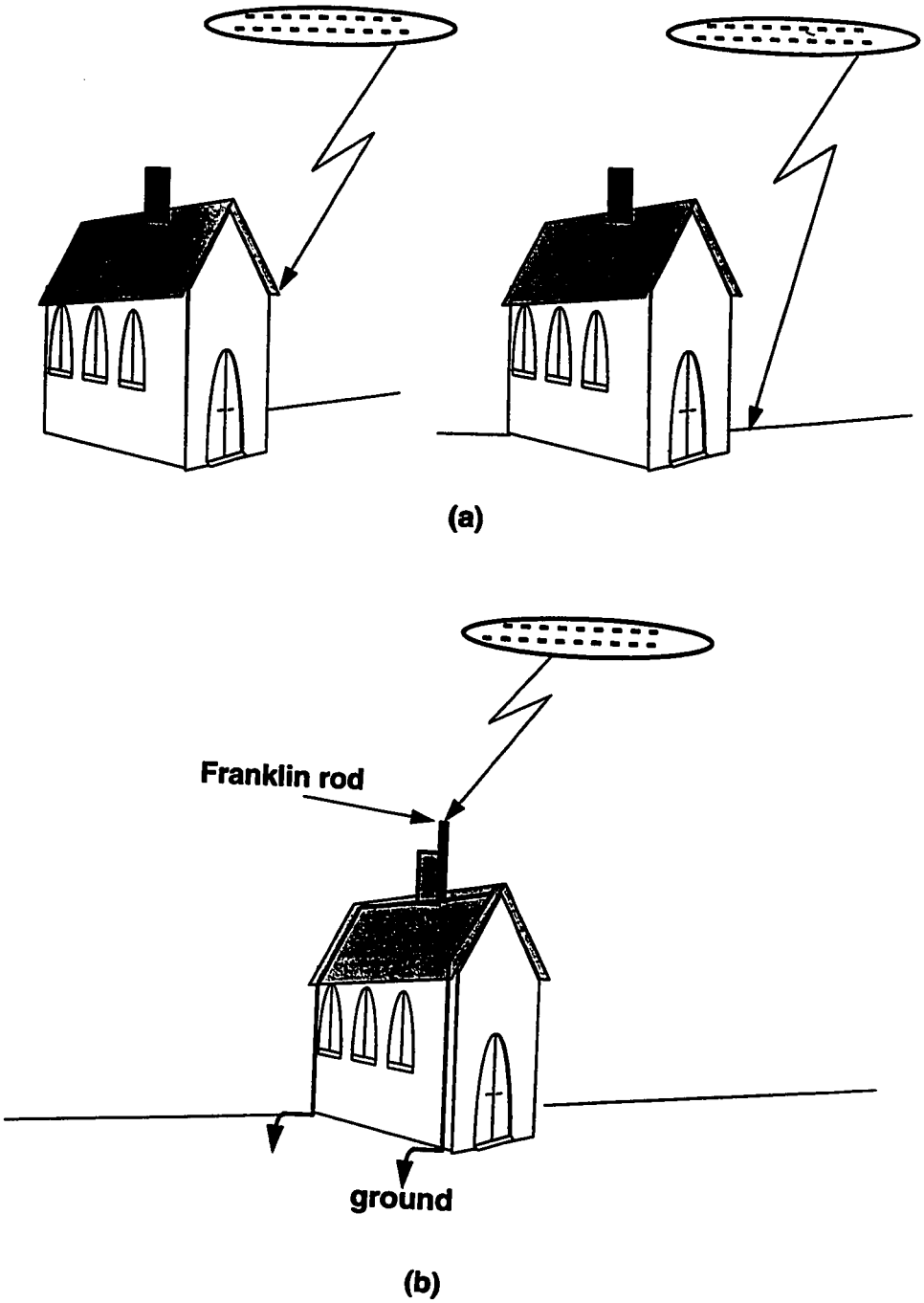

Fig. 2.3 a) Lightning may hit unprotected structure.

b) Lightning never hits the protected structure.

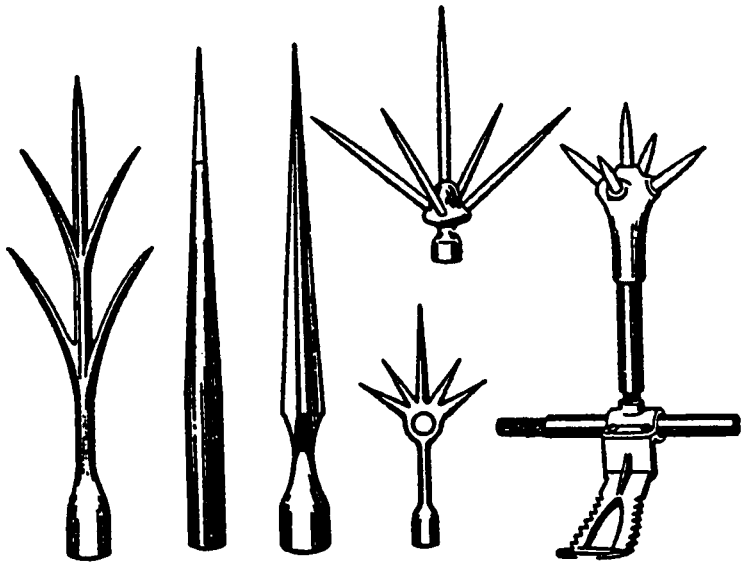

Fig. 2.4 Points of the lightning rod [15]

lower the electric field strength in the vicinity of the protected structure [15].

1- Franklin rod scheme

Franklin rod is an important device for protecting houses, electrical power substations and other structures against lightning. This is accomplished in two ways. First, corona from the sharp tip of the Franklin rod creates a protective ion cloud above the structure and secondly, in the event of a direct hit by lightning, the Franklin rod will force the electric charge to dissipate into ground and prevent damage to the structure. Lightning protection consists of two types of protection, internal and external. External protection concerns the safety of the roof and sidings of a structure while interior protection deals with sparks between metal objects inside the structure including power transformers and relay sets in substations and appliances, radios, and telephone lines in houses [8,23].

2- Faraday cage scheme

It has been noticed that a lightning rod attracts to a building a greater number of discharges than in its absence and that therefore fewer discharges would occur in the region surrounding the rod. Thus, the Faraday cage was proposed in place of the usual lightning rod. The interior of a completely enclosed metal shell is free from the effects of any external changes of the electric field, Fig. 2.5. If lightning strikes the top of a metal shell and proceeds to earth from its underside, the potential drop across the points of entry and exit is simply given by the product of the

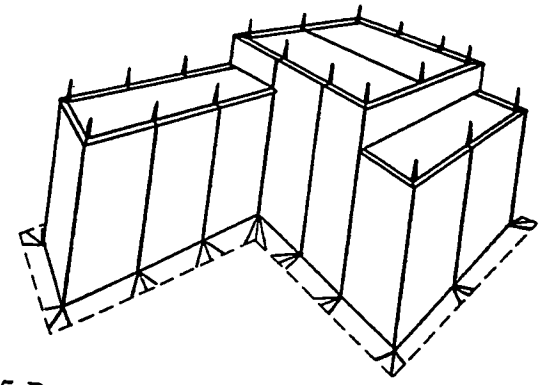

Fig. 2.5 Protection of structure by Faraday cage.

lightning current and the effective ohmic resistance of the discharge path over the shell and this can be made negligibly low. There is an important limitation to the use of a Faraday cage for the purpose of lightning protection where there is an electric conductor or cable lead goes into the structure from the outside. Dangerous potential differences can be introduced inside the "cage" through the cable and special precautions have to be taken to discharge the related currents. Apart form special cases, a genuine Faraday cage hardly constitutes a practical solution to the lightning problem. This scheme is also very costly compare to the Franklin rod [1].

With a deeper knowledge of the lightning phenomena during the twentieth century, several attempts have been attempted to improve the effectiveness of the classical Franklin rod in lightning protection.

3- Spline Ball Ionizer (SBI)

Lightning Eliminators & Consultants (LEC). has afforded [2] an improved electrogeometric model of a lightning protection scheme which they named it Spline Ball Ionizer (SBI). They claim that the operating principle of their design can be explained according to Fig. 2.6. SBI is simply a sharp grounded point whose height above the ground plane is determined by the size of the structure being protected. Under cloudy condition, the electrostatic field at the sharp point increases with subsequent ionization of the surrounding air. Thus, SBI looks like a point charge emitting ions in the space. This ionization process creates current

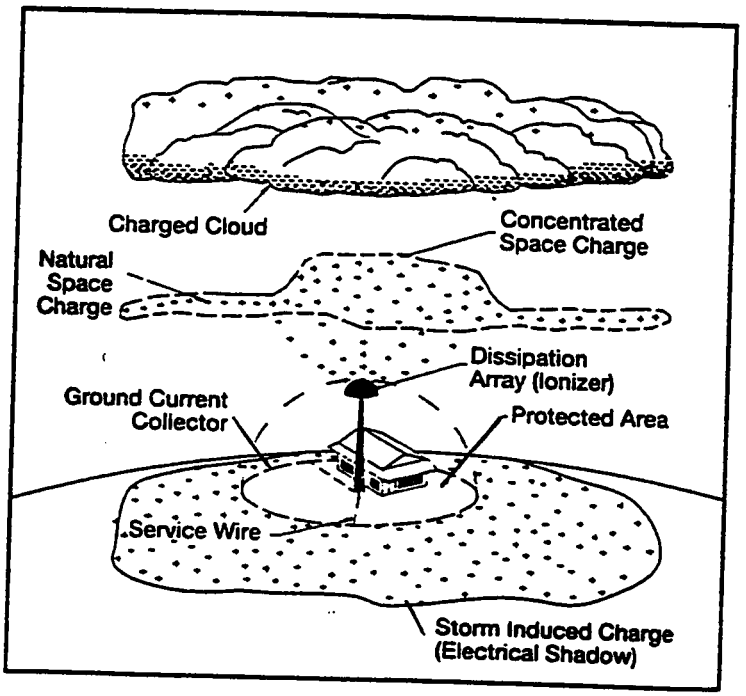

Fig. 2.6 Spline Ball Ionizer of LEC [2].

flowing through SBI. This current increases exponentially with the storm's electrostatic field which can reach as high as 30 kV per meter of elevation above earth during a mature storm. The emitted ions screen the structure where most of the electrostatic field lines terminate on the emitted ions, and not on the structure. This reflects itself on a decrease of the field at the structure and the latter appears as being isolated from direct stroke. This is because much of the storm induced charge has been removed and transferred to the ionized air molecules which subsequently form an intervening space charge that functions as a Faraday Shield. The cloud will dissipate its energy away from the protected structure where the induced electrostatic field is higher.

4- Laser-triggered scheme

Recent advances of laser applications suggest the possibility of laser-triggered lightning protection [3,4]. When a giga power laser beam is focused in air, a high degree of ionization is produced in a brilliant bead at the focus. This is a well-known phenomenon called optical breakdown. If the power of the laser is high enough, a chain of air-breakdown plasmas are produced along the laser beam. This type of breakdown has been achieved for up to 60 m away from the laser source. These plasmas have the ability to guide the downward leader toward the lightning rod, Fig. 2.7. If the power of the laser is increased more, such long air-breakdown plasmas can be produced which may be able to attract far lightning stroke through the rod.

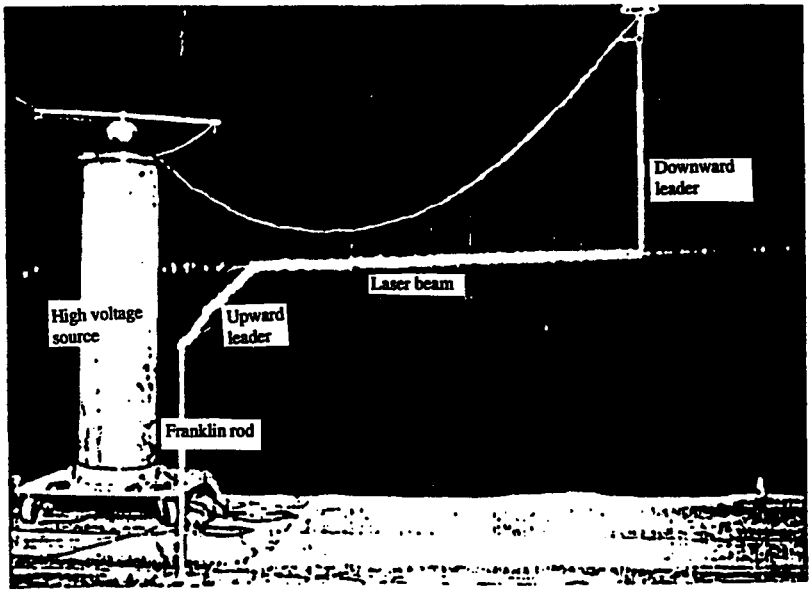

Fig. 2.7 Laser triggering the downward leader [3,4].

5- Radioactive material

A question has been raised whether the effect of a classical Franklin rod in attracting lightning strokes could be increased by the addition of a radioactive source. The idea of the scheme is to use α , γ or β - radioactive material to ionize the air at the tip of the Franklin rod. Many investigations to answer this question lead to the conclusion that radioactive Franklin rods are no more effective than the classical Franklin rods of the same dimensions. This conclusion is supported by the failure of a radioactive lightning rod to prevent the 22 m height papal crest on the Vatican's Bernini Colonnade in Rome being knocked off by a lightning strike on 1976. In additional, there is a possible danger of intense radiation to human [1].

6- Energized Franklin rod

Helita in France [5,6,7] has designed and manufactured an energized lightning rod, Fig. 2.8. The Franklin rod is energized by a high voltage signal at controlled repetition rate and amplitude. Experiments have been performed [5,6,7] to confirm an increase in the protection efficiency of energized rod when compared with the classical Franklin rod. The aim of their experiments is to confirm earlier triggering of streamers from energized rod in comparison with classical Franklin rods. They measured the gain in triggering time of streamers due to rod energization. This gain in time was considered a measure for the increase of the protection area on using energized rod.

1- emit the high-voltage pulse and capture the lightning current and convey it to the ground.

2- designed to convey the lightning current from point (1) to the ground.

3- contain the electrical device that will generate the high-voltage pulse.

4- fix the lightning rod.

5- fix the rod with the down conductor.

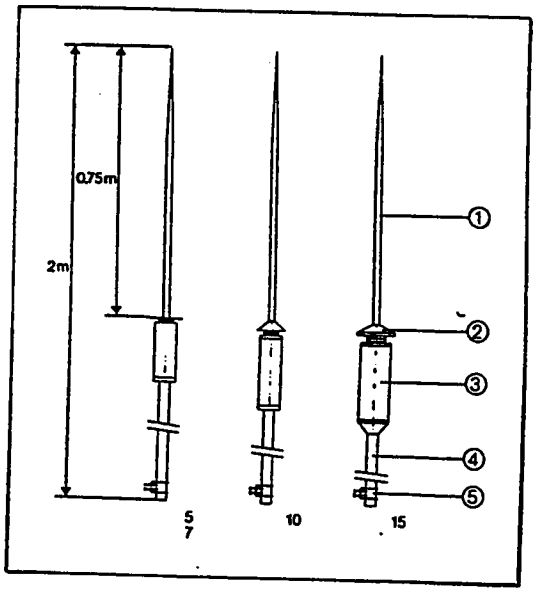

Fig. 2.8 Energized Franklin rod of Helita [5,6,7] .

They claim [5,6,7] that the voltage pulse applied to the rod will enhance the corona discharge at the tip of the rod and eventually will result in faster launching of the upward leader which will result in a more efficient lightning rod. To the author's knowledge, the parameters of the pulse voltage applied to the lightning rod, as regards to the amplitude and repetition rate are unknown. They were chosen [5,7] to ensure streamer formation at the tip of the lightning rod without steady glow. The latter will reduce the electric field in the vicinity of the rod as reported by Wahlin [15].

On the other hand, Frydenlund [24] and Mackerras [25] were not in favor with all the new concepts proposed in the literature [1-7] to improve the effectiveness of lightning protection by Franklin rod. They insist that lightning protection using classical Franklin rod is still the only credible system. Mackerras [25] made a survey over about two decades in Singapore and found that most of the failures occur when any of the new concepts of lightning protection is adopted to protect a larger range than that of the classical Franklin rod. The following is a list of examples extracted from his survey made over 100 radioactive lightning protection schemes.

a) Building A: 180 m high, with claimed radius of protection for the protection scheme of 50 m. It was reported that the side of the building was struck and the protective scheme had failed.

b) Building B: 168 m high, it was reported that a direct strike was seen by an occupant to the side of the building several floors below the top floor- indicating a failure in the protective scheme.

c) Building C: 6 m high, two strokes was seen within the zone of protection with a considerable damage.

d) Building D: 177 m high, the building was struck and a large fragment of the concrete from the edge of the roof fell to the ground. Investigations confirmed that the damage caused by this lightning flash was well within the claimed zone of protection.

2.4 Corona Under Impulse Voltage

Corona literally means the disk of the light that appears around the sun. The term was borrowed by physicists and electrical engineers to describe generally the partial discharges that develop in zones of highly concentrated electric fields, like those at the tip of lightning rod. This partial breakdown of air is quite distinct in nature and appearance from the complete breakdown of air gap between the cloud and the earth.

Transient over-voltage due to lightning cause a steep build-up of voltage wave on structures. Experimental investigations showed that these waves have a rise time of 0.5-10 μs and decay time to 50% of the peak value of the order of 30-200 μs. Lightning over-voltages can be represented as double exponential waves expressed as:

$$V(t) = V_L\left[\exp(-\psi_1 t) - \exp(-\psi_2 t)\right] \qquad (2.1)$$

where V_L is related to the peak of the wave and ψ_1 and ψ_2 are constants (expressed in sec^{-1}). The general wave shape is shown in Figure 2.9. Impulse waves are specified by defining their front time T_1 and tail time T_2 to 50% of the peak value. Thus, 1.2/50 μs wave represents an impulse voltage with a front time of 1.2 μs and tail time to 50% of the peak value of 50 μs. The American standards specify 1.5/40 μs wave and the British standards specify 1/50 μs wave as standard impulse. The tolerances allowed in the front and tail times are respectively ±30% and ±20%.

Impulse positive corona discharge takes place at the tip of Franklin rod due to the negative downward leader and the positive pulse voltage applied to the Franklin rod, if it is energized. Impulse corona discharge is different from a steady (dc) voltage, because the applied pulse voltage declines to about one-half of its magnitude in a few microseconds, so, the ionic space-charge drift and accumulation can be neglected.

Because of transient development of the ionization processes under such pulse conditions, their detection has always been quite difficult. In one case, repetitive pulse were used in order to produce a detectable effect as adopted by Helita in their energized rods, and in other cases the voltage had to be raised well above the onset for the same reason [5,6].

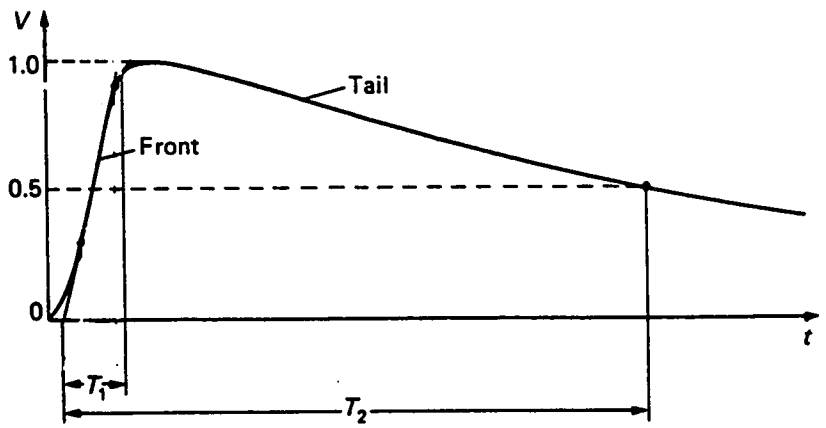

Fig. 2.9 General shape of lightning impulse voltage.

The corona starts in an air gap almost clear of any space charge. Therefore, electron avalanches and streamers extend over significant distances. The observations show that the streamers branch out radially with different lengths. If the electric field at the tip of the Franklin rod increases, the avalanches and streamers grow upward both in length and number of branches with a subsequent transfer into upward leaders. The velocity of streamers increases rapidly with the electric field increase [26].

2.5 Electron Avalanche and Associated Fields

Electrical corona is simply an initiatory avalanche, triggered by free electrons available in space, followed by a succession of generations of avalanches. These avalanches grow in the ionization-zone around the coronating electrode (Franklin rod) where the coefficient of ionization by electron collision α exceeds that of the electron attachment coefficient η. Initiatory electrons may originate around the Franklin rod by ultraviolet, or from the surrounding air volume by ionization by any means. They could also be produced at a later stage by photons from the discharge itself.

Due to the effect of the electric field of the downward leader and the pulse voltage applied to the Franklin rod, if energized, the initiatory electron accelerates toward the Franklin rod, gaining energy with distance. If the electron acquires enough energy, it will ionize an air molecule by

collision. Leaving a positive ion behind, the new electron, together with the initiatory electron, proceed along the resultant field and repeat the process forming an avalanche. The avalanche can produce successor avalanches if the discharge is self-sustained as discussed in detailed in chapter 4.

With one electron starting to multiply in a non-uniform field at point P_1 (of Z-coordinate $=z_1$), Fig. 2.10a, the number of electrons produced by the avalanche at point P_2 (of Z-coordinate $=Z_2$) is given by :

$$N_e(z) = \exp\left[\int_{z_1}^{z_2}(\alpha(z) - \eta(z))dz\right] \qquad (2.2)$$

where:

$\alpha(z)$ is the coefficient of ionization by electron collision at z.

$\eta(z)$ is the coefficient of electron attachment at z.

The head of the avalanche is a build-up of electrons while its wake is populated by positive ions. These ions will produce a space-charge field which opposes the field accelerating the electrons at the avalanche head. This retarding space-charge field could be disregarded during the initial stages of avalanche growth. To quantify the space charge field, the positive ions in the avalanche wake was represented [27] by fictitious point charge located at a distance $1/\alpha(z)$ from the avalanche tip, Fig. 2.10a.

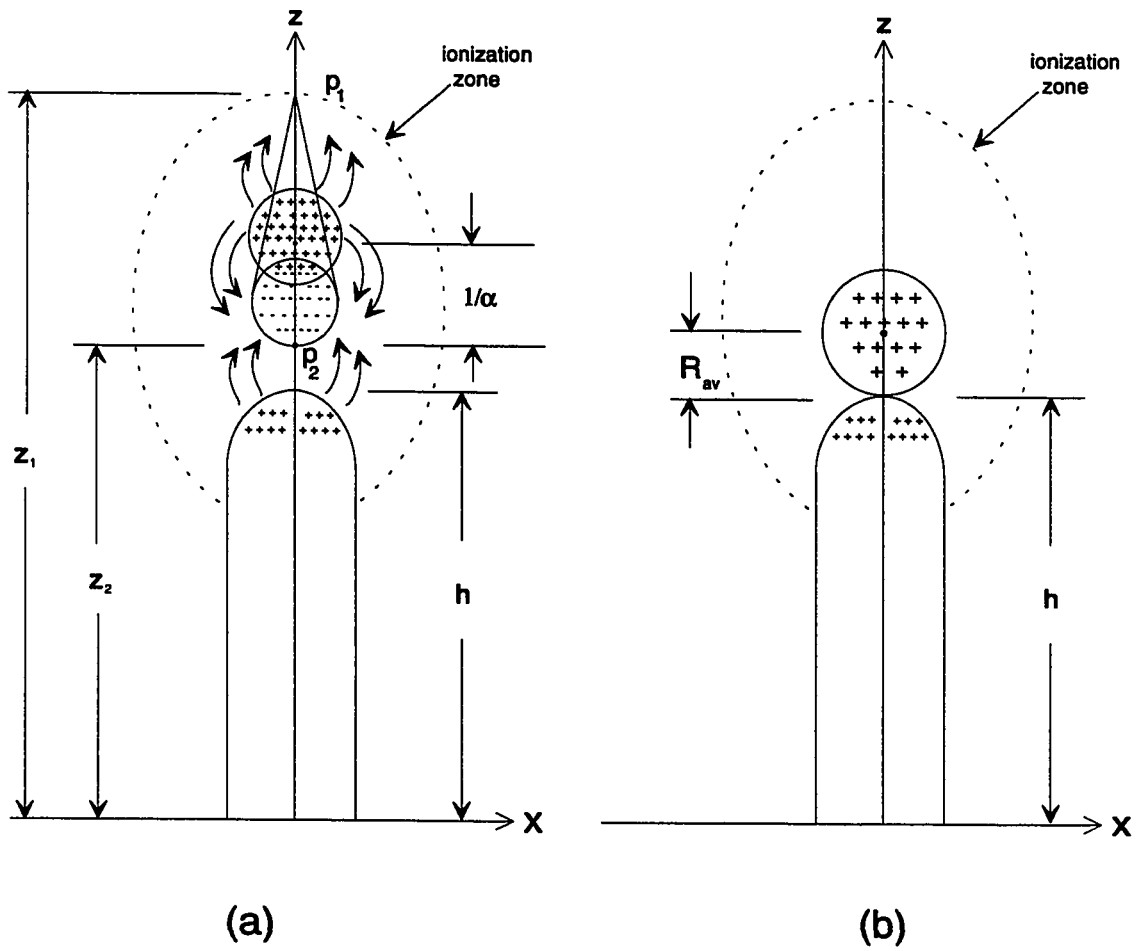

Fig. 2.10 (a) Initiatory avalanche development.
(b) Positive ions left behind the initiatory avalanche.

Thus, the space-charge field produced by the positive ions is expressed as:

$$E_{sc}(z) = \frac{e \cdot (N_e(z) - 1)}{4\pi\varepsilon_o [1/\alpha(z)]^2} \approx \frac{e \cdot N_e(z) \cdot \alpha(z)^2}{4\pi\varepsilon_o} \tag{2.3}$$

where:

e is the electron charge ($= 1.6 \times 10^{-19}$ C).

ε_o is the permittivity of air ($= \frac{1}{36\pi} \times 10^{-9}$ F / m).

When the initiatory avalanche reaches the Franklin rod, all the electrons will be absorbed there. The positive ions left behind the avalanche will be simulated by a point charge Q located at distance R_{av} above the tip of the Franklin rod, Fig. 2.10b, where R_{av} is the radius of the head of the initiatory avalanche and expressed as:

$$R_{av} = \sqrt{6 D_e \tau} \tag{2.4}$$

where:

D_e is the electron diffusion coefficient (m^2/s).

τ is the avalanche transit time (s).

The justification for this assumption is that the avalanche growth is concentrated in the last few steps of the avalanche [17].

The electric field caused by the positive ions left behind the initiatory avalanche at any point located at radial distance r_s from the simulation charge Q can be as:

$$E_{psc} = \frac{Q}{4\pi\varepsilon_o \cdot r_s^2} = \frac{e \cdot N_{+1}}{4\pi\varepsilon_o \cdot r_s^2} \tag{2.5}$$

where:

N_{+1} is the size of the initiatory avalanche and is expressed as:

$$N_{+1} = \exp\left[\int_{z_1}^{h}[\alpha(z) - \eta(z)]dz\right] \tag{2.6}$$

where:

h is the rod height, Fig. 2.10a.

z_1 is the starting point of the initiatory avalanche, Fig. 2.10a.

CHAPTER 3

ELECTRIC FIELD

3.1 Introduction

As is well known, evaluation of the electric field in the vicinity of the tip of the Franklin rod is a pre-requisite for determining the onset condition of upward streamer at the surface of the rod. Such evaluation of the electric field in the presence of a charged cloud and downward leader approaching the rod, Fig. 3.1, is not a simple problem. It calls for a numerical solution of Laplace's equation. Many numerical techniques have been suggested to solve Laplace's equation. Among these techniques, finite-element, finite-difference, and charge-simulation techniques (CST) have been applied in the literature [8-13]. The finite-elements and finite-differences must be applied to bounded arrangements and evaluate the electric field through numerical differentiation of the potential. However, ballooning technique has been proposed to adopt the finite element solution to open-boundary arrangements [28,29]. The accurate CST is adopted for the present calculation of the electric field .

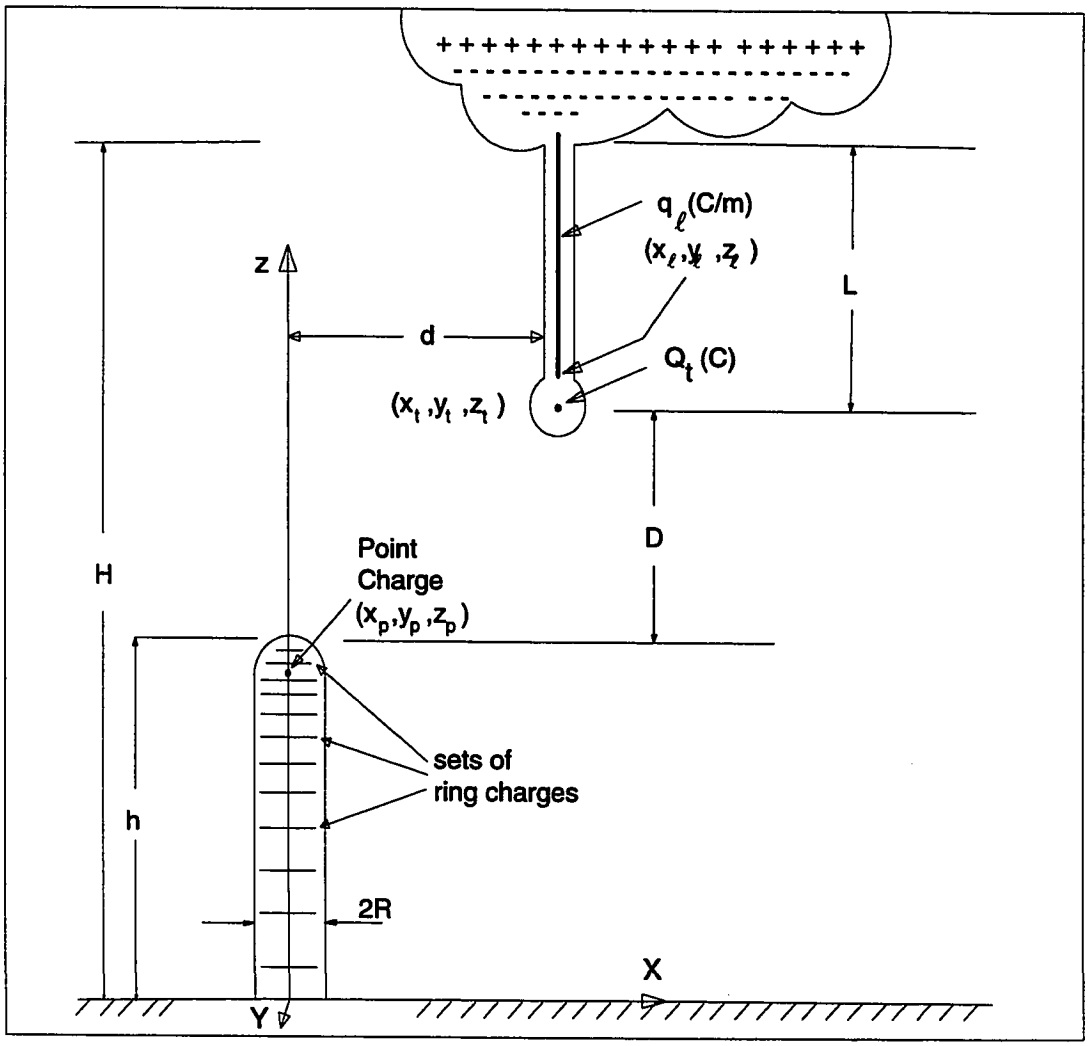

Fig. 3.1 Charge simulation of the downward leader and lightning rod.

The selection of the CST among others techniques is based on the following advantages:

1- Simplicity in representing the equipotential surface of the lightning rod.

2- Direct calculation of the field strength.

3- Suitability to unbounded (open-boundary) arrangements.

4- Possibility of computation of three-dimensional fields without symmetry with reasonable amount of computations.

3.2 Charge Simulation Technique (CST)

The Charge Simulation Technique (CST) can be used successfully for the computation of the electric field in the vicinity of the lightning rod. In CST, the surface charge of the electrode is replaced by a fictitious discrete set of inner charge distributions, whose position and type are predetermined, but whose magnitude is unknown. The important point is that if some classical charge distributions are chosen, explicit expressions are obtained for the potential and field distributions.

The basic mathematical equations that describe the electrostatic field distribution in the investigated arrangement:

$$\nabla \overline{E} = 0 \tag{3.1}$$

$$\nabla \Phi = -\overline{E} \tag{3.2}$$

Equation (3.1) is Laplace's equation and equation (3.2) is the electric field in terms of the potential Φ.

In order to determine the magnitude of the simulation charges, boundary points on the surface of the electrode, equal to the number of the simulation charges, are chosen and is required to satisfy the potential boundary conditions at any of these points. The boundary condition at the ith boundary point on the electrode surface is that the calculated potential Φ_i due to the simulation charges should be equal to the applied voltage V_{ap_i} at the ith boundary point.

$$\Phi_i = \sum_{j=1}^{n} P_{i,j} q_j = V_{ap_i} \tag{3.3}$$

where:

q_j is the jth simulation charge.

$P_{i,j}$ is the potential coefficient calculated at the ith boundary point due to the jth simulation charge.

If the electrode is at a finite height from the ground plane, then the images of the simulation charges are considered to take into account the effect of the ground plane.

Satisfying the boundary condition expressed by equation (3.3) at all the boundary points formulates a set of simultaneous equations whose solution determines the unknown simulation charges;

$$[P]\cdot[q]=[V_{ap}] \tag{3.4}$$

where:

$[V_{ap}]$ $n\times 1$ matrix of the applied voltage at the boundary points.
$[P]$ $n\times n$ matrix of the potential coefficients.
$[q]$ $n\times 1$ matrix of the simulation charges to be determined.

Once the unknown charges are determined, the electric field $\overline{E}$ at any point on or close to the electrode surface can be calculated as:

$$[\overline{E}]=[\overline{f}]\cdot[q] \tag{3.5}$$

where:

$[\bar{f}]$ $n \times n$ matrix of the electric field coefficients.

3.3 Modeling the System

The components of the system that will be modelled are the negative downward leader developed from the thundercloud toward the Franklin rod and the energized Franklin rod, Fig. 3.1.

3.3.1 Simulation of Downward Leader's Charge

The negative downward leader that develops from the thundercloud toward the ground is modelled [8,30,31] as 10% of the leader charge is concentrated at the leader tip and the remaining 90% is equally distributed along the leader length. Under this condition, the total charge Q of the downward leader at any time can be expressed as follows:

$$Q = Q_t + q_\ell L \tag{3.6}$$

where:

L is the downward leader length.

q_ℓ is the semi-infinite line charge per unit length.

Q_t is the downward leader tip charge which is equal to 0.1Q.

It should be noted that q_ℓ is a constant value for a given leader. Therefore, both the total charge Q and the tip-carried charge 0.1Q are function of the leader length L [8,30].

Accordingly, the downward leader -as discussed above-is simulated by a known point charge Q_t at its tip and semi-infinite line charge of density q_ℓ. The coordinates of this point charge is (X_t, Y_t, Z_t). The coordinates of the starting point of the semi-infinite line charge is (X_ℓ, Y_ℓ, Z_ℓ).

3.3.2 Simulation of Charge on Franklin Rod

Franklin rod is a hemispherical capped rod, so it has been divided into two portions, cylindrical and hemispherical portions as shown in Fig. 3.1. Due to the absence of rotational symmetry (due to the presence of the downward leader), each Z-level of the cylindrical portion has been simulated by a set of M rings [8,9]. The radius of these rings is related to the rod radius. Each ring has a constant, but unknown charge. The number of Z-levels at the higher part of the rod is chosen denser than that at the bottom of the rod.

The hemispherical cap of the rod has been simulated also by a set of rings at each Z-level, the radius of these rings is variable from level to level. Each ring has also a constant, but unknown charge [8,9].

For both the cylindrical and hemispherical portions of the rod, the nth simulated ring has a radius denoted as r_{j_n} and coordinates of the center as $(X_{r_n}, Y_{r_n}, Z_{r_n})$, Fig. 3.2.

The distance between the center of the nth ring and a boundary point of coordinated (X_b, Y_b, Z_b) projected in the X-Y plane, Fig. 3.2, is denoted as r_{xy_n} and expressed as:

$$r_{xy_n} = \sqrt{(X_b - X_{r_n})^2 + (Y_b - Y_{r_n})^2} \tag{3.7}$$

In additional to the ring charges at the different Z-levels, a point charge is placed at the center of the hemispherical cap of the lightning rod with coordinates (X_p, Y_p, Z_p), Fig. 3.1. Experience has shown the importance of this point charge for simulation to maintain the radial field pattern at the cap of the rod.

If N_Z is the number of the Z-levels for both portions then the total number of unknowns charges will be $(N_Z \times M) + 1$.

3.4 Determining of the Unknown Charges

As mentioned before, a set of equations is formulated at a set of boundary points chosen on the rod surface, to determine these unknown

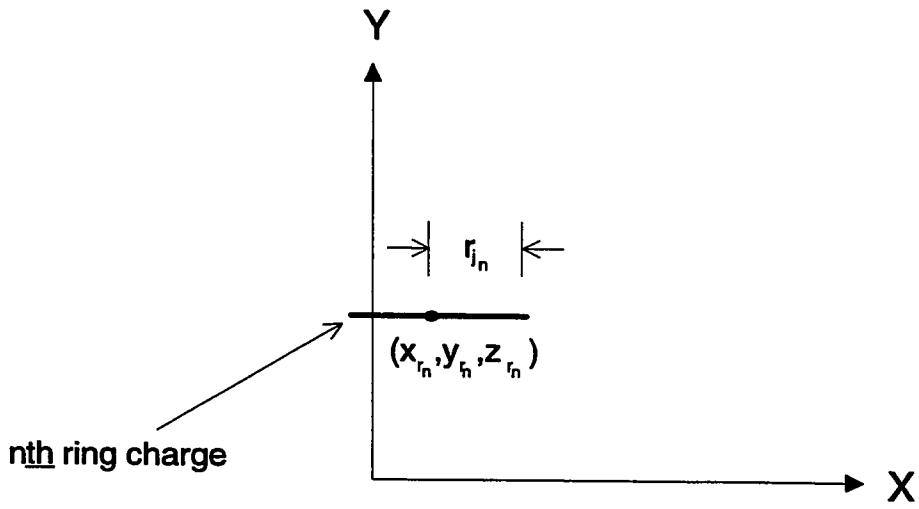

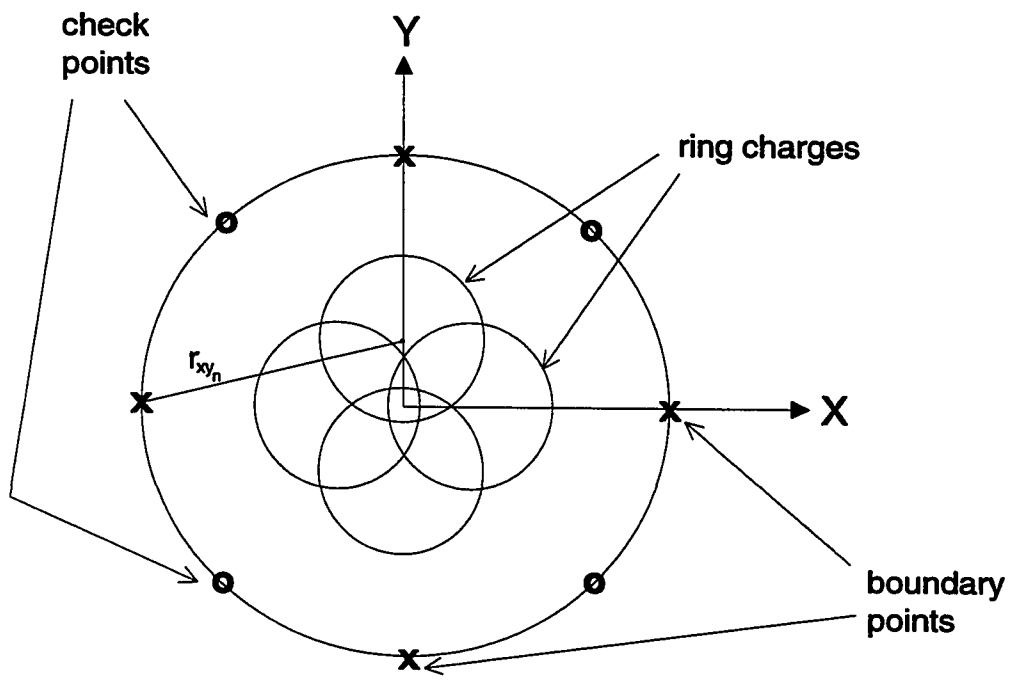

Fig. 3.2 Arrangement of simulation ring charges.

charges. The number of boundary points is equal to the number of the unknown charges. The potential at each boundary point in the presence of the downward leader expressed as:

$$\sum_{n=1}^{M \cdot N_z} \left\{ P_{r_n} Q_{r_n} \right\} + P_p Q_p + P_\ell q_\ell + P_t Q_t = V_{ap}(t)$$

or

$$\sum_{n=1}^{M \cdot N_z} \left\{ P_{r_n} Q_{r_n} \right\} + P_p Q_p = -P_\ell q_\ell - P_t Q_t + V_{ap}(t) \qquad (3.8)$$

where:

Q_{r_n} is the value of the nth simulation ring charge in the rod.

Q_p is the value of the simulation point charge in the rod.

$V_{ap}(t)$ is the instantaneous value of pulse voltage applied to the lightning rod, which may be expressed by the double exponential wave form (see equation (2.1)) as:

$$V_{ap}(t) = A\left[\exp(-\varphi_1 t) - \exp(-\varphi_2 t)\right] \qquad (3.9)$$

where A, φ_1 and φ_2 are the constants determining the shape of the pulse voltage.

P_{r_n} is the potential coefficient of the nth simulation ring charge calculated at a boundary point of coordinates (X_b, Y_b, Z_b). The coefficient P_{r_n} is expressed as [8,9]:

$$P_{r_n} = \frac{1}{4\pi\varepsilon_o} \cdot \frac{2}{\pi}\left[\frac{K_1(k_1)}{\gamma_1} - \frac{K_1(k_2)}{\gamma_2}\right] \tag{3.10}$$

with:

$$\gamma_1 = \sqrt{(r_{xy_n} + r_{j_n})^2 + (z_b - z_{r_n})^2}$$

$$\gamma_2 = \sqrt{(r_{xy_n} + r_{j_n})^2 + (z_b + z_{r_n})^2}$$

$$k_1 = \frac{2 \cdot \sqrt{r_{j_n} \cdot r_{xy_n}}}{\gamma_1}$$

$$k_2 = \frac{2 \cdot \sqrt{r_{j_n} \cdot r_{xy_n}}}{\gamma_2}$$

$K_1(k_1)$ and $K_1(k_2)$ are the complete elliptic integrals of the first kind.

P_p is the potential coefficient of the simulation point charge at the center of the hemispherical cap of the lightning rod calculated at a boundary point of coordinates (X_b, Y_b, Z_b). The coefficient P_p is expressed as [8,9]:

$$P_p = \frac{1}{4\pi\varepsilon_o}\left[\frac{1}{D_{pc}} - \frac{1}{D_{pi}}\right] \tag{3.11}$$

with:

D_{pc} is the distance between the point charge Q_p and the boundary point, and is expressed as:

$$D_{pc} = \sqrt{(X_b - X_p)^2 + (Y_b - Y_p)^2 + (Z_b - Z_p)^2}$$

D_{pi} is the distance between the image of the point charge Q_p and the boundary point, and is expressed as:

$$D_{pi} = \sqrt{(X_b - X_p)^2 + (Y_b - Y_p)^2 + (Z_b + Z_p)^2}$$

P_t is the potential coefficient of the simulation point charge at the tip of the downward leader calculated at a boundary point of coordinates (X_b, Y_b, Z_b). The coefficient P_t is expressed as [9]:

$$P_t = \frac{1}{4\pi\varepsilon_o}\left[\frac{1}{D_{tc}} - \frac{1}{D_{ti}}\right] \tag{3.12}$$

with:

D_{tc} is the distance between the point charge Q_t and the boundary point, and is expressed as:

$$D_{tc} = \sqrt{(X_b - X_t)^2 + (Y_b - Y_t)^2 + (Z_b - Z_t)^2}$$

D_{ti} is the distance between the image of the point charge Q_t and the boundary point, and is expressed as:

$$D_{ti} = \sqrt{(X_b - X_t)^2 + (Y_b - Y_t)^2 + (Z_b + Z_t)^2}$$

P_ℓ is the potential coefficient of the simulation semi-infinite line charge of the downward leader calculated at a boundary point of coordinates (X_b, Y_b, Z_b). The coefficient P_ℓ can be derived by integrating the potential coefficient due to an infinitesimal length Δz over the semi-infinite line which extends along the Z-axis, Fig. 3.3, i.e.:

$$P_\ell = \int_{z_\ell}^{\infty} \frac{1}{4\pi\varepsilon_o}\left[\frac{1}{D_{ic}} - \frac{1}{D_{ii}}\right] dz \tag{3.13}$$

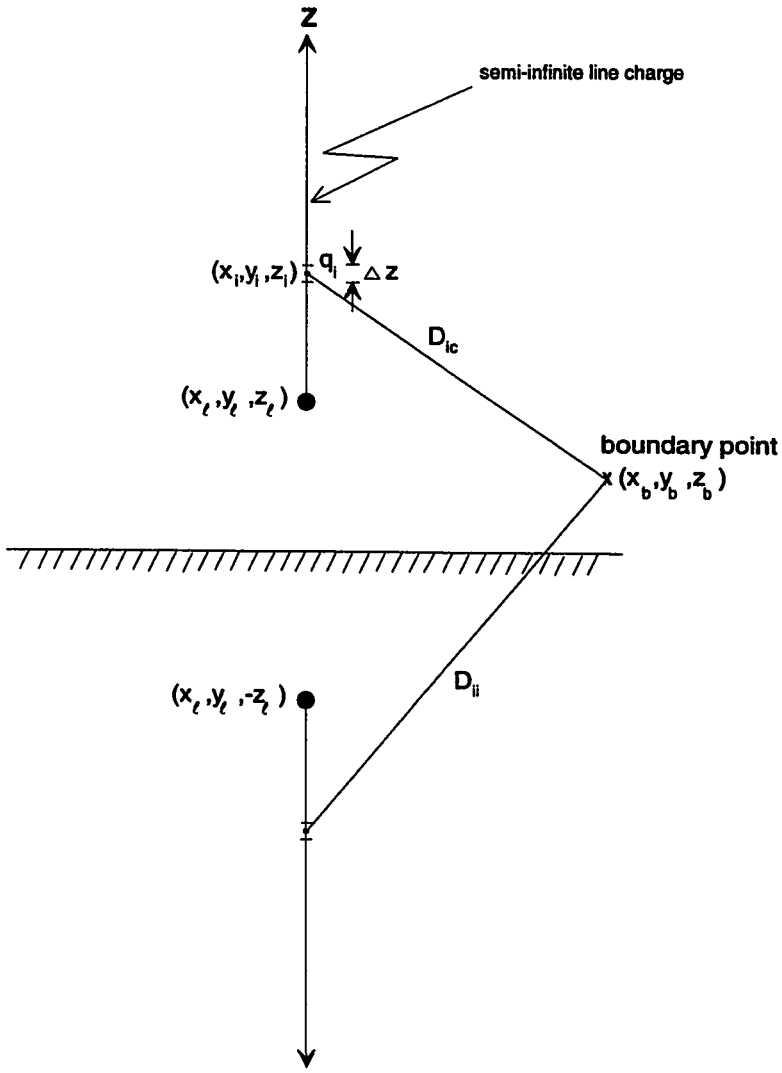

Fig. 3.3 Potential coefficient of the semi-infinite line charge.

The infinitesimal length Δz is considered as equivalent to a point charge of coordinates (X_i, Y_i, Z_i), then

D_{ic} is the distance between the equivalent point charge and the boundary point, and is expressed as:

$$D_{ic} = \sqrt{(X_b - X_i)^2 + (Y_b - Y_i)^2 + (Z_b - Z_i)^2}$$

D_{ii} is the distance between the image of equivalent point charge and the boundary point, and is expressed as:

$$D_{ii} = \sqrt{(X_b - X_i)^2 + (Y_b - Y_i)^2 + (Z_b + Z_i)^2}$$

Then,

$$P_\ell = \frac{1}{4\pi\varepsilon_\circ}\left[\int_{z_\ell}^{\infty}\frac{dz}{D_{ic}} - \int_{z_\ell}^{\infty}\frac{dz}{D_{ii}}\right] \qquad (3.14)$$

Then, from the integration tables, one obtains:

$$P_\ell = \frac{1}{4\pi\varepsilon_\circ}\cdot \mathrm{Ln}\left[\frac{Z_\ell + Z_b + D_{\ell i}}{Z_\ell - Z_b + D_{\ell c}}\right] \qquad (3.15)$$

with:

$D_{\ell c}$ is the distance between the starting point of the semi-infinite line charge q_ℓ and the boundary point, and is expressed as:

$$D_{\ell c} = \sqrt{(X_b - X_\ell)^2 + (Y_b - Y_\ell)^2 + (Z_b - Z_\ell)^2}$$

$D_{\ell i}$ is the distance between the starting point of the image of the semi-infinite line charge q_ℓ and the boundary point, and is expressed as:

$$D_{\ell i} = \sqrt{(X_b - X_\ell)^2 + (Y_b - Y_\ell)^2 + (Z_b + Z_\ell)^2}$$

Equation (3.4) in a matrix form can be written as:

$$\begin{bmatrix} P_{1,r_1} & P_{1,r_2} & \cdot\ \cdot & P_{1,r_{M\cdot N_z}} & P_{1,p} \\ P_{2,r_1} & P_{2,r_2} & \cdot\ \cdot & P_{2,r_{M\cdot N_z}} & P_{2,p} \\ \cdot & \cdot & \cdot\ \cdot & \cdot & \cdot \\ \cdot & \cdot & \cdot\ \cdot & \cdot & \cdot \\ P_{M\cdot N_z,r_1} & P_{M\cdot N_z,r_2} & \cdot\ \cdot & P_{M\cdot N_z,r_{M\cdot N_z}} & P_{M\cdot N_z,p} \\ P_{M\cdot N_z+1,r_1} & P_{M\cdot N_z+1,r_2} & \cdot\ \cdot & P_{M\cdot N_z+1,r_{M\cdot N_z}} & P_{M\cdot N_z+1,p} \end{bmatrix} \cdot \begin{bmatrix} Q_{r_1} \\ Q_{r_2} \\ \cdot \\ \cdot \\ Q_{r_{M\cdot N_z}} \\ Q_p \end{bmatrix} = \begin{bmatrix} -P_{1,\ell}\cdot q_\ell \\ -P_{2,\ell}\cdot q_\ell \\ \cdot \\ \cdot \\ -P_{M\cdot N_z,\ell}\cdot q_\ell \\ -P_{M\cdot N_z+1,\ell}\cdot q_\ell \end{bmatrix} + \begin{bmatrix} -P_{1,t}\cdot Q_t \\ -P_{2,t}\cdot Q_t \\ \cdot \\ \cdot \\ -P_{M\cdot N_z,t}\cdot Q_t \\ -P_{M\cdot N_z+1,t}\cdot Q_{t_1} \end{bmatrix} + \begin{bmatrix} V_{ap}(t) \\ V_{ap}(t) \\ \cdot \\ \cdot \\ V_{ap}(t) \\ V_{ap}(t) \end{bmatrix}$$

(3.16)

It is important to mention that $V_{ap}(t)$ is the same at all boundary points as the Franklin rod is an equipotential. Then the matrix (3.16) solved for the unknown rings and point charges simulating the rod.

$$\begin{bmatrix} Q_{r_1} \\ Q_{r_2} \\ \cdot \\ \cdot \\ Q_{r_{M \cdot N_z}} \\ Q_p \end{bmatrix}$$

After determining the unknown simulation charges, it is necessary to check whether the calculated set of charges satisfies the actual boundary conditions. It must be emphasized that only $(M \cdot N_z + 1)$ discrete boundary points of the real electrode system have been used to solve equation (3.16), and thus the potentials at any other contour points, different from the boundary points might deviate from $V_{ap}(t)$. Therefore, the potentials at a number of "check points", Fig. 3.2, located on the rod boundary (with the known potential) must be computed using equation (3.17). The number of the check points is taken for simplicity equal to the number of the boundary points i.e. $(M \cdot N_z + 1)$ where a check point is selected between two successive boundary points.

$$V_{ch} = \sum_{n=1}^{M \cdot N_z} \left\{ P_{r_n} Q_{r_n} \right\} + P_p Q_p + P_\ell q_\ell + P_t Q_t \qquad (3.17)$$

The difference between these potentials and the given boundary potential, $V_{ap}(t)$, is then a measure of the accuracy and applicability of the proposed simulation.

3.5 Field Calculation Near the Franklin Rod

The geometry of the downward leader and the lightning rod, Fig. 3.1, calls for a 3-dimensional field analysis. In the particular case when the downward leader extends along the axis of the rod, Fig. 3.4, the rotational symmetry results in a simpler 2-dimensional field problem and the M rings at each Z-level will have the same charge value. In this section the mathematical formulation for calculating electric field will be explained.

Once the unknown simulation charges are known, the electric field E(X,Y,Z) at any point of coordinates (X,Y,Z) close to the tip of the lightning rod could be calculated as follows:

$$\overline{E}(X,Y,Z) = \sum_{n=1}^{M \cdot N_Z} \left\{ \overline{f}_{r_n} Q_{r_n} \right\} + \overline{f}_p Q_p + \overline{f}_\ell q_\ell + \overline{f}_t Q_t \qquad (3.18)$$

where:

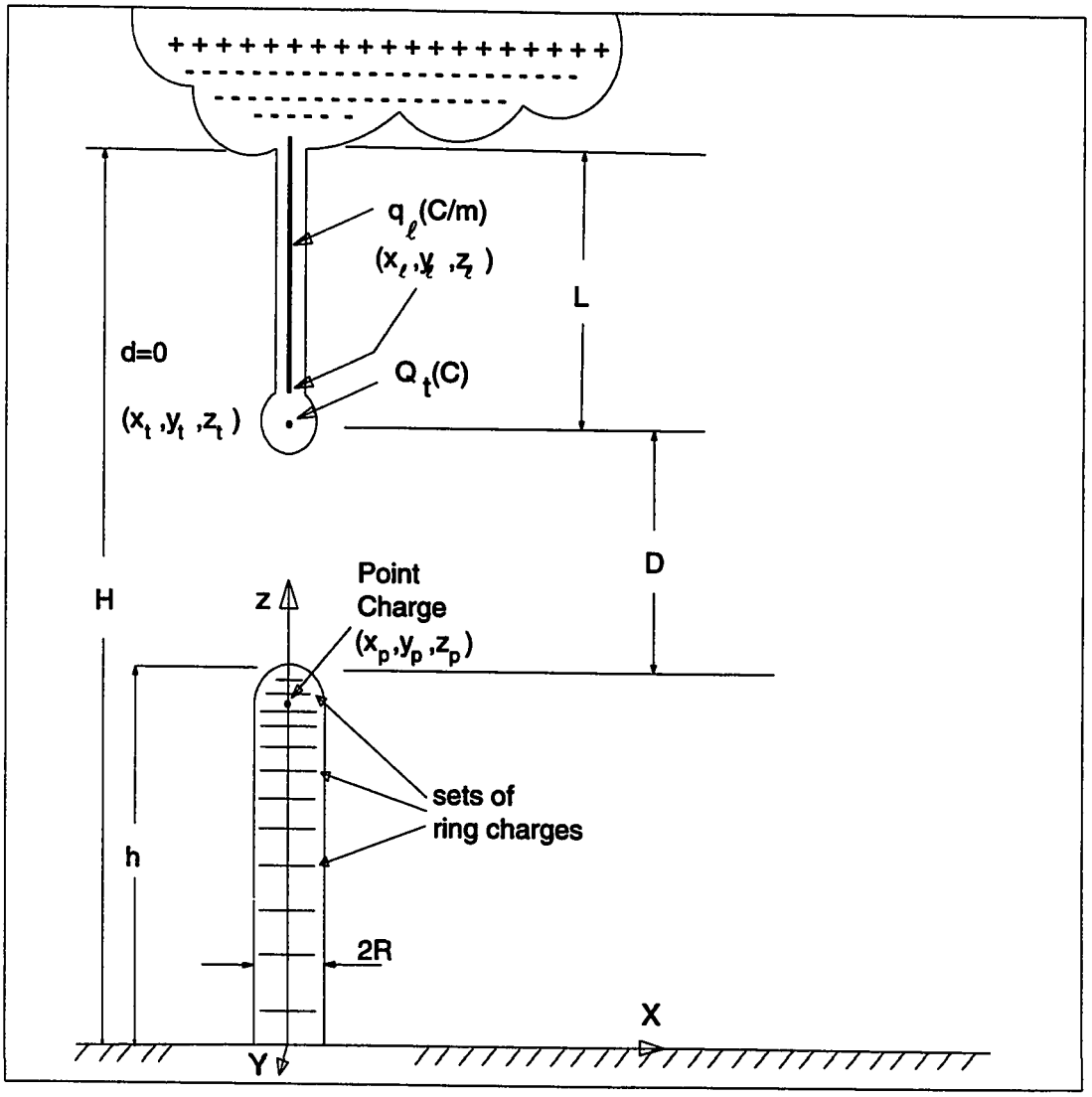

Fig. 3.4 Charge simulation of the downward leader and lightning rod for the special case when the leader is along the axis of the rod.

$\bar{f}_{r_n}$ is three dimensional electric field coefficients (f_{rx_n}, f_{ry_n} and f_{rz_n}) of the nth simulation ring charge calculated at any point of coordinates (X,Y,Z). The coefficients f_{rx_n}, f_{ry_n} and f_{rz_n} are expressed [9] as follows :

$$f_{rx_n} = f_{rr_n} \cos(\theta) \tag{3.19}$$

$$f_{ry_n} = f_{rr_n} \sin(\theta) \tag{3.20}$$

$$f_{rz_n} = \frac{-1}{4\pi\varepsilon_o} \cdot \frac{2}{\pi} \cdot \left\{ \frac{(Z_{r_n} - Z) \cdot K_2(k_1)}{\gamma_1 \cdot \gamma_3^2} + \frac{(Z_{r_n} + Z) \cdot K_2(k_2)}{\gamma_2 \cdot \gamma_4^2} \right\} \tag{3.21}$$

with

f_{rr_n} is the radial component in the X-Y plane and it has been reported in [9] as follows, Fig. 3.5:

$$f_{rr_n} = \frac{-1}{4\pi\varepsilon_o} \frac{1}{\pi r} \left[\frac{\left[r_{j_n}^2 - r_{xy_n}^2 + (Z - Z_{r_n})^2\right] \cdot K_2(k_1) - \gamma_3^2 \cdot K_1(k_1)}{\gamma_1 \cdot \gamma_3^2} - \frac{\left[r_{j_n}^2 - r_{xy_n}^2 + (Z + Z_{r_n})^2\right] \cdot K_2(k_2) - \gamma_4^2 \cdot K_1(k_2)}{\gamma_2 \cdot \gamma_4^2} \right] \tag{3.22}$$

$$\sin(\theta) = \frac{Y - Y_{r_n}}{r_{xy_n}} \tag{3.23}$$

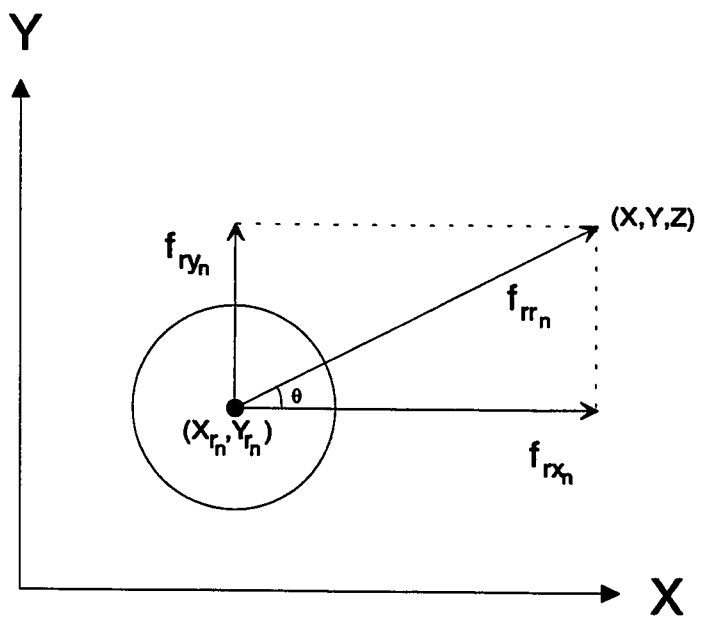

Fig. 3.5 Electric field coefficient components in the X-Y plane of the nth ring charge.

$$\cos(\theta) = \frac{X - X_{r_n}}{r_{xy_n}} \tag{3.24}$$

$$\gamma_3 = \sqrt{(r_{xy_n} - r_{j_n})^2 + (z - z_{r_n})^2}$$

$$\gamma_4 = \sqrt{(r_{xy_n} - r_{j_n})^2 + (z + z_{r_n})^2}$$

Where $K_2(k_1)$ and $K_2(k_2)$ are the complete elliptic integrals of the second kind.

$\bar{f}_p$ is three dimensional electric field coefficients (f_{px}, f_{py} and f_{pz}) of the point charge at the center of the cap of the lightning rod calculated at any point of coordinates (X,Y,Z). This three component coefficient could be derived from potential coefficient P_p as follows [9]:

$$f_{px} = \frac{-\partial P_p}{\partial X} = \frac{\partial}{4\pi\varepsilon_o \partial x}\left[\frac{1}{D_{pc}} - \frac{1}{D_{pi}}\right] \tag{3.25}$$

$$f_{px} = \frac{X - X_p}{4\pi\varepsilon_o}\left[\frac{1}{D_{pc}^3} - \frac{1}{D_{pi}^3}\right] \tag{3.26}$$

Similarly;

$$f_{py} = \frac{Y - Y_p}{4\pi\varepsilon_o}\left[\frac{1}{D_{pc}^3} - \frac{1}{D_{pi}^3}\right] \tag{3.27}$$

$$f_{pz} = \frac{1}{4\pi\varepsilon_o}\left[\frac{Z - Z_p}{D_{pc}^3} - \frac{Z + Z_p}{D_{pi}^3}\right] \tag{3.28}$$

$\bar{f}_t$ is three dimensional electric field coefficients (f_{tx}, f_{ty} and f_{tz}) of the point charge at tip of the downward leader calculated at any point of coordinates (X,Y,Z). This three component coefficient could be also expressed as follows [9]:

$$f_{tx} = \frac{X - X_t}{4\pi\varepsilon_o}\left[\frac{1}{D_{tc}^3} - \frac{1}{D_{ti}^3}\right] \tag{3.29}$$

$$f_{ty} = \frac{Y - Y_t}{4\pi\varepsilon_o}\left[\frac{1}{D_{tc}^3} - \frac{1}{D_{ti}^3}\right] \tag{3.30}$$

$$f_{tz} = \frac{1}{4\pi\varepsilon_o}\left[\frac{Z - Z_t}{D_{tc}^3} - \frac{Z + Z_t}{D_{ti}^3}\right] \tag{3.31}$$

$\bar{f}_\ell$ is three dimensional electric field coefficients ($f_{\ell x}$, $f_{\ell y}$ and $f_{\ell z}$) of the simulation semi-infinite line charge of the downward

leader calculated at any point of coordinates (X,Y,Z). This three components coefficient could be derived from the potential coefficient P_ℓ as follows:

$$f_{\ell x} = \frac{-\partial P_\ell(X,Y,Z)}{\partial x} = \frac{-\partial}{4\pi\varepsilon_\circ\,\partial x}\cdot \mathrm{Ln}\left[\frac{Z_\ell + Z + D_{\ell i}}{Z_\ell - Z + D_{\ell c}}\right] \tag{3.32}$$

$$f_{\ell x} = \frac{X - X_\ell}{4\pi\varepsilon_\circ}\cdot\left\{\frac{1}{D_{\ell c}[Z_\ell - Z + D_{\ell c}]} - \frac{1}{D_{\ell i}[Z_\ell + Z + D_{\ell i}]}\right\} \tag{3.33}$$

Similarly;

$$f_{\ell y} = \frac{Y - Y_\ell}{4\pi\varepsilon_\circ}\cdot\left\{\frac{1}{D_{\ell c}[Z_\ell - Z + D_{\ell c}]} - \frac{1}{D_{\ell i}[Z_\ell + Z + D_{\ell i}]}\right\} \tag{3.34}$$

and

$$f_{\ell z} = \frac{-\partial P_\ell(X,Y,Z)}{\partial z} = \frac{-\partial}{4\pi\varepsilon_\circ\,\partial z}\cdot \mathrm{LN}\left[\frac{Z_\ell + Z + D_{\ell i}}{Z_\ell - Z + D_{\ell c}}\right] \tag{3.35}$$

$$f_{\ell z} = \frac{-1}{4\pi\varepsilon_\circ}\cdot\left\{\frac{1 + (Z + Z_\ell)/D_{\ell i}}{Z_\ell + Z + D_{\ell i}} + \frac{1 + (Z_\ell - Z)/D_{\ell c}}{Z_\ell - Z + D_{\ell c}}\right\} \tag{3.36}$$

If the electric field in the vicinity of grounded Franklin rod is denoted as $\overline{E}_{dl}$. Then the electric field component due to the applied pulse voltage is expressed as:

$$\overline{E}_{ap} = \overline{E}_{to} - \overline{E}_{dl} \tag{3.37}$$

where $\overline{E}_{to}$ is the electric field in the vicinity of energized rod.

The next section describes a computer program written using the above model to calculate the electric field in the vicinity of the Franklin rod.

3.6 Programming the CST for the Present Model

In this section, an iterative computer program to calculate the electric field at any point in the vicinity of the energized Franklin rod will be explained (see Appendix-A). The following steps and the flow chart of Fig. 3.6 describe briefly the computation of the electric field at any point (X,Y,Z) in the vicinity of the rod.

1- Defining the values and the coordinates of the simulation charges of the simulation charges for the downward leader, section 3.3.1.

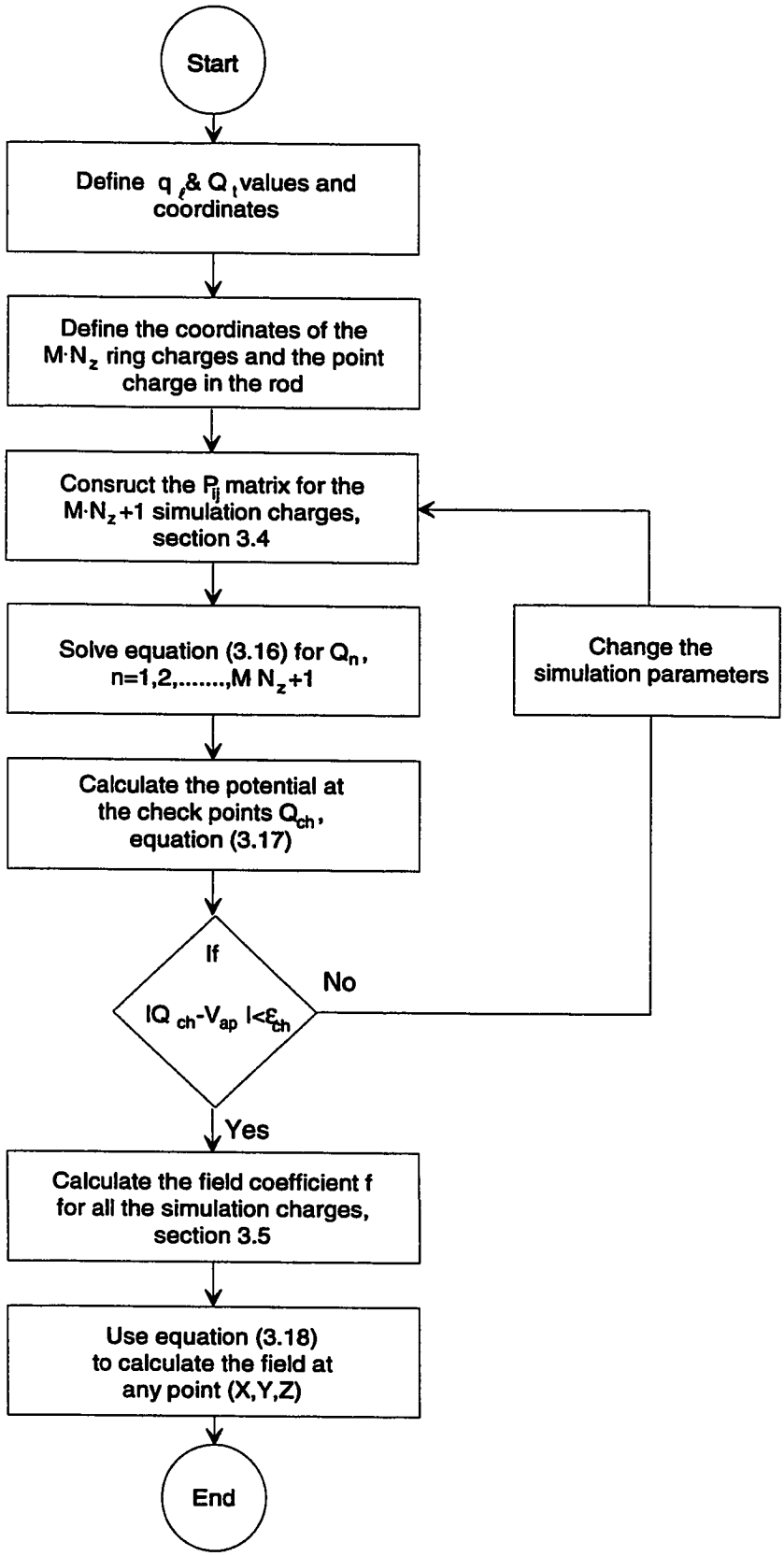

Fig. 3.6 Flow chart for calculating the electric field in the vicinity of the Franklin rod.

2- Defining the coordinates of the simulation charges on the rod, section 3.3.2.

3- Construction of the potential coefficient $(M \cdot N_z + 1)$ square matrix at the boundary points as explained in section 3.4.

4- Solve equation (3.16) for the unknown simulation charges.

5- Calculate the potential at the $(M \cdot N_z + 1)$ check points using equation 3.17.

6- If the difference between the potential given in step 5 and the boundary potential is accepted, then computation of the unknown charges is completed. Otherwise, the simulation charges parameters (number and coordinates) should be modified and then proceed to step 3.

7- Calculate the electric field coefficients $\bar{f}$ for all the simulation charges at any point (X,Y,Z) as explained in section 3.5.

8- Use equation (3.18) to calculate the electric field $\bar{E}(X,Y,Z)$ at any point (X,Y,Z) in the vicinity of the energized Franklin rod.

3.7 Numerical Data

The physical parameters used in calculating the electric field in the vicinity of the energized Franklin rod are quantified in the following sections.

3.7.1 Downward Leader Simulation Charges Data

The downward leader simulation charges described in section 3.3.1 is expressed as a function of the peak current of the first lightning stroke. For practical applications, the following relations are often reported in the literature [8,30]:

$$Q_t(C) = \frac{I(kA)}{150.0} \tag{3.38}$$

and

$$q_\ell(C/m) = \frac{0.9I(kA)}{15H(m)} \tag{3.39}$$

where:

H is the height of the cloud above the ground plane where the downward leader originates, Fig. 3.1.

I is the peak current of the first lightning stroke, when L=H, Fig. 3.1.

3.7.2 Energized Franklin Rod Simulation Charges Data

Due to the absence of rotational symmetry (due to the presence of the downward leader), each Z-level has been simulated by a set of 4 rings. In the special case when the leader extends along the rod axis, one ring can be used to simulate the rod.

The number of rings simulating the rod has been selected based on the best results obtained. It has been observed that there is an optimum number of simulating charges at which the best accuracy of the calculated potential at the check points is achieved (see Appendix-B).

For the Cylindrical portion, different number of rings was attempted and 160 rings was found satisfactory. The radius of these rings is constant and related to the rod radius. It was found that if the ring radius is 0.85 of the rod radius, the best accuracy in the calculated potential at the check points was achieved. The number of Z-levels at the higher part of the rod is chosen denser than that at the bottom of the rod. Therefore, the Z-coordinate of these Z-levels is determined according to the following formula:

$$Z_i = Z_{i-1} - \frac{2 \cdot h}{(N_{zc}+1)\cdot(N_{zc}+2)} \cdot i \qquad (3.40)$$

where:

Z_i is the Z-coordinate of the ith level.

N_{zc} is the number of Z-level in the cylindrical portion.

This formula has been tested and found that it gives the best result of the electric field calculation (see Appendix-B).

For the hemispherical cap portion, the number of the rings in this portion is 32. The radius of these rings is variable from level to level and depends on the radius of the cap at that level. It was found that if the ring radius is 0.85 of the cap radius, the best accuracy in the potential at the check points was achieved (see Appendix-B).

3.8 Results

The electric field in the vicinity of the Franklin rod is a prerequisite for determining the onset condition of the upward streamer. To check the accuracy of the calculated electric field values in the vicinity of the Franklin rod, a comparison is made against the values reported by Berger [32].

In order to exclude the effect of the downward leader on the field values, the current of the leader was set equal to zero. In this case, the

field established in the vicinity of the rod is due to the voltage applied to the rod.

Let s is the Z-coordinate of a point along the axis of Franklin rod where $s \geq h$, the height of the Franklin rod. For different s-values, the electric field is calculated and normalized to the peak value at the rod tip.

Figures 3.7-3.10 show the normalized field values versus the ratio s/h, i.e. the Z-coordinate of the point normalized to the rod height. The field values in these figures are those obtained by the present method and those reported before [32] for different h/R values where R is the rod radius.

It is quite clear that the present calculated values agree satisfactorily with those reported before [32]. This reflects itself on the accuracy of the calculated field values and the correctness of the algorithm developed for field calculation in the vicinity of the rod in the presence of the downward leader.

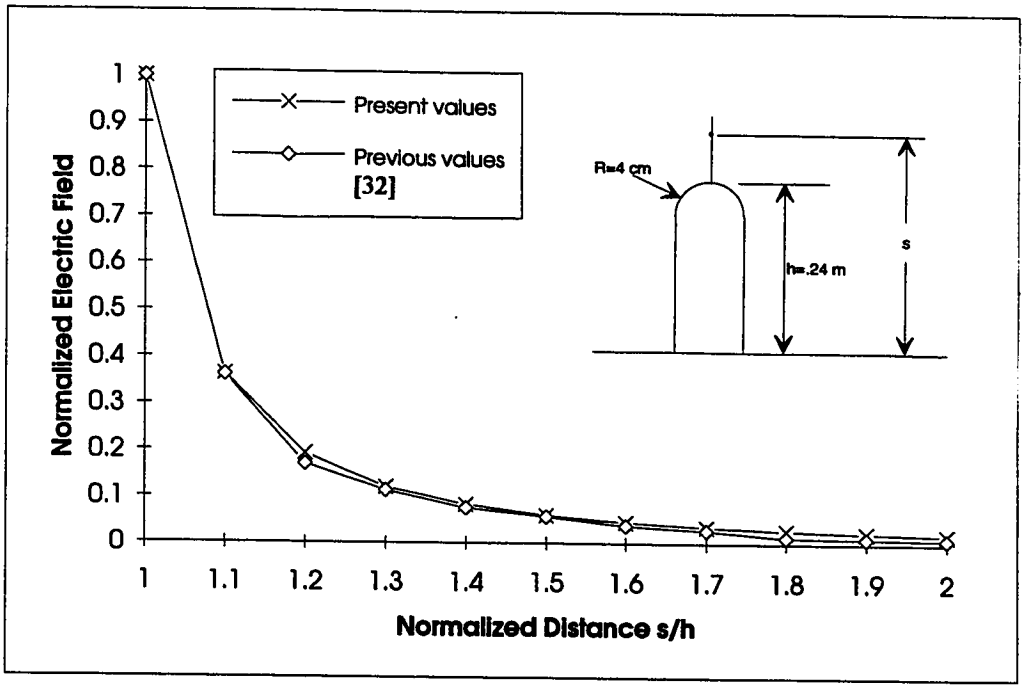

Fig. 3.7 Electric field distribution along the axis of the Franklin rod versus the normalized distance s/h for h/R=6.

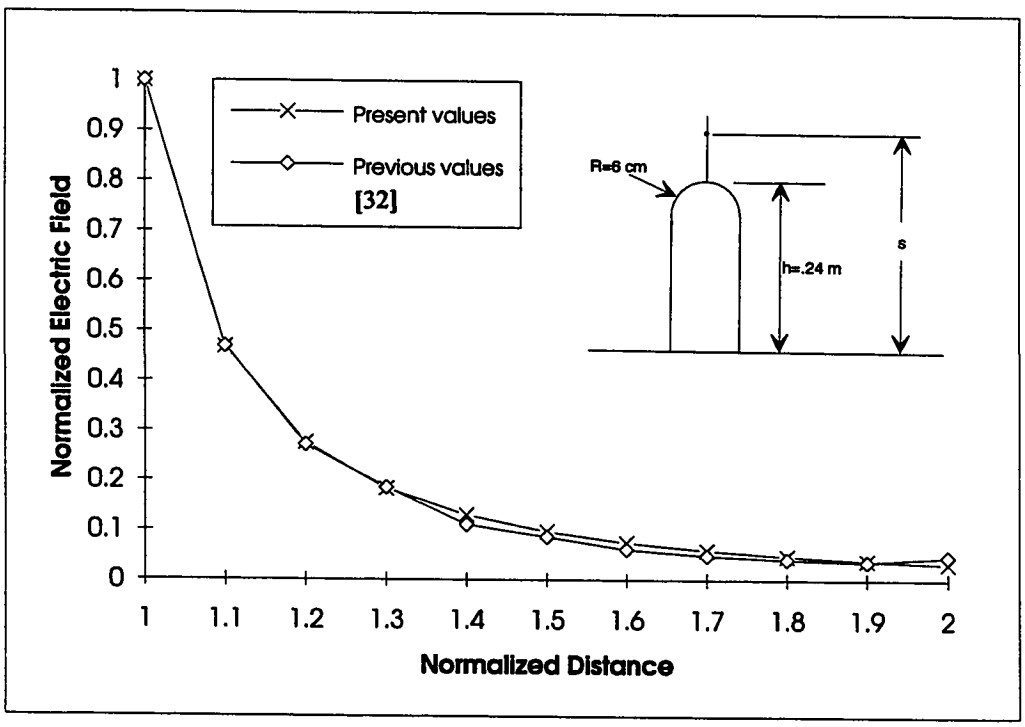

Fig. 3.8 Electric field distribution along the axis of the Franklin rod versus the normalized distance s/h for h/R=4.

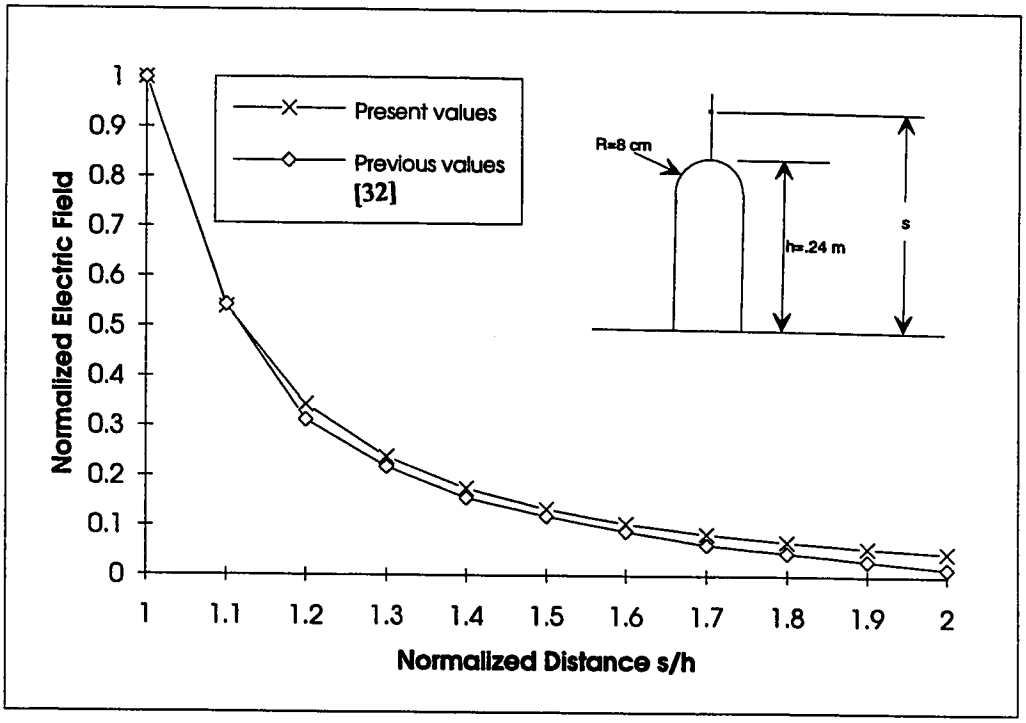

Fig. 3.9 Electric field distribution along the axis of the Franklin rod versus the normalized distance s/h for h/R=3.

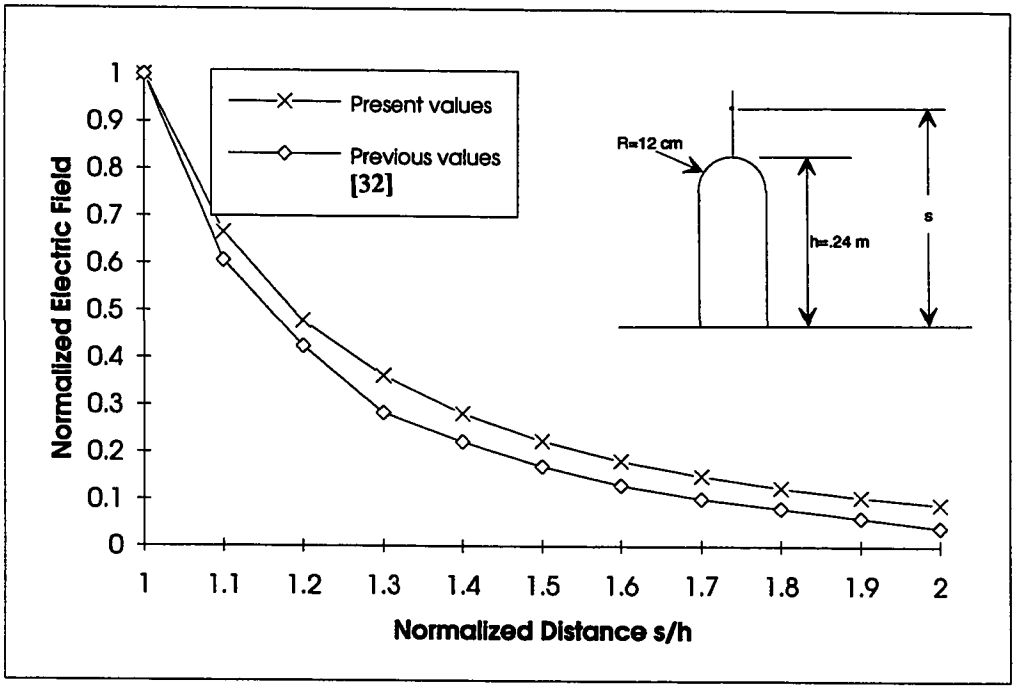

Fig. 3.10 Electric field distribution along the axis of the Franklin rod versus the normalized distance s/h for h/R=2.

CHAPTER 4

ONSET CRITERIA OF THE UPWARD STREAMER

4.1 Introduction

Under stormy conditions, it is believed that the upper portion of the cloud is usually positively charged whereas the lower portion and base are predominantly negative as discussed in Chapter 2. When the electric field at some points on the base of the cloud exceeds the breakdown value of the moist air (≈10 kV/cm), a negative electric streamer (pilot streamer) starts toward the ground with a velocity of a bout 1/10 times that of the light. This streamer eventually turns into a negative downward (stepped) leader. Simultaneously, with propagation of the downward leader, the field is amplified at the tip of Franklin rod. When the field exceeds the breakdown value of air, a corona discharge takes place at the rod tip, which may turn into a positive upward leader.

The two opposite leaders influence each other, the result being a bending of the downward leader towards the upward leader.

When both leaders meet, the lightning stroke takes place and the lightning current falls into the ground through the rod.

Therefore, lighting protection is tied up with the formation of corona at the tip of Franklin rod and its transition into an upward leader. The sooner the launching of the upward leader, the more efficient is the Franklin rod [5,6,7]. Therefore, stressing the Franklin rod by a pulse voltage may enhance its effectiveness in protection against lightning. This is because of the earlier development of the streamer corona. Thus, the onset of corona streamer at the tip of the energized rod is one of the main parameters to be investigated.

4.2 The Criterion of the Corona Onset

In this section, the onset criterion of the breakdown will be briefly described and then the criterion will be formulated mathematically in the next section.

When the downward leader starts its propagation from the cloud toward the ground, the electric field at the ground level will increase and the maximum increase will be at tip of the Franklin rod. This increase will create an ionization-zone around the tip of the rod. In this zone, the field is so high that the ionization coefficient by electron collision ,α, exceeds the electron attachment coefficient,

η, Fig. 4.1. If any electron appears inside this zone, it will accelerate toward the rod building an electron avalanche Fig. 4.2.

Assuming that an initiatory electron starts at the boundary of the ionization zone creating an electron avalanche on its way toward Franklin rod. This avalanche is called the primary avalanche (representing the first generation of avalanches), where the electrons are populated at the head leaving behind positive ions in the wake of the avalanche. The electrons of the primary avalanche accelerate under the resultant of the field induced by the downward leader, the field produced by the pulse voltage applied to the energized Franklin rod, and the field resulting from the avalanche-produced positive space charge, Fig. 2.10.

It should be recalled that during the build-up of the primary avalanche, excitation of air atoms has been taking place at the same time ionization have been occurring. Excited states have lifetime that can be as short as 10^{-13} second. Therefore, before the primary avalanche has reached its full size, photons will be emitted from these excited states as they return to the ground level [26]. The number of excited states is a fraction f_2 of the number of ionization events.

These photons will be heading in all directions and will be absorbed at various distances from their origin, depending on the absorption coefficient μ of the air, Fig. 4.2.

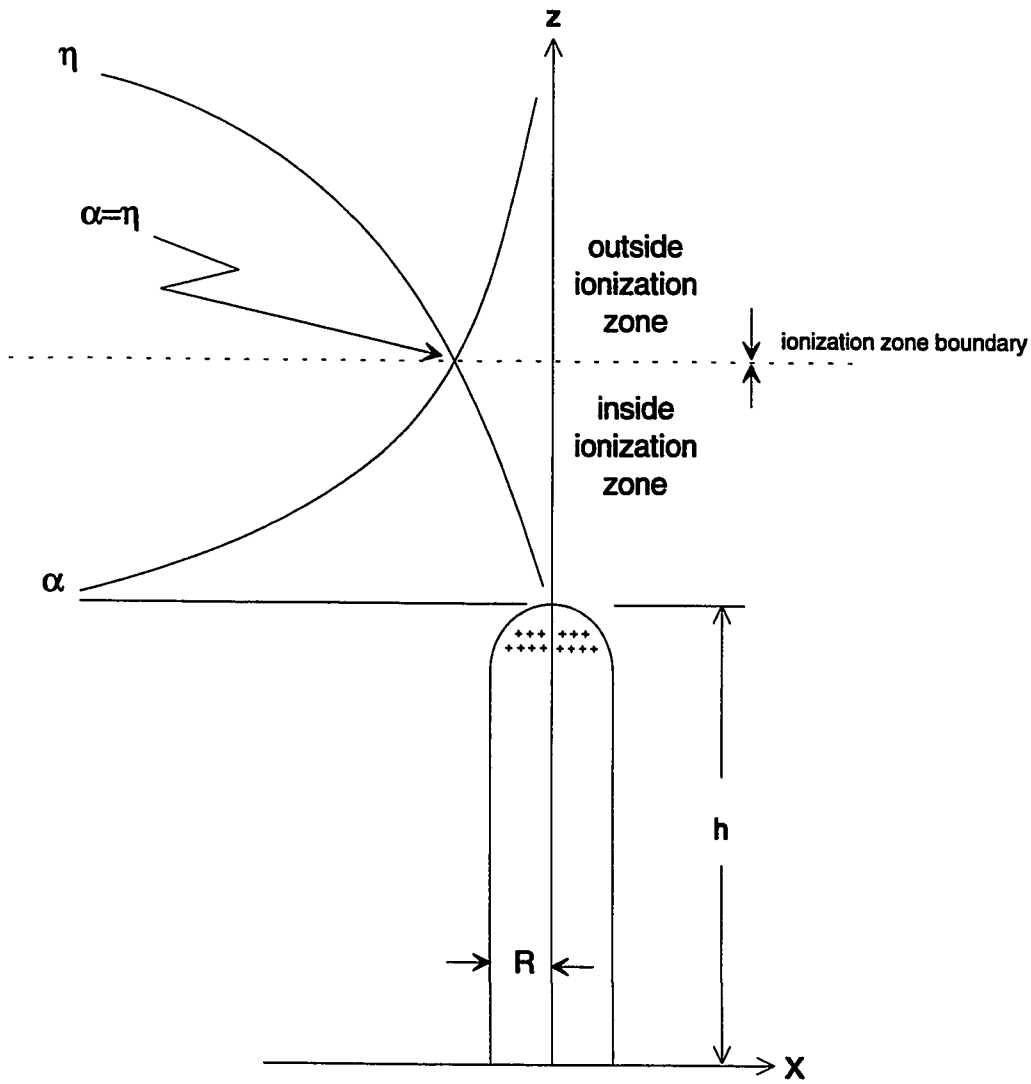

Fig. 4.1 Axial distribution of the ionization α and attachment η coefficients above the rod.

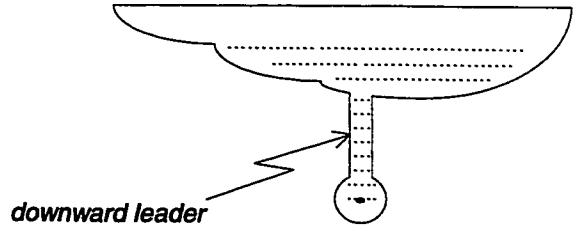

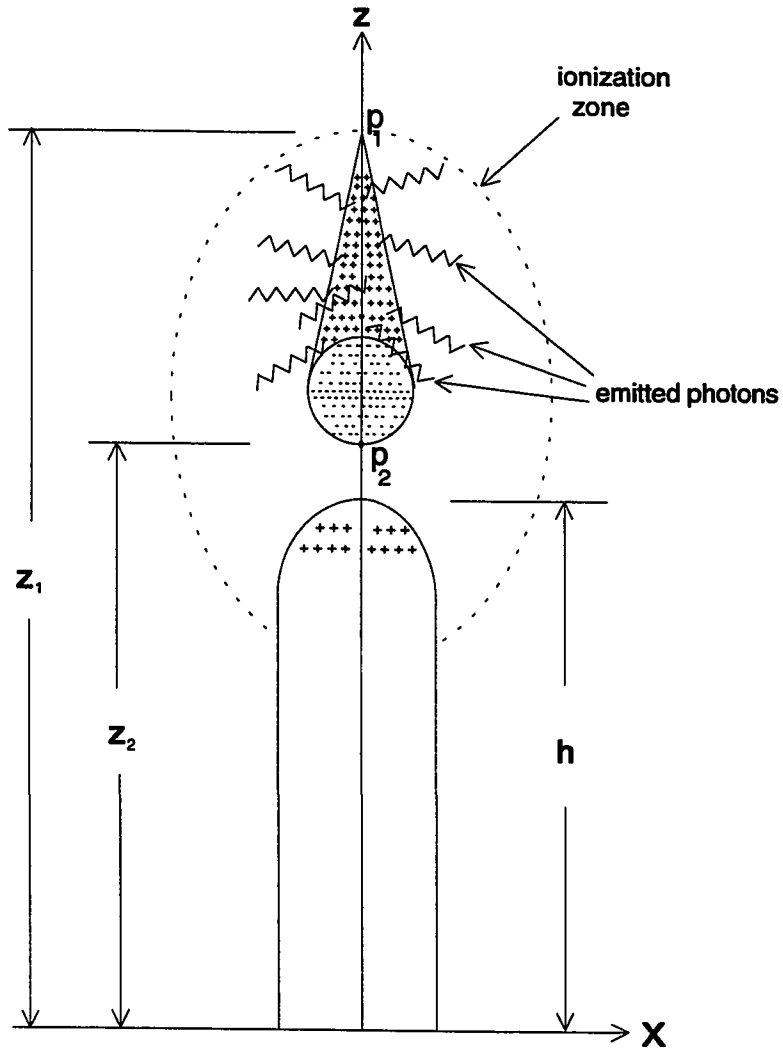

Fig. 4.2 Emitted photons from the primary avalanche.

When the photons are absorbed, many processes take pace which may lead to photoionization of the air inside the ionization-zone with probability factor f_1.

New photoelectrons are now available in the air to start successor avalanches (of the second generation) that is still advancing toward the Franklin rod, Fig. 4.3.

The growth of each successor avalanche takes place under the resultant of the four components of the electric field; the field induced by the downward leader, the field produced by the pulse voltage applied to the energized Franklin rod, the field resulting from the positive ions left behind the primary avalanche, and the field due to the space charge of the successor avalanche itself.

Similarly, all successor avalanches of the second generation will emit photons as they are being formed. These photons create new photoelectrons that are ready to give rise to third-generation avalanches and so on.

The accumulation of the positive ions created by the primary avalanche has grown toward the downward leader by the charges of the successor avalanches of the second generation and the succeeding generations. This constitutes the growth of the streamer

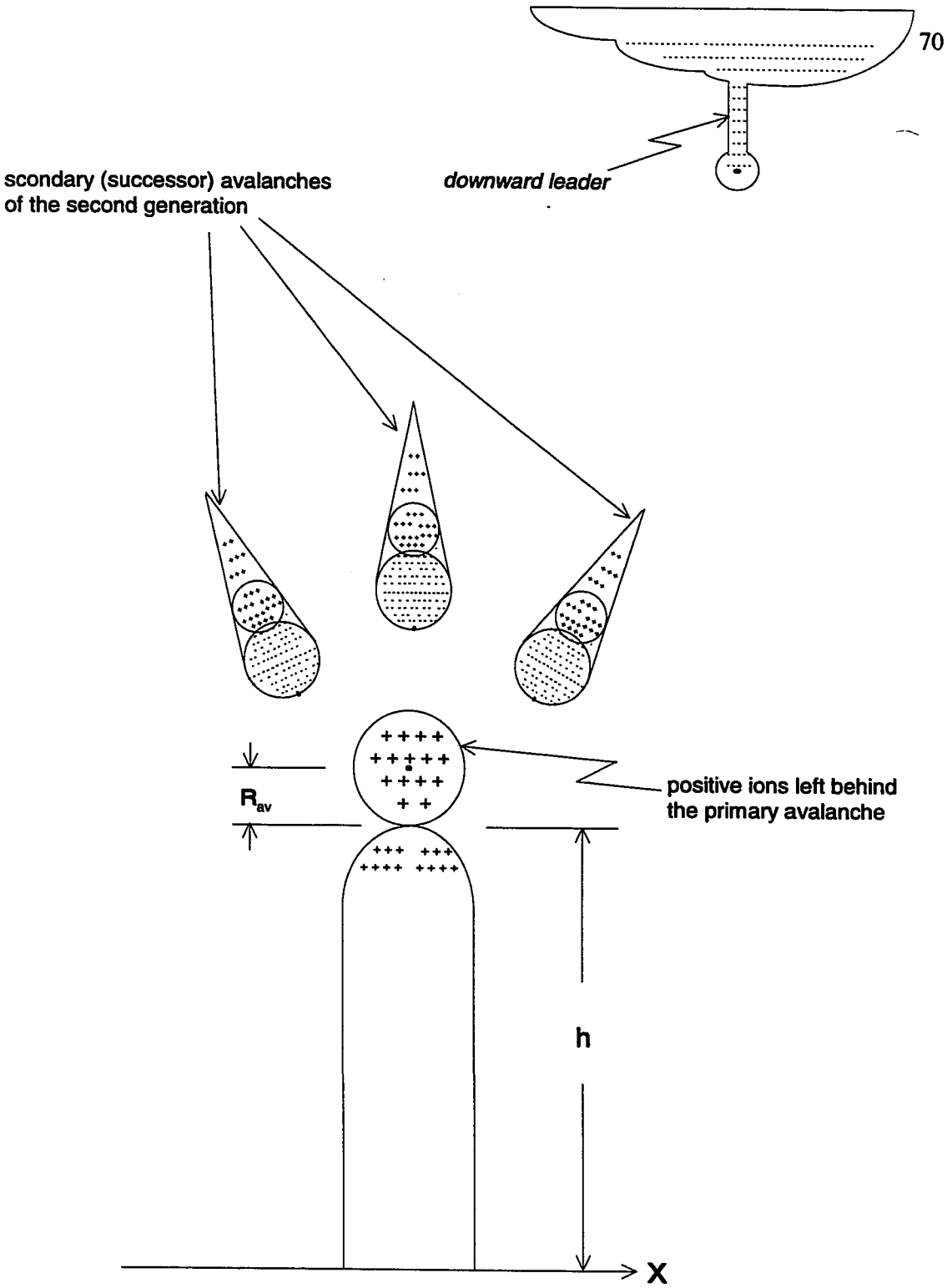

Fig. 4.3 Secondary avalanches feeding into primary avalanche.

from the Franklin rod toward the downward leader, Fig. 4.4. Thus, the propagation of the streamer tip upwards depend on ionization yield of the avalanches feeding into it.

The criterion of the primary avalanche-to-streamer transition [1,8,26] is that the total number of positive ions (N_{+2}) created by the successor avalanches forming the second generation is equal to the number of positive ions of the primary avalanche (N_{+1}). This will ensure that the discharge process becomes self-maintained or self-sustained.

4.3 Mathematical Formulation of the Onset Criteria

The physical phenomenon outlined in the previous section is mathematically formulated in this section. Assume one initiatory electron is available at the ionization-zone boundary i.e. (at $z = z_1$, Fig. 4.2). Under the prevailing field, the electron accelerates forming the primary avalanche.

The number of electrons $N_e(z)$ at the head of the growing primary avalanche growing to $z = z_2$, Fig. 4.2:

$$N_e(z) = \exp\left(\int_{z_1}^{z_2}[\alpha(z) - \eta(z)]dz\right) \tag{4.1}$$

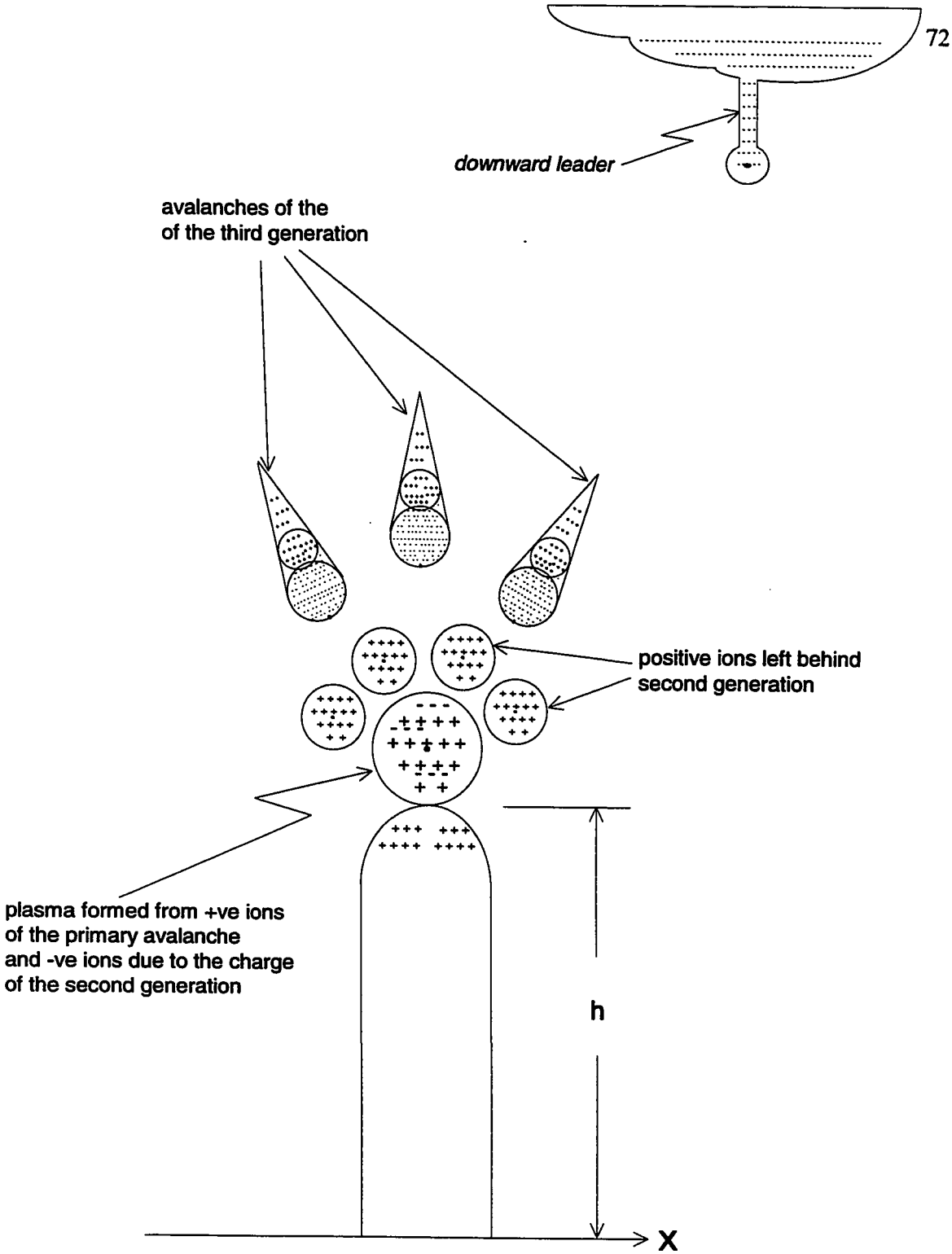

Fig. 4.4 Growth of the streamer from Franklin rod.

where z is the distance traveled by the avalanche.

The coefficients $\alpha(z)$ and $\eta(z)$ depend on the prevailing electric field $\overline{E}(z)$. The latter, given by equation (4.2), is the resultant of the field induced by the downward leader $\overline{E}_{dl}(z)$, the field resulting from the pulse applied to Franklin rod $\overline{E}_{ap}(z)$, and the field produced by the positive space charge of the primary avalanche $\overline{E}_{psc}(z)$. The field components $\overline{E}_{dl}(z)$ and $\overline{E}_{ap}(z)$ are determined as evaluated in Chapter 3. The component $\overline{E}_{psc}(z)$ is expressed by equation (2.5).

$$\overline{E}(z) = \overline{E}_{dl}(z) + \overline{E}_{ap}(z) + \overline{E}_{psc}(z) \tag{4.2}$$

The number of photons emitted while the avalanche is growing, is expressed as:

$$n_{ph} = N_e(z) \cdot f_2 \tag{4.3}$$

where:

f_2 is the ratio between the number of exciting states and the number of ionizing events.

If the downward leader is displaced from the Franklin-rod axis, Fig. 3.1, the electric field would not be symmetrical around the rod, and the ionization-zone will be divided into shells along the Z-

direction, each with a thickness Δz. Each shell is divided into strips along the X-direction each with thickness Δy. Then, each strip is subdivided into sections of thickness Δx along the Y-direction, Fig. 4.5. Thus, the ionization zone is divided into segments, each with volume $\Delta x \cdot \Delta y \cdot \Delta z$. Because the volume of the segment is very small the electric field is assumed the same over the segment volume. Then, the number of photons incident on each segment can be calculated as:

$$(n_{ph})_{\text{incident to segment}} = \frac{\Delta x \cdot \Delta y}{4\pi\rho_s^2} \cdot f_2 \cdot N_e(z) \qquad (4.4)$$

where:

ρ_s is the distance from the head of the primary avalanche to the segment, Fig. 4.5.

If μ is the coefficient of absorption, the number of photons absorbed in each segment of thickness Δz is:

$$(n_{ph})_{\text{absorbed in segment}} = \frac{\Delta x \cdot \Delta y}{4\pi\rho_s^2} \cdot f_2 \cdot N_e(z) \cdot \mu \cdot \exp(-\mu\rho_s) \cdot \Delta z \qquad (4.5)$$

Only a small fraction, f_1, of the absorbed photons will produce photoelectrons. This depends on the probability of ionization of the

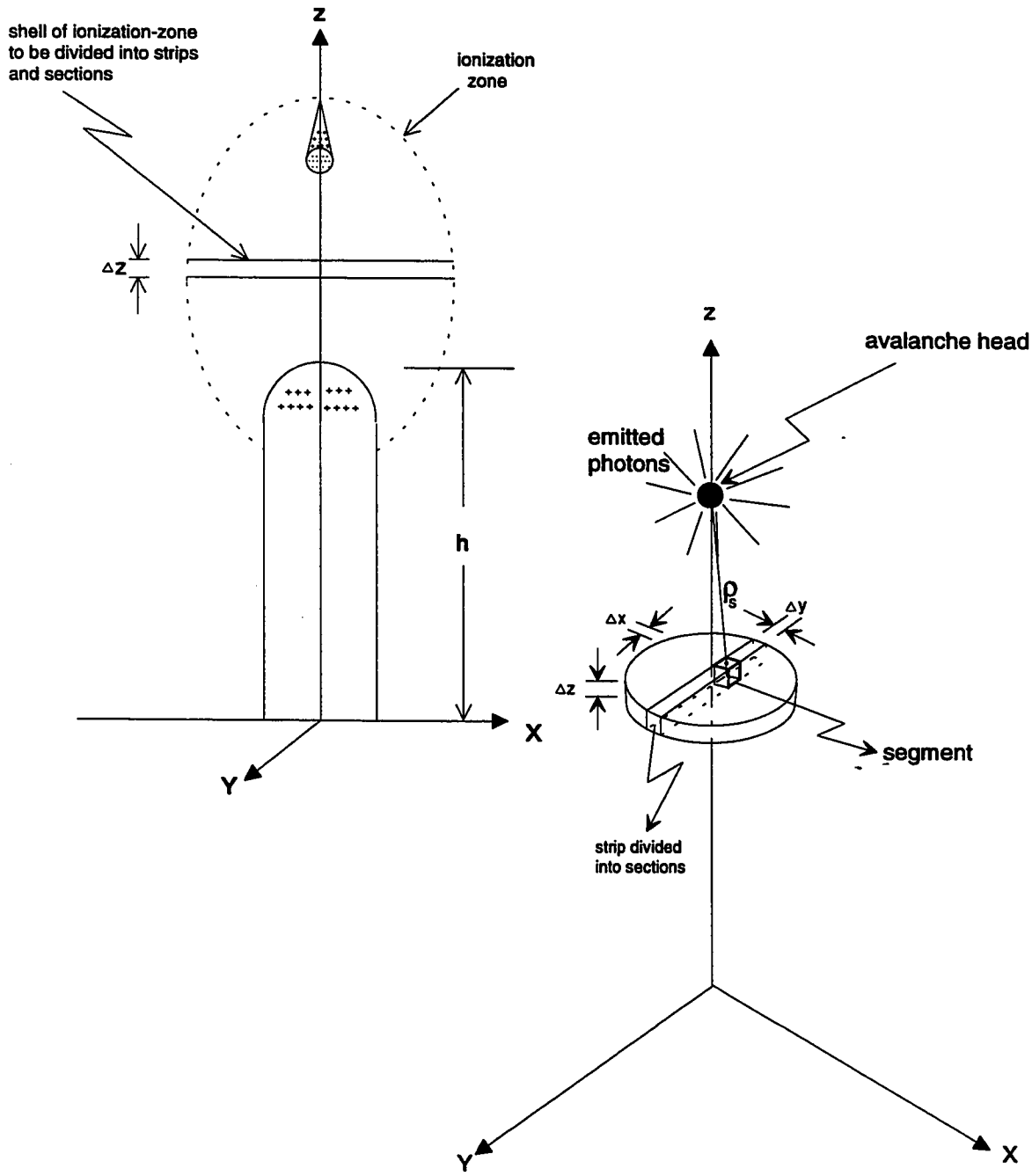

Fig. 4.5 Division of the ionization-zone into small segments.

radiation being emitted. Then, the number of photoelectrons produced in each segment is:

$$n_{\text{ph.electrons in segment}} = \frac{\Delta x \cdot \Delta y}{4\pi\rho_s^2} \cdot f_1 \cdot f_2 \cdot N_e(z) \cdot \mu \cdot \exp(-\mu\rho_s) \cdot \Delta z \qquad (4.6)$$

Then, the total number of the photoelectrons created in each segment can be obtained by integrating equation (4.6) along the whole avalanche growth.

$$n_{\text{tot.ph. elect. in segment}} = \int_{z_1}^{h} \frac{\Delta x \cdot \Delta y}{4\pi\rho_s^2} \cdot f_1 \cdot f_2 \cdot N_e(z) \cdot \mu \cdot \exp(-\mu\rho_s) \cdot \Delta z \cdot dz \qquad (4.7)$$

All the photoelectrons created in the ionization-zone will be accelerated along the actuating field to produce successor avalanches. Each photoelectron will produce a number of positive ions given by the following expression:

$$N_{+\text{secondary/photoelecrton}} = \exp\left[\int_{\ell_1}^{\ell_2} (\alpha(\ell) - \eta(\ell)) d\ell\right] \qquad (4.8)$$

where:

ℓ_1 is determined by the coordinates of the segment from which the successor avalanche starts its growth.

ℓ_2 is determined by the coordinates of the end point at which the successor avalanche will terminate. The successor avalanche may terminate at the rod surface or

at the positive space charge left by the primary avalanche.

ℓ is the distance measured along the direction of growth of successor avalanche.

The actuating field through which the successor avalanche accelerates is the resultant of four components namely:

a- The field due to the downward leader $\overline{E}_{dl}(\ell)$ as discussed in Chapter 3.

b- Field produced by the pulse voltage applied to the energized lightning rod $\overline{E}_{ap}(\ell)$ as discussed also in Chapter 3.

c- The field due to the positive space charge left by the primary avalanche $\overline{E}_{psc}(\ell)$ as expressed by equation (2.5).

d- The field resulting from the positive space charge of the successor avalanche itself $\overline{E}_{ssc}(\ell)$, which is expressed (in analogy with equation 2.3) as:

$$E_{ssc}(\ell) = \frac{e \cdot N_e(\ell) \cdot \alpha^2(\ell)}{4\pi\varepsilon_o} \tag{4.9}$$

$$\overline{E}(\ell) = \overline{E}_{dl}(\ell) + \overline{E}_{ap}(\ell) + \overline{E}_{psc}(\ell) + \overline{E}_{ssc}(\ell) \tag{4.10}$$

The number of the positive ions produced by each segment $N_{segment}$ is obtained by multiplying the number of photoelectrons created in each segment, equation (4.7), by the number of positive ions produced by each photoelectron as expressed by equation (4.8). This gives:

$$N_{segment} = \int_{z_1}^{h} \frac{\Delta x \cdot \Delta y}{4\pi\rho_s^2} \cdot f_1 \cdot f_2 \cdot N_e(z) \cdot \mu \cdot \exp(-\mu\rho_s) \cdot \Delta z \cdot dz \cdot \left\{ \exp\left[\int_{\ell_1}^{\ell_2} (\alpha(\ell) - \eta(\ell)) d\ell \right] \right\} \tag{4.11}$$

Then, the total number of positive ions produced by all successor avalanches is expressed as:

$$N_{+2} = \sum_{i=1}^{K} \int_{z_1}^{h} \frac{\Delta x_i \cdot \Delta y_i}{4\pi\rho_{s_i}^2} \cdot f_{1_i} \cdot f_{2_i} \cdot N_e(z) \cdot \mu_i \cdot \exp(-\mu_i\rho_{s_i}) \cdot \Delta z_i \cdot dz \cdot \left\{ \exp\left[\int_{\ell_{1_i}}^{\ell_{2_i}} (\alpha_i(\ell) - \eta_i(\ell)) d\ell \right] \right\} \tag{4.12}$$

where:

K is the total number of segments in the ionization-zone as whole.

The criterion for primary avalanche-streamer transition (i.e. condition of self-propagating streamer) is that the total number of positive ions created by the successor avalanches, as expressed by equation (4.12), be equal to the number of the positive ions produced by the primary avalanche;

$$N_{+1} = \int_{z_1}^{h} [\alpha(z) - \eta(z)] dz \qquad (4.13)$$

The streamer onset voltage V_o is the critical value which fulfills the equality (4.14).

$$N_{+2} = N_{+1} \qquad (4.14)$$

The next section explains an iterative digital computer algorithm to fulfill the equality (4.14) seeking the assessment of the onset-condition of streamer corona at the tip of Franklin rod..

Special case

If the downward leader is in alignment with Franklin-rod axis, then the electric field will be symmetrical around the rod axis, Fig. 3.4. In this case, the problem will be much simpler and the ionization-zone can be divided into shells as before. Each shell has a thickness Δz and is sub-divided into rings, Fig. 4.6. Then, equations (4.4)-(4.8), and (4.12) can be rewritten, respectively, for this case, as follows:

$$(n_{ph})_{\text{incident to ring}} = \frac{2\pi r_r \cdot \Delta r}{4\pi \rho_r^2} \cdot f_2 \cdot N_e(z) \qquad (4.4a)$$

where:

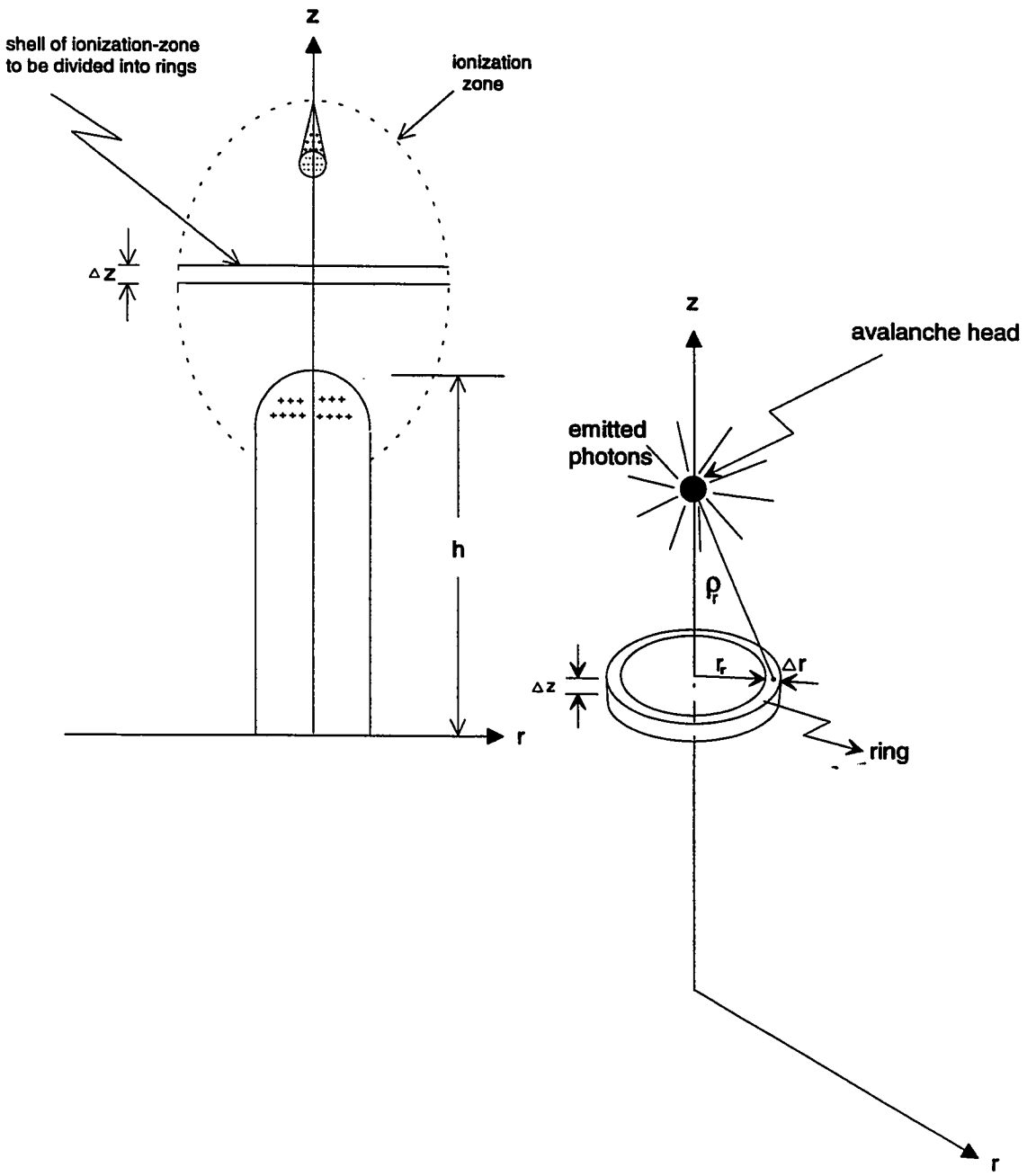

Fig. 4.6 Division of the ionization-zone into small rings if the downward leader extends along the rod axis.

ρ_r is the distance from the head of the primary avalanche to any point on the ring periphery, Fig. 4.6.

r_r is the ring radius, Fig. 4.6.

Δr is the ring thickness, Fig. 4.6.

$$(n_{ph})_{\text{absorbed in ring}} = \frac{2\pi r_r \cdot \Delta r}{4\pi\rho_r^2} \cdot f_2 \cdot N_e(z) \cdot \mu \cdot \exp(-\mu\rho_r) \cdot \Delta z \qquad (4.5a)$$

$$n_{\text{ph.electrons in ring}} = \frac{2\pi r_r \cdot \Delta r}{4\pi\rho_r^2} \cdot f_1 \cdot f_2 \cdot N_e(z) \cdot \mu \cdot \exp(-\mu\rho_r) \cdot \Delta z \qquad (4.6a)$$

$$n_{\text{tot.ph.elect. ring}} = \int_{z_1}^{h} \frac{2\pi r_r \Delta r}{4\pi\rho_r^2} \cdot f_1 \cdot f_2 \cdot N_e(z) \cdot \mu \cdot \exp(-\mu\rho_r) \cdot \Delta z \cdot dz \qquad (4.7a)$$

$$N_{+\text{secondary/photoelecrton}} = \exp\left[\int_{\ell_1'}^{\ell_2'} \left(\alpha(\ell') - \eta(\ell')\right) d\ell'\right] \qquad (4.8a)$$

where:

ℓ_1' is determined by the coordinates of any point of the ring periphery from which the successor avalanche starts its growth.

ℓ_2' is determined by the coordinates of the end point at which the successor avalanche will terminate. The successor avalanche may terminate at the rod surface or at the positive space charge left by the primary avalanche.

ℓ' is the distance measured along the direction of growth of successor avalanche.

$$N_{+2r} = \sum_{i=1}^{K_r} \int_{z_1}^{h} \frac{2\pi r_{r_i} \Delta r_i}{4\pi \rho_{r_i}^2} \cdot f_{1_i} \cdot f_{2_i} \cdot N_e(z) \cdot \mu_i \cdot \exp\left(-\mu_i \rho_{r_i}\right) \cdot \Delta z_i \cdot dz \cdot \left\{ \exp\left[\int_{\ell_1'}^{\ell_2'} \left(\alpha(\ell') - \eta(\ell')\right) d\ell' \right] \right\} \tag{4.12a}$$

where:

K_r is the total number of rings in the ionization-zone.

4.4 Programming the Onset Criteria

In this section an iterative algorithm to fulfill the equality (4.14) will be explained (see Appendix-A).

4.4.1 Ionization Zone Boundary

The ionization-zone is a small volume of space at the tip of the lightning rod where the field strength is high enough such that the coefficient of ionization by electron-collision, α, exceeds the attachment coefficient η. The ionization-zone boundary is defined where $\alpha = \eta$. The flow chart given in Fig. 4.7 and the following steps describe the methodology for determining the ionization-zone boundary and segments.

1- Set the angle $\theta_{zone} = 0$, Fig. 4.8.

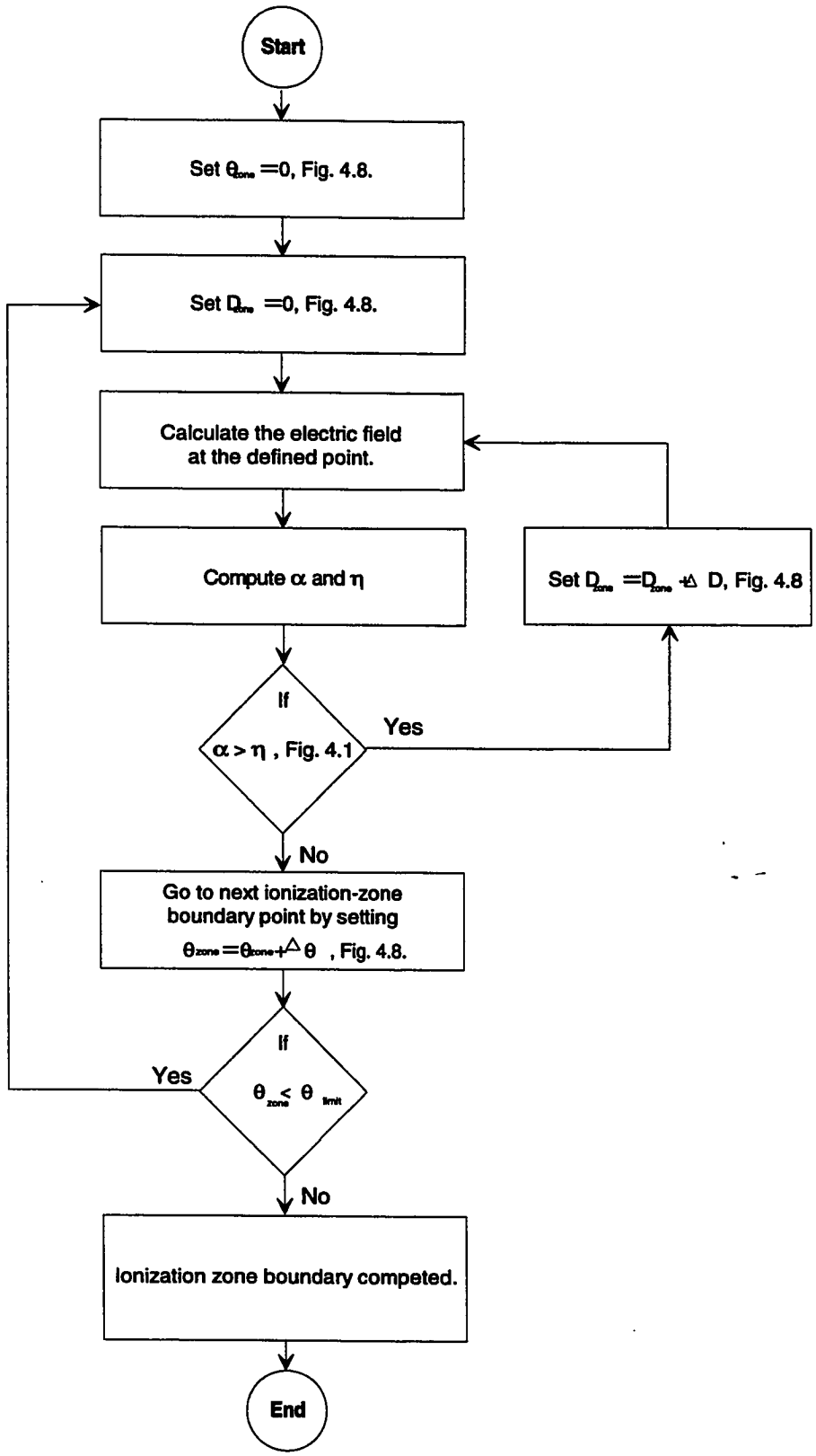

Fig. 4.7 Flow chart for determining the ionization-zone boundary.

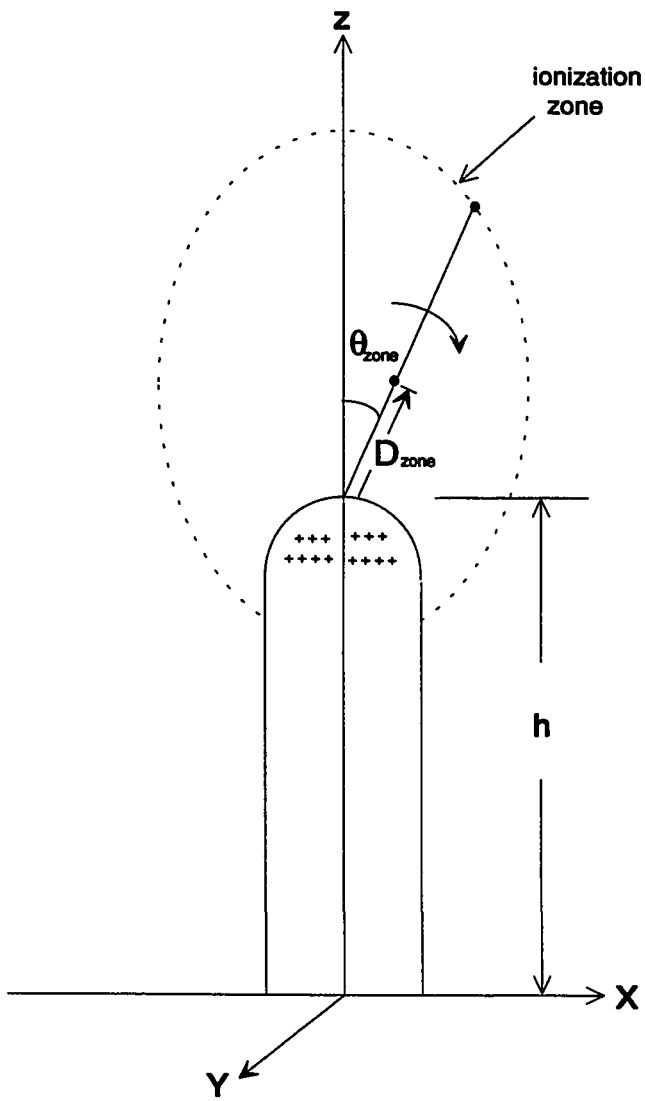

Fig. 4.8 Detemining the ionization-zone boundary.

2- Set the distance D_{zone} along the direction of θ_{zone} equal to zero, Fig. 4.8.

3- Calculate the electric field components as described in section 4.3.

4- Calculate the ionization coefficient α and the attachment coefficient η using the computed field in step 3.

5- If α exceeds η, Fig. 4.1, increase the distance D_{zone} by an increment ΔD_{zone} and proceed to step 3. Otherwise, go to the next ionization boundary point by increasing θ_{zone} with an increment $\Delta\theta_{zone}$ and proceed to step 2.

6- This completes the ionization-zone boundary.

4.4.2 Primary Avalanche and the Generated Photoelectrons

After determining the ionization-zone boundary, this zone is divided into small segments as described in section 4.3 and Fig. 4.5. The growth of the primary avalanche and the evaluation of the emitted photons from it which create photoelectrons in these segments are described in the following steps in conformity with the flow chart of Fig. 4.9.

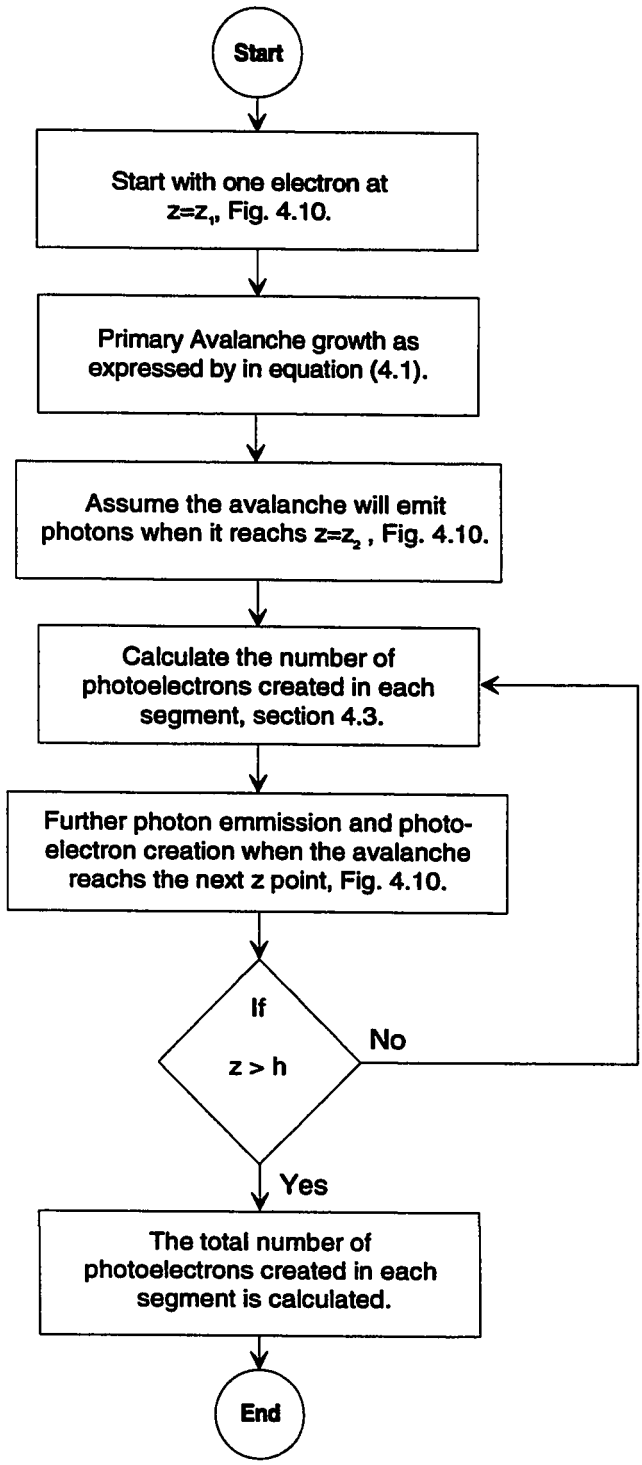

Fig. 4.9 Flow chart for calculating the number of photoelectrons created in each segment.

1- Start with an initiatory electron at $z = z_1$ to trigger a primary avalanche, Fig. 4.10.

2- The primary avalanche will grow according to equation (4.1).

3- When the avalanche travels an incremental distance and reaches $z = z_2$ it will emit photons, Fig. 4.10. The segments of the ionization-zone will receive some of these photons, with a subsequent generation of photoelectrons in each segment.

4- The number of photoelectrons created in each segments is calculated as explained in section 4.3.

5- The primary avalanche will continue growing to the next point, Fig. 4.10, with more photoelectron generation in each segment. This procedure will continue until the primary avalanche reach the rod tip at z=h, Fig. 4.10.

4.4.3 Positive Ions Produced by the Secondary Avalanches

In section 4.4.2, the number of the photoelectrons created in each segment is calculated. The secondary avalanches result of the growing of these photoelectrons in the actuating field. The number

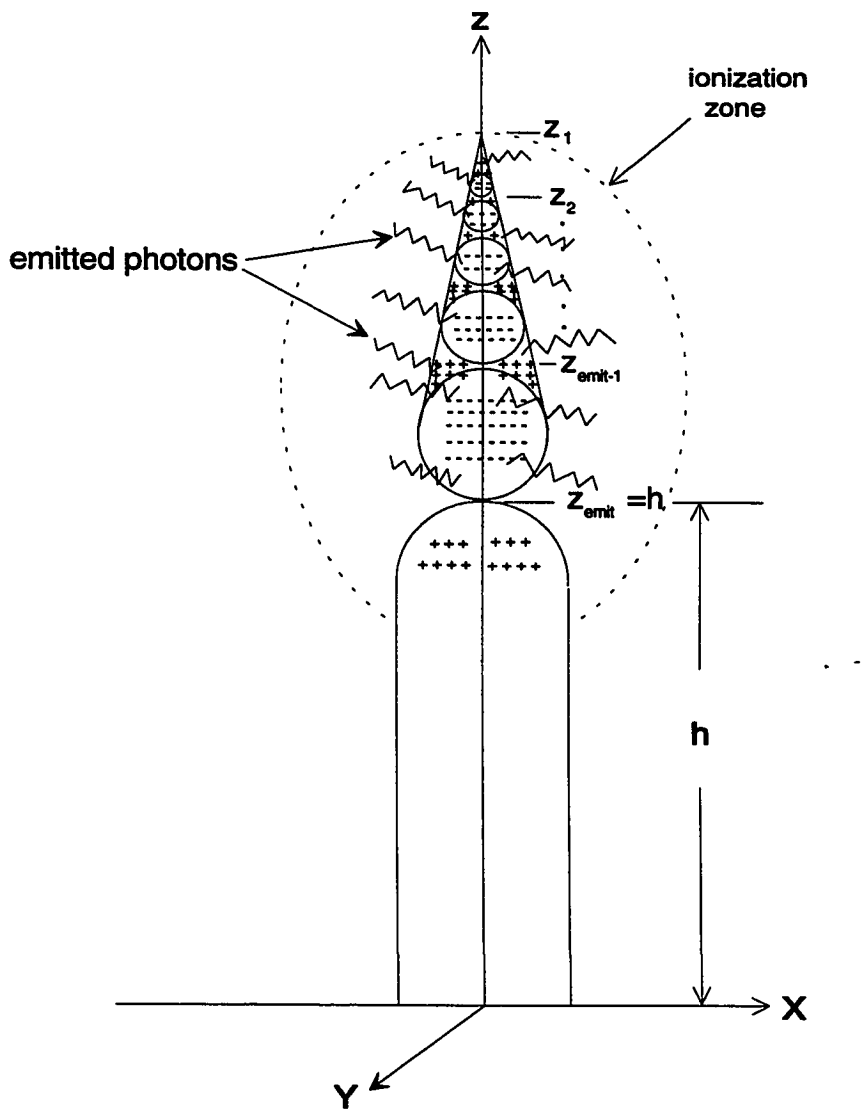

Fig. 4.10 Growth of the primary avalanche and the associated photon emission.

of the positive ions produced by the growth of the secondary avalanches is explained in the following steps in conformity with the flow chart of Fig. 4.11.

1- Set the segment number i=1.

2- Calculate the electric field due to the four field components, equation (4.10), along the route of the secondary avalanche starting from the ith segment.

3- Use equation (4.8) to calculate the number of the positive ions create by each photoelectron using the computed field in step 2.

4- Multiply the number of positive ions calculated in step 3 by the number of the photoelectrons created in each segment to get the number of positive ions produced by each segment.

5- Set the segment number i=i+1 and proceed to step 2.

6- After completing the K segments, then the total number of positive ions will be the summation of the positive ions produced by each segment obtained in step 4, equation (4.12).

7- Compare the number of positive ions produced by the secondary avalanches, step 6, with the number of positive ions produced by

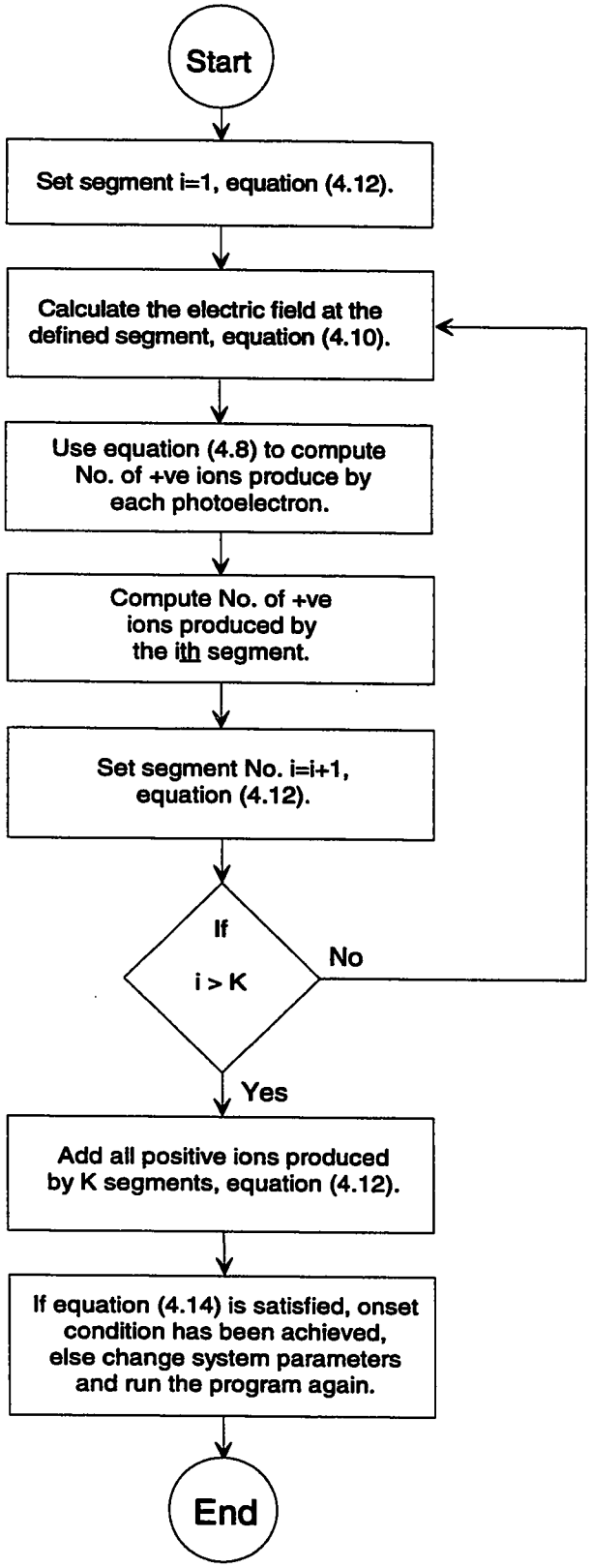

Fig. 4.11 Flow chart for computing the number of positive ions produced by the secondary avalanches.

the primary avalanche obtained in section 4.4.2. If the equality (4.14) is satisfied within a predefined mismatch, onset streamers will develop. Otherwise, the system parameters (leader height, leader current, rod height, rod radius, lateral distance or the applied pulse voltage) should be changed for a new run of the program.

4.5 Numerical Data

The physical parameters used in formulating the streamer onset condition, equation (4.14), are quantified in the following sections.

4.5.1 Coefficient of Ionization by Electron Collision α

In the absence of electric field, the rate of electron and positive ions generation form a state of equilibrium. This equilibrium state will be upset in a case of applying sufficient high field where each electron accelerates in the field and collides with the gas molecules. The ionization coefficient α is defined as the number of ionizing collisions per unit length of the electron path in the direction of the field.

Different empirical formulas have been reported in [33] to correlate α to the actuating electric field as shown in Fig. 4.12 and 4.13 [33,34]. As shown from these figures, the best equation that fits the experimental data is the one proposed by Sarma and Janischewskyj [33]. Accordingly, the following empirical formulas have been used in the present analysis.

$$\frac{\alpha}{p} = 4.7786e^{-221p/E} \quad 25 \leq E/p \leq 60 \ \text{V/cm.torr} \tag{4.15}$$

$$\frac{\alpha}{p} = 9.682e^{-264.2p/E} \quad 60 \leq E/p \leq 240 \ \text{V/cm.torr} \tag{4.16}$$

where:

p is the atmospheric pressure in torr (= 760 torr).

E is the electric field in V/cm.

4.5.2 Coefficient of Electron Attachment η

When an electron gets attached to neutral molecule or atom, it produces a negative ion. Negative ions play an important role in the corona and full breakdown. The suppression of electrons from an ionized gas by attachment is expressed by the attachment coefficient η. This coefficient is defined by analogy with the ionization coefficient α as the number of the attachments produced in the path

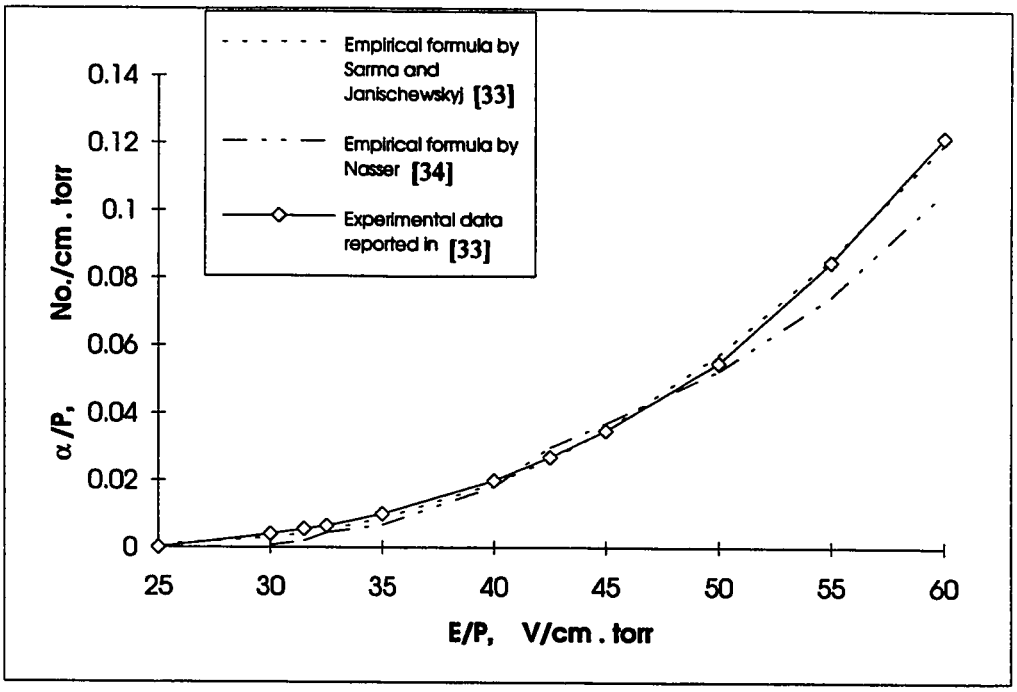

Fig. 4.12 Comparison between experimental data and different empirical equations reported for the ionization coefficient in the range 25≤E/p≤60

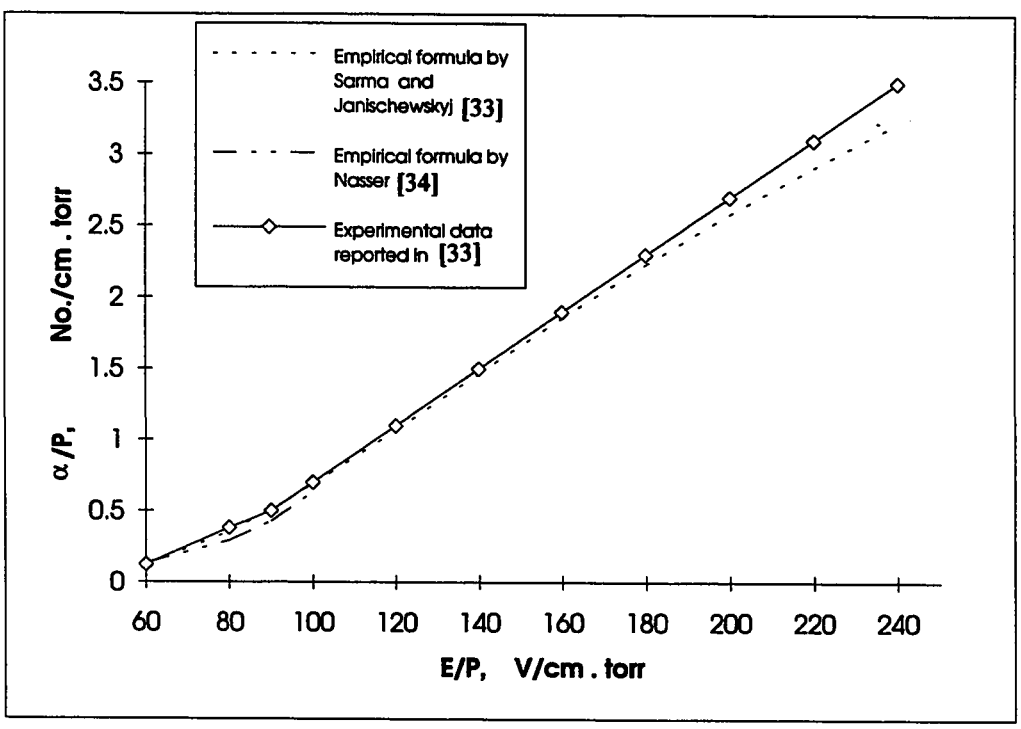

Fig. 4.13 Comparison between experimental data and different empirical equations reported for the ionization coefficient in the range 60≤E/p≤24

of a single electron traveling a unit distance in the direction of the field.

An empirical equation proposed by Sarma and Janischewskyj that fits the experimental data of Harrison and Geballe is shown in Fig. 4.14 [33]. Accordingly, the following empirical equation has been used in the present analysis.

$$\frac{\eta}{p} = 0.01298 - 0.541\times10^{-3}(E/p) + 0.87\times10^{-5}(E/p)^2 \qquad (4.17)$$

4.5.3 Electron mobility k_e

The mobility of a particle is defined as the ratio of its velocity in field direction to the magnitude of field intensity, or the drift velocity per unit applied field. Thus, the electron mobility is:

$$k_e = \frac{v_e}{E} \quad \left(\frac{m^2}{V\cdot sec}\right) \qquad (4.18)$$

The electron velocity v_e (m/sec) was expressed as [8,35]:

$$v_e = 1.217\times10^4 E^{0.715} \qquad \text{for } E \le 76 \text{ kV/cm} \qquad (4.19)$$

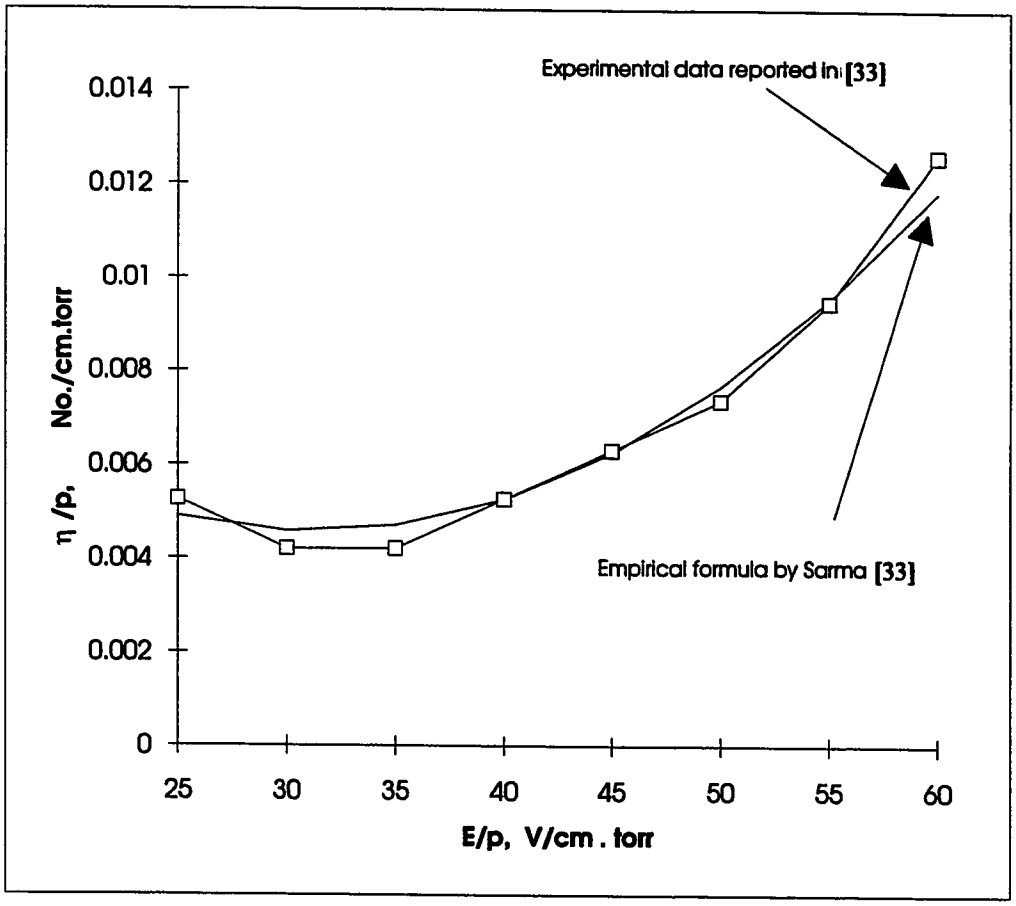

Fig. 4.14 Comparison between experimental data and empirical equation reported for attachment coefficient.

$$v_e = 1.837 \times 10^4 E^{0.62} \qquad \text{for } E > 76 \text{ kV/cm} \qquad (4.20)$$

4.5.4 Diffusion coefficient D_e

The diffusion can be simply defined as the constant of proportionality between the rate of flow and the concentration gradient.

$$J = -D_e \cdot \nabla n \qquad (4.21)$$

where:

J is the rate of flow of charges from the high density to the low density.

∇n is the concentration gradient in three dimensional space.

A fundamental relation was developed by Loeb in 1965 correlating the mobility k_e to the diffusion coefficient D_e:

$$\frac{k_e}{D_e} = \frac{e}{K_{bol} \cdot T_e} \qquad (4.22)$$

where:

K_{bol} is the Boltzmann's constant (1.37×10^{-23} W·sec/K).

T_e is the electron temperature in K.

Then,

$$D_e = k_e \frac{K_{bol} \cdot T_e}{e} = k_e \frac{K_{bol}}{e} \left(\frac{T_e}{T_g} \right) \cdot T_g \tag{4.23}$$

where:

T_g is the gas temperature (= 298 K at N.T.P.).

The temperature ratio $\frac{T_e}{T_g}$ was measured and expressed as [8,35]:

$$\frac{T_e}{T_g} = 12.267 + 3.16 \cdot \ln E \qquad \text{for } E < 0.532 \ \text{kV/cm} \tag{4.24}$$

$$\frac{T_e}{T_g} = 20.632 + 14.29 \cdot \ln E \qquad \text{for } E \geq 0.532 \ \text{kV/cm} \tag{4.25}$$

4.5.5 Avalanche radius R_{av}

The radius of the avalanche head R_{av} can be obtained from the diffusion equation and is expressed as [8,34]:

$$R_{av} = \sqrt{6 \cdot D_e \cdot \tau} \tag{4.26}$$

where:

τ is the avalanche transit time and can be evaluated from equation (4.27) and the limits of integration are the starting and end points of the avalanche growth.

$$\tau = \int \frac{dl}{v_e} \qquad (4.27)$$

4.5.6 Absorption coefficient μ

The absorption coefficient μ is a proportionately factor that relates the reduction in the photons intensity dI from the initial intensity I as they travel a distance dx at x from their origin. This relation can be written as:

$$-dI = \mu I \, dx \qquad (4.29)$$

The absorption coefficient was measured in [36] and expressed as:

$$\mu = 100 \cdot e^{-31.568+6.785 \cdot \ln E} \quad \text{for } 26.6 \le E \le 190 \text{ kV/cm} \qquad (4.30)$$

$$\mu = 100 \cdot e^{-11.743+2.78 \cdot \ln E} \quad \text{for } E > 190 \text{ kV/cm} \qquad (4.31)$$

4.5.7 Photoionization product $f_1.f_2$

The factor f_1 is the factor that relates the number of the excited states created by the electron collisions to the number of ionizing events.

The factor f_2 is the probability of the small fraction of the absorbed photons that will produce photoelectrons.

The product of the two factors has been measured and an equation that fits the data has been set by Uber and Penny [37,38] as follows:

$$f_1 \cdot f_2 = 2.46e^{-696.92\rho_s} + 28.3e^{-3002\rho_s} + 528e^{-30590\rho_s} \qquad (4.32)$$

where:

ρ_s is the radial distance shown in Fig. 4.5.

4.5.8 Photons Emitted from Primary Avalanche

The primary avalanche is continuously emitting photons during its travel from the ionization-zone boundary to the Franklin rod. Since, the primary avalanche will have a life time in the range

of 0.5×10^{-7} second. One of the assumptions made in the present analysis is that the avalanche emits photons every $0.5\times10^{-7}/50$ seconds i.e. the avalanche emits photons 50 times during its growth.

4.5.9 Avalanche Integration Steps

The avalanche size highly depends on the electric field. Therefore, the integration step has been selected to be a function of the electric field as follows:

$$\text{step} = \frac{1}{9\cdot\alpha} \tag{4.33}$$

The ionization coefficient α increases dramatically with the electric field, Fig. 4.1. The factor 9 was selected based on a compromise between the accuracy of the results and the program execution time.

4.6 Results

The positive onset criterion proposed in this study was checked against the widely used empirical formula for the DC

positive corona inception field in rod-plane gap [39]. The expression of this formula is given as:

$$E_o = 22.8\left[1+\frac{1}{\sqrt[3]{R}}\right] \qquad kV/cm \qquad (4.34)$$

Table 4.1 shows calculated onset field values using the proposed onset criterion and the empirical formula (4.34) for different values of rod radius R. To exclude the effect of the cloud and the downward leader on the calculated field values, the current was set to zero. In this case, the field established in the ionization zone is due to the voltage applied to the rod.

The deviation of the calculated onset field values from those obtained by the formula is simply attributed to the presence of the ground plane at the base of the Franklin rod, Fig. 4.15. The image charges considered to account for the ground plane will reduce the field within the ionization zone with a subsequent increase of the corona onset value and the corresponding onset field value. This is why the present calculated onset field values exceed those obtained by the formula, even the difference is around 10%. However, it is worthy to mention that any empirical formula is tailored to fit some experimental values. The latter may change from laboratory to laboratory depending on the weather conditions and the near-by objects to the experimental set-up.

Rod radius (R) (cm)	0.5	1	2	3	4
Onset field values (formula (4.34)) (kV/cm)	51.5	45.6	40.9	38.6	37.2
Present onset field values (kV/cm)	56.9	51.3	45.2	42.5	40.8

Table 4.1 Present corona onset field values against those obtained by formula.

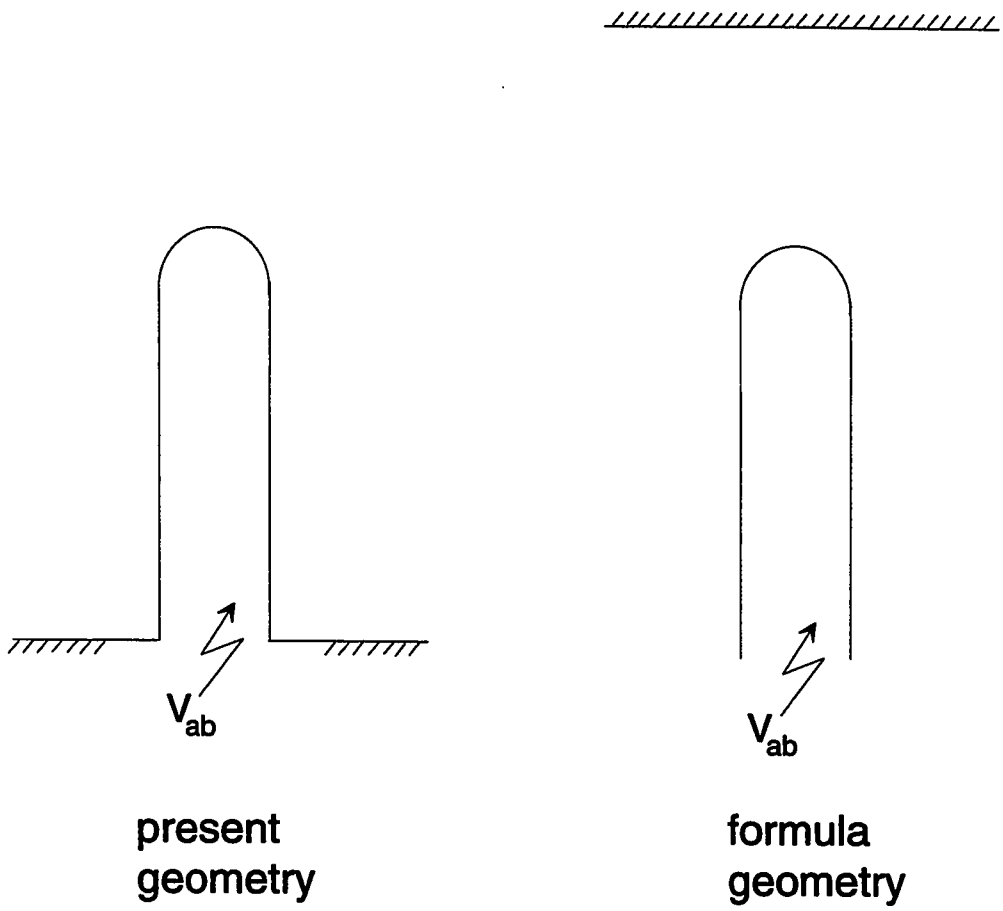

Fig. 4.15 Present geometry against the one used for the formula.

CHAPTER 5

RESULTS AND DISCUSSION

The onset criteria discussed in chapter 4 was applied to evaluate onset condition of upward streamer at the tip of the Franklin rod. Among the objectives of this chapter is to investigate the effect of different system parameters including those of the downward leader and those of the Franklin rod on the onset condition of upward streamer. The downward leader parameters are the leader current and height above the ground plane. The Franklin rod parameters are the radius and height of the rod, the lateral distance between the rod and the leader and the amplitude of the applied pulse voltage. In this analysis, a step-pulse voltage applied to the rod was assumed for simplicity.

Also, the virtual increase in the rod height due to the applied pulse voltage was calculated. This virtual increase in the rod height is a measure of the increase of the protection radius as discussed in this chapter. The computed values of the radius of protection are compared with the available published data.

5.1 Parameter Study of the Streamer Onset Condition

In Fig. 5.1, the rod height, the amplitude of the pulse voltage applied to the rod and the lateral distance between the Franklin rod and the downward leader are kept constants at 0.5 m, 10 kV and 150 m, respectively. For the same value of the leader current, Fig. 5.1, the electric field at the tip of the rod is higher for lower radii of the rod. This can be explained in the light of the fact that the electric field (due to the leader and applied pulse voltage) tends to concentrate at the sharp points. Subsequently, the larger the electric field concentration at the tip point of the rod, the faster the launching of the upward streamers at a higher leader height which will result in an increase in the radius of protection. This is why most of the lightning rods are shaped sharpy at their tip, Fig. 2.4. The manufacturers of lightning rods tends to reduce the tip radius of the rod with the limitation that it should carry safely the current of the downward leader. Of course, the larger the leader current the higher is the height of the downward leader at the onset condition of the upward streamer at the rod. An important observation drawn from Fig. 5.1 is that with rod radius of 2 cm and above, the lightning rod may not be able to attract lightning strokes with current less than 50 kA. Thus, the rod loses its function in providing protection against lightning strokes with currents less than 50 kA. For rod radius of 1 cm, the lightning rod may not be able to provide protection against lightning strokes with currents less than 20 kA.

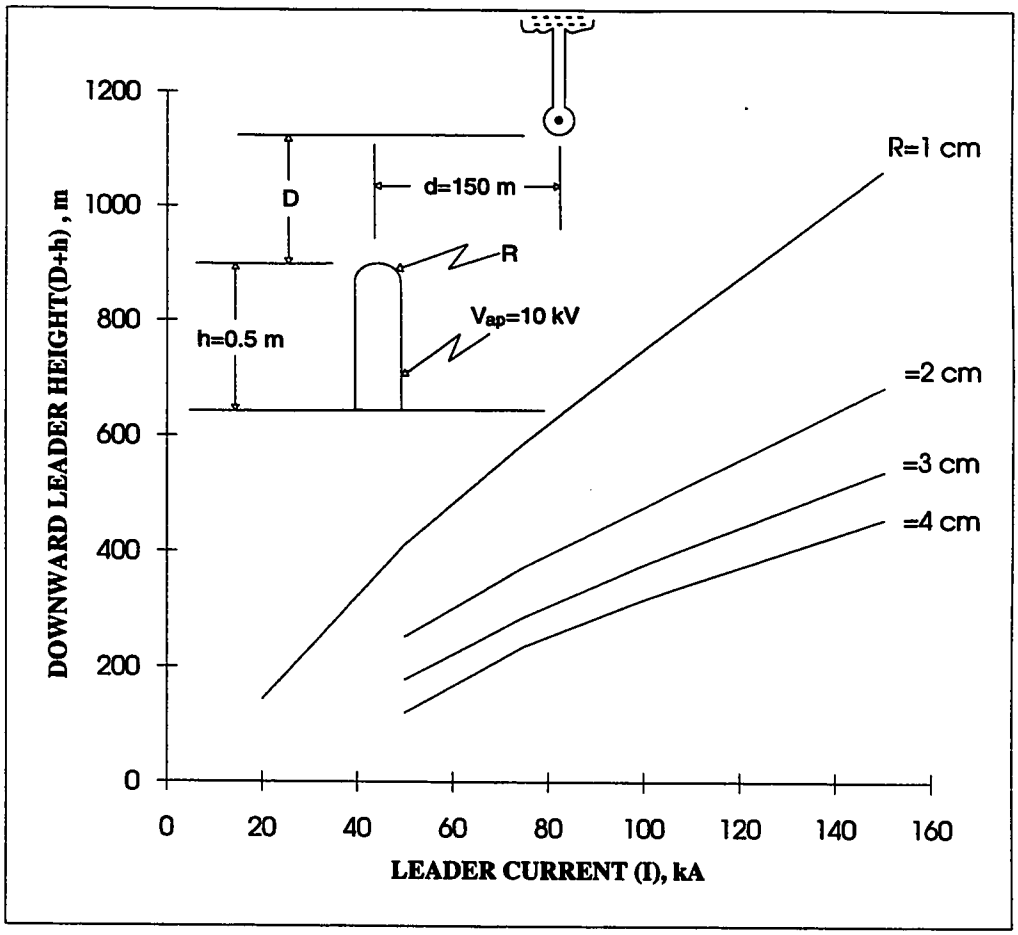

Fig. 5.1 Downward leader height versus leader current for different tip radii of the lightning rod.

In Fig. 5.2 the rod radius , the amplitude of the pulse voltage applied to the rod and the lateral distance between the Franklin rod and the downward leader are kept constants at 2 cm, 10 kV and 150 m, respectively. For the same value of the leader current, Fig. 5.2, the height of the leader increases with the increase of the rod height in order to satisfy the onset condition of the upward streamers. The electric field due to the leader and the applied pulse voltage tends to concentrate more at the longer rod. Doubling the height of the lightning rod at 75 kA leader-current results in an increase by about 60% of the leader height, at which the onset condition for the upward streamer is met. However, the height of the lightning rod should not be too long to prevent side and ascending strokes and to withstand mechanical stresses due to winds. Fig. 5.2 dictates that for rod heights of 0.75 m and below, the lightning rod may not be able to attract lightning strokes with currents less than 50 kA and loses its function in providing protection against lightning strokes with these currents. For rod height of 1 m, the lightning rod may not be able to provide protection against lightning strokes with currents less than 20 kA.

In Fig. 5.3, the rod height and radius and the amplitude of the pulse voltage applied to the rod are kept constants at 0.5 m, 2 cm and 10 kV, respectively. For the same value of the leader current, Fig. 5.3, the height of the leader decreases with the increase of the lateral distance between the Franklin rod and the leader in order to satisfy the onset condition of the upward streamers. This is attributed to the decrease of the electric field

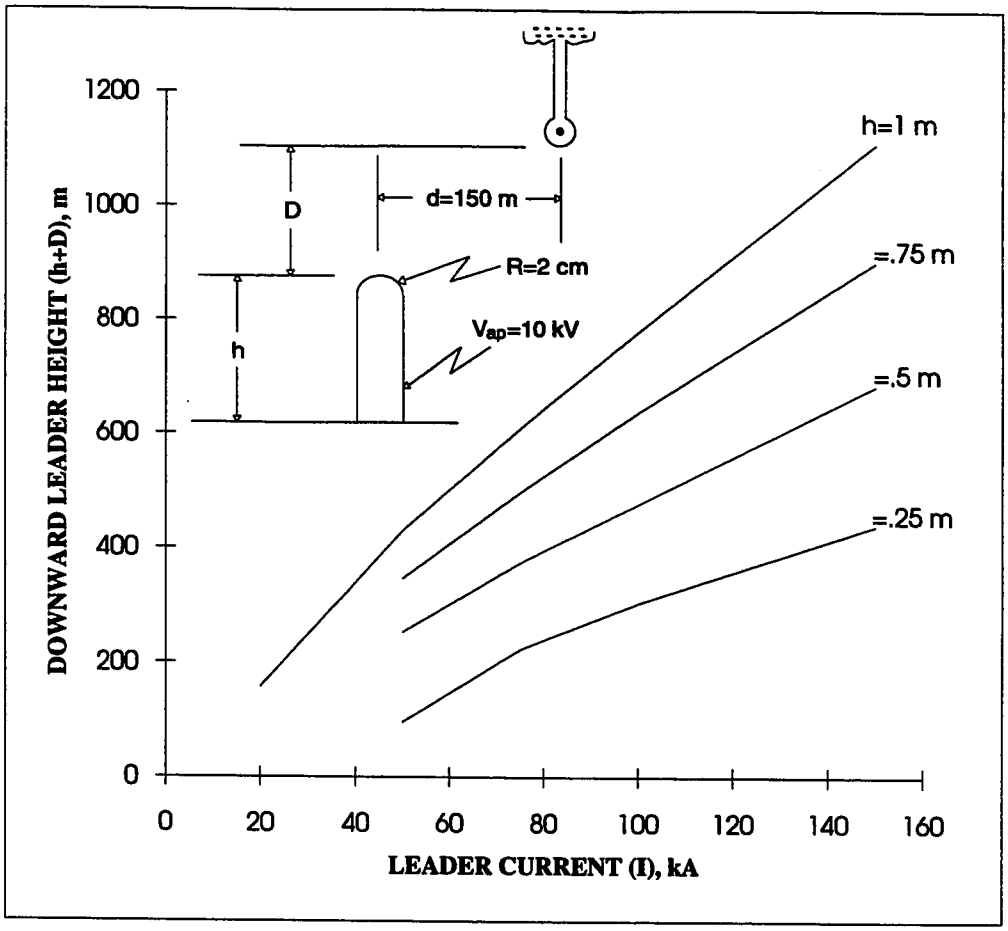

Fig. 5.2 Downward leader height versus leader current for different heights of the lightning rod.

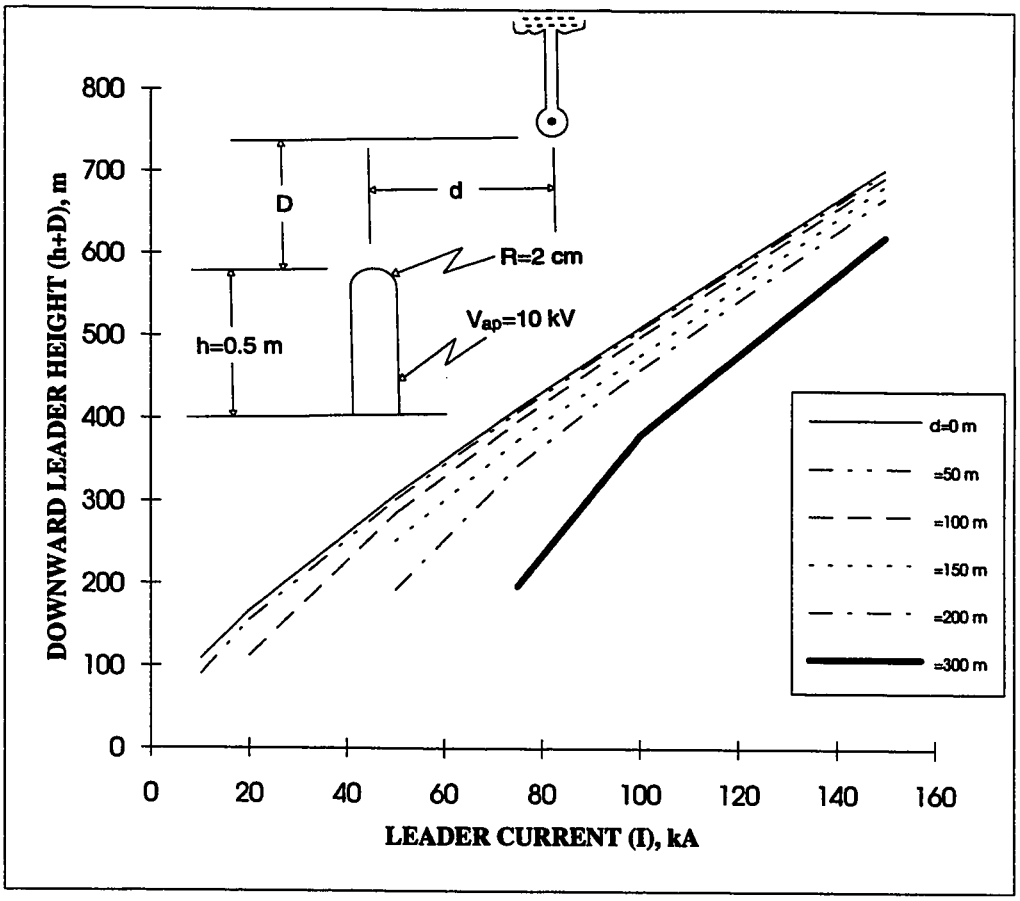

Fig. 5.3 Downward leader height versus leader current for different lateral distances measured from the rod.

due to the downward leader at the tip of the lightning rod. Figure 5.3 indicates that for lateral distances greater than 50 m the lightning rod may not be able to attract lightning strokes of low lightning currents. Thus, for low lightning currents the rod may lose its function in providing protection against lightning strokes with lateral distances gteater than 50 m.

In Fig. 5.4-5.9, the rod radius is kept constant at 0.02 m. For rod height (h=0.5 m) and lateral distance (d=50 m), Fig. 5.4 shows the leader current versus the leader height at the onset of upward streamer. In Fig. 5.4, the effect of the pulse voltage applied is very small at low leader currents and increases gradually with the increase of the leader current. This observation can be explained in the light of the fact that the onset of streamers takes place at low leader heights for low leader current values. In this case, the electric field due to the leader depends highly on the relative spacing between the leader and the rod and it is the dominant factor among the others. In the other case, the onset codition for the upward streamer occured at higher downward leader for the high leader current and it will change gradually with downward leader height. In this case, other factors such as the applied voltage will cause a significant increase in the height of the downward leader. Figure 5.5 and 5.6 are plotted for different values (150 m and 250 m) of the lateral distance between the leader and the rod axis. It is clear that the larger the lateral distance the higher is the effect of the pulse voltage applied to the rod, Fig. 5.4-5.6. For the case of rod height h=1m, Fig. 5.7-5.9 show the leader height at the onset of the upward streamer versus the leader current for different values of the lateral

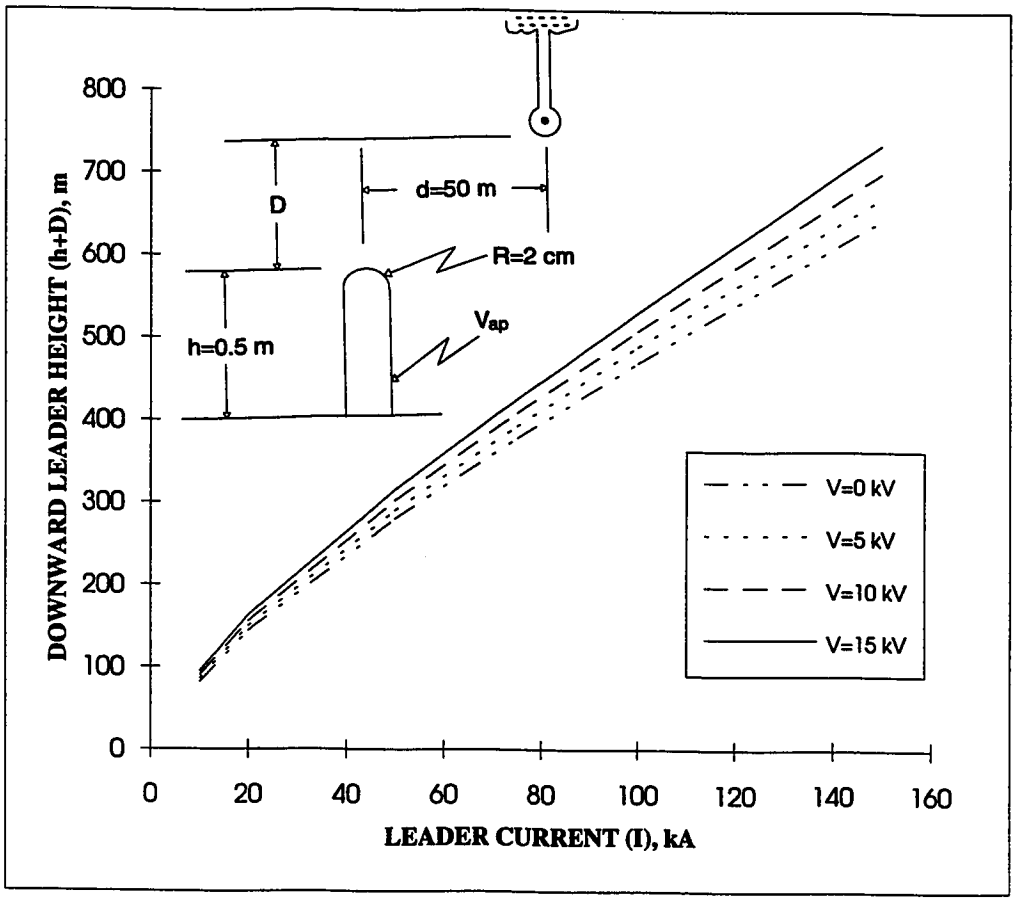

Fig. 5.4 Downward leader height versus leader current for different values of the applied pulse voltage (d=50 m rod h= 0.5 m).

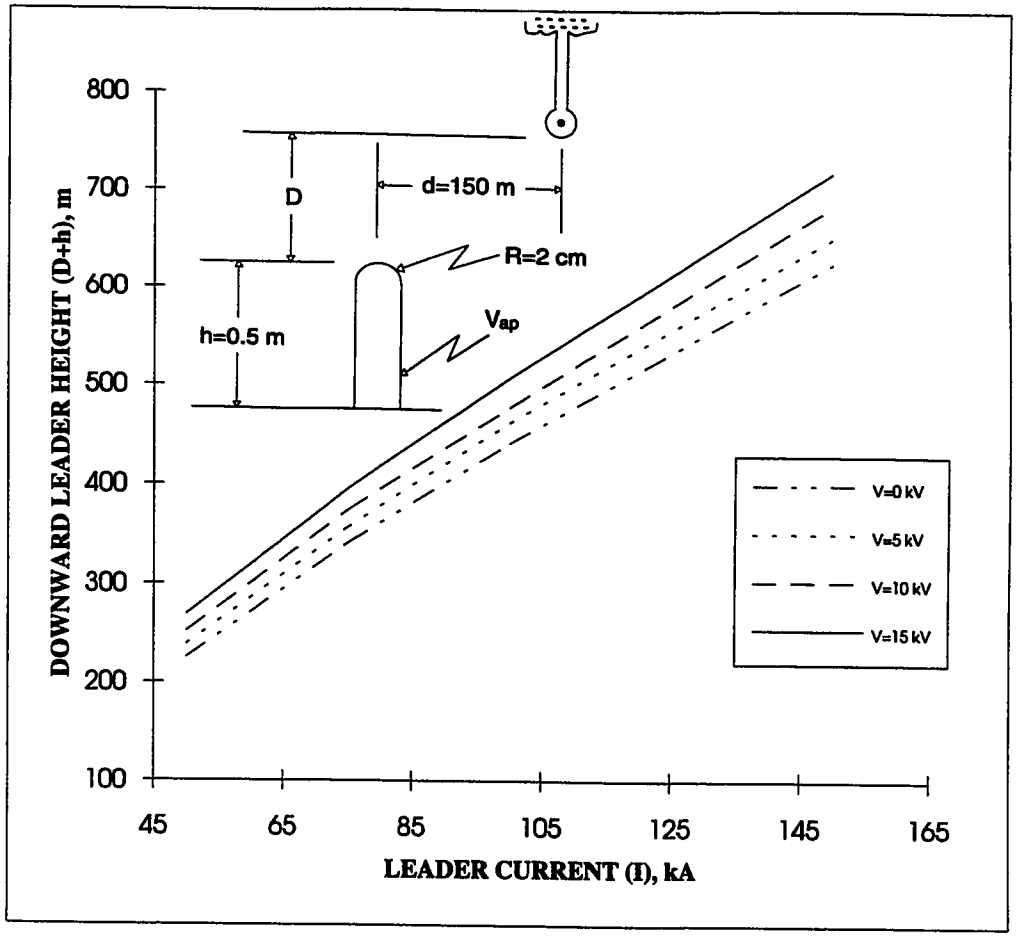

Fig. 5.5 Downward leader height versus leader current for different values of the applied pulse voltage (d=150 m rod h= 0.5 m).

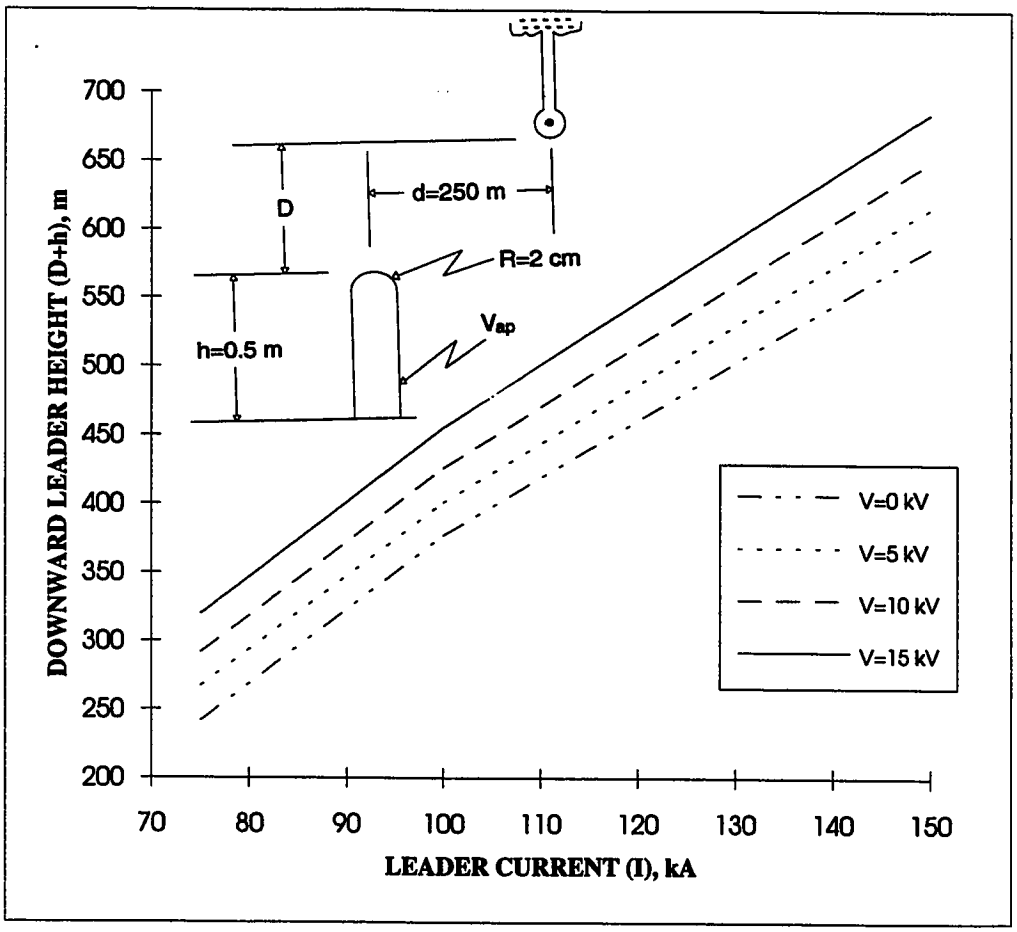

Fig. 5.6 Downward leader height versus leader current for different values of the applied pulse voltage (d=250 m and h=0.5 m).

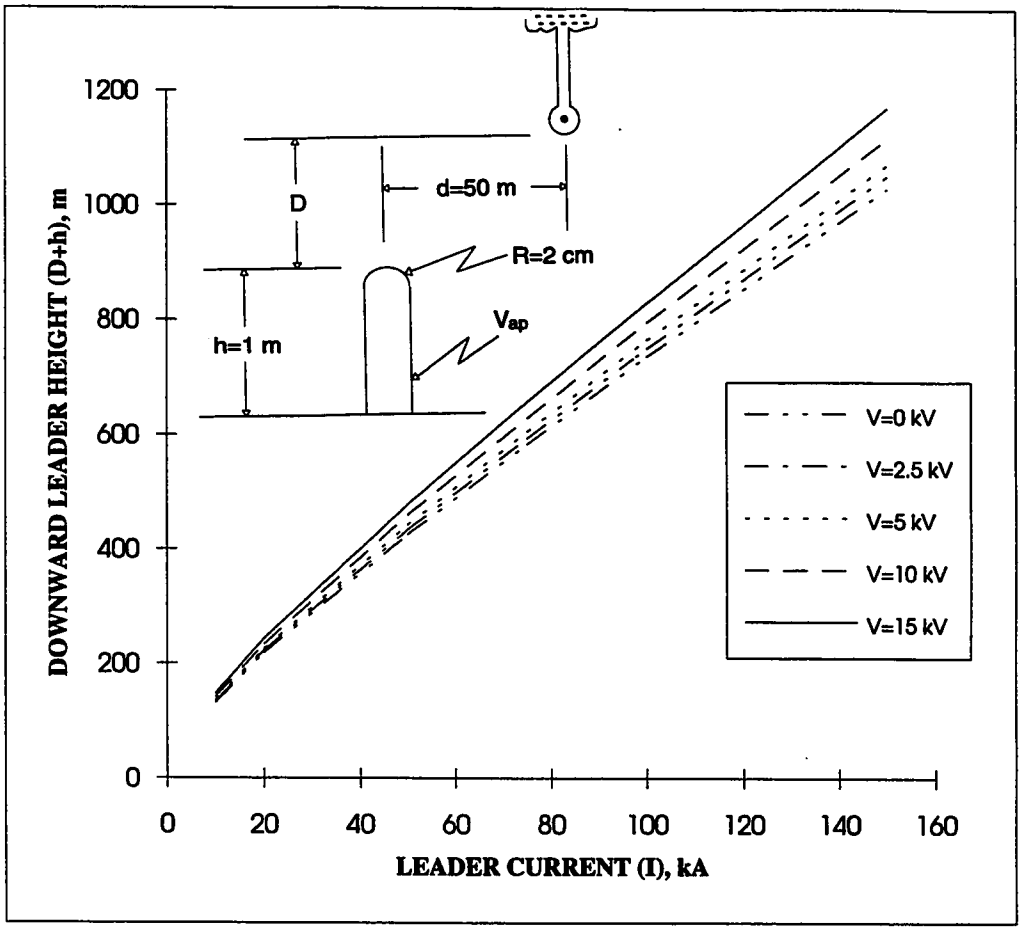

Fig. 5.7 Downward leader height versus leader current for different values of the applied pulse voltage (d=50 m and h=1 m).

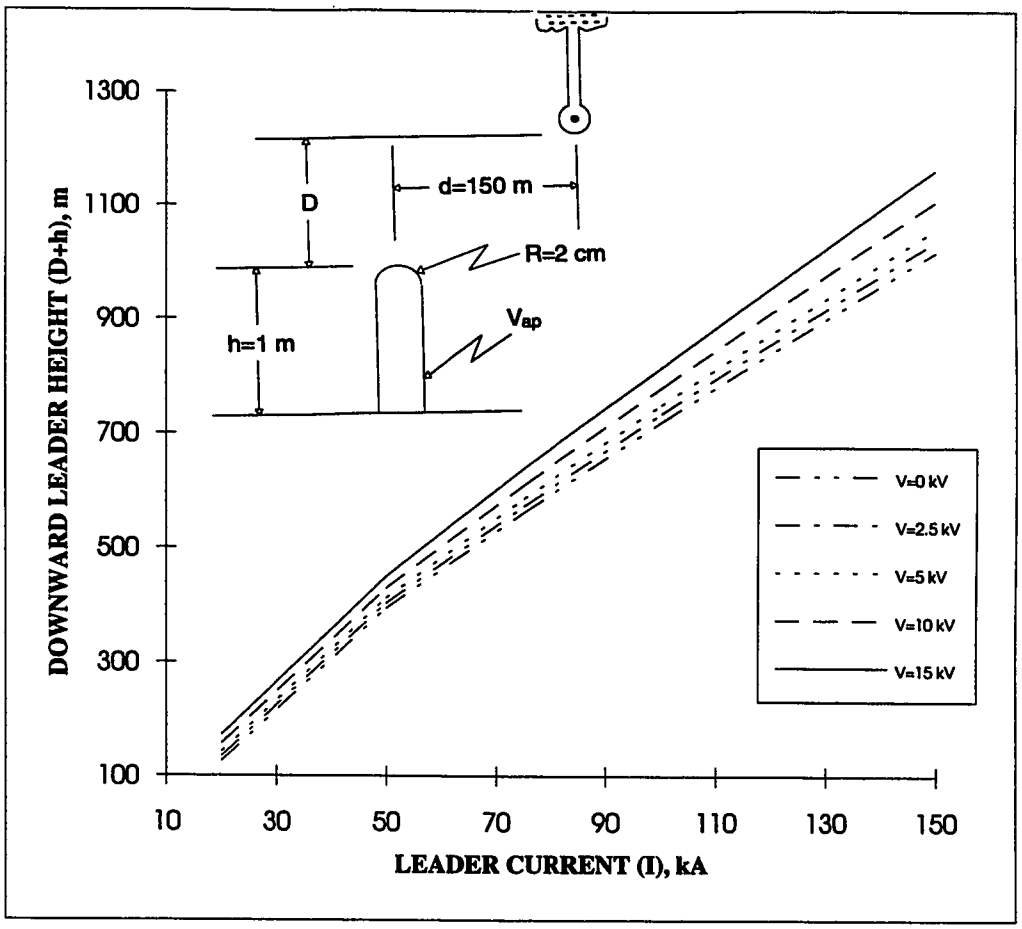

Fig. 5.8 Downward leader height versus leader current for different values of the applied pulse voltage (d=150 m and h=1 m).

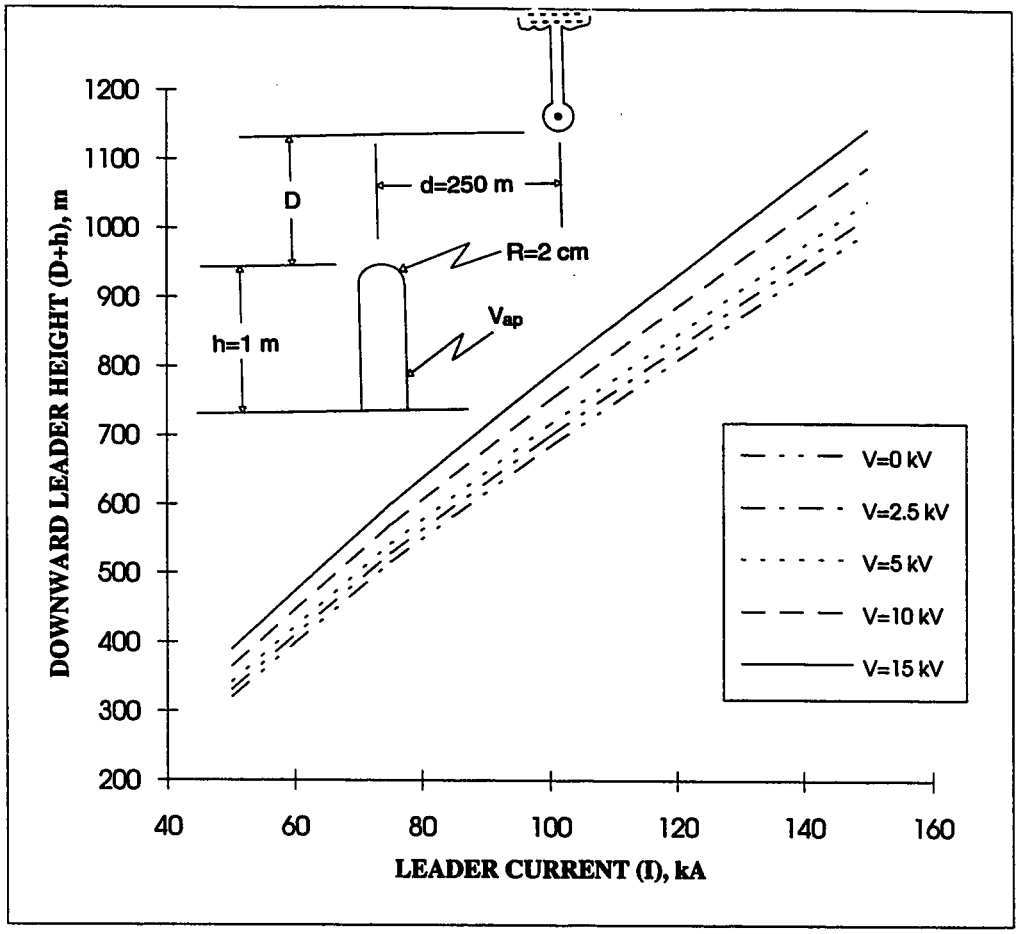

Fig. 5.9 Downward leader height versus leader current for different values of the applied pulse voltage (d=250 m and h=1 m).

distance and the applied voltage. The behavior discussed for h=0.5 m is applicable for rod height of h=1 m, the only difference is the higher the rod height the more effective is the applied voltage on triggering the onset steamer at the rod tip.

Figure 5.10 shows a trace for the point of maximum lateral distance at the lowest leader current value (I=10 kA) where the rod height, rod radius and the applied voltage are kept constants at 1 m, 2 cm and 10 kV, respectively. It can be seen from this figure that the downward leader height at the onset of the upward streamer decreases with the increase of the lateral distance, initially at a slow rate and later at a faster rate. The zone under the curve will be the zone of the onset of upward streamer. The maximum lateral distance that the rod con attract the downward leader is 104 m at a leader height of 64.5 m. If the lateral distance exceeds this value the electric field at the tip of the rod will not be high enough to cause an onset streamer.

At the onset condition of upward streamer Fig. 5.11 shows the increase in the maximum lateral distance due to the applied pulse voltage at the lowest leader current (I=10 kA) where the rod height and rod radius are kept constants at 1 m and 2 cm, respectively. At first, the maximum lateral distance when there is no applied pulse voltage is defined and found 92 m at leader height of 84.5 m. Then, on applying 5 kV to the rod the maximum lateral distance increases by 3.5 m for the same leader height (84.5 m). For 10 kV applied pulse voltage, the increase in the maximum

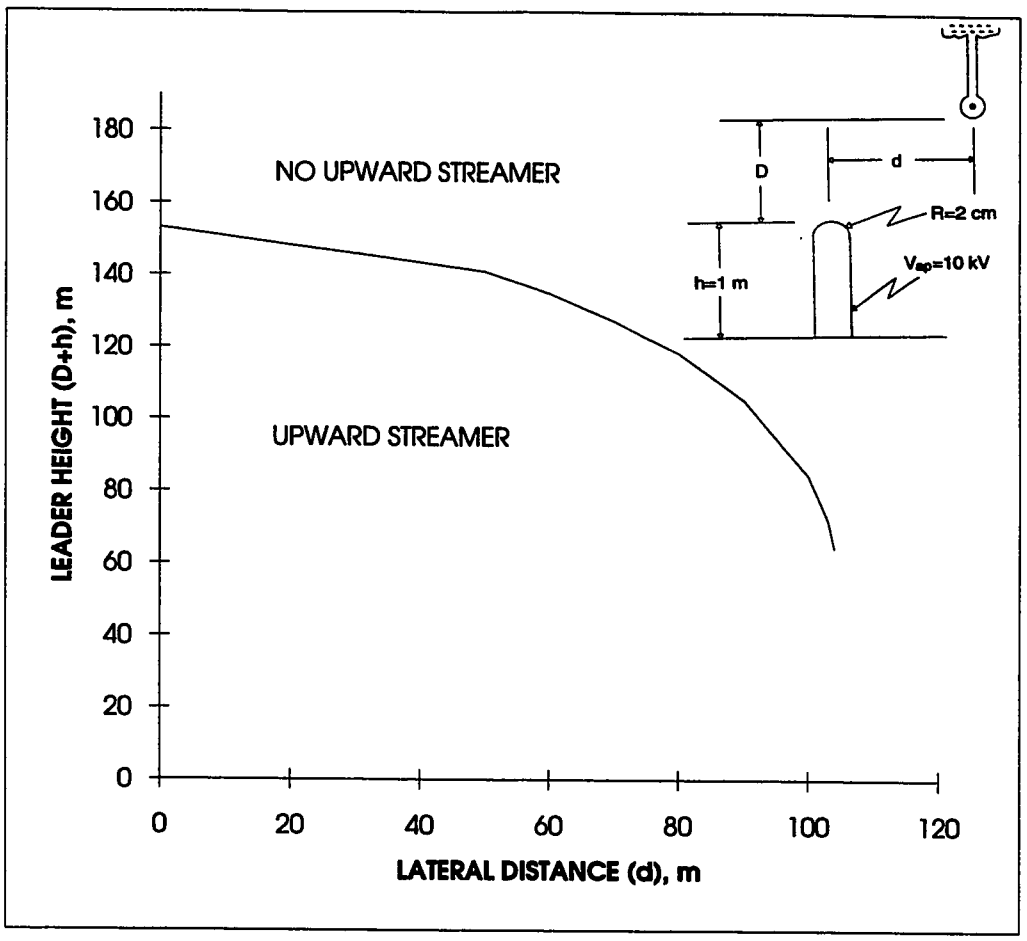

Fig. 5.10 Leader height versus lateral distance at the lowest value of the leader current (I=10 kA).

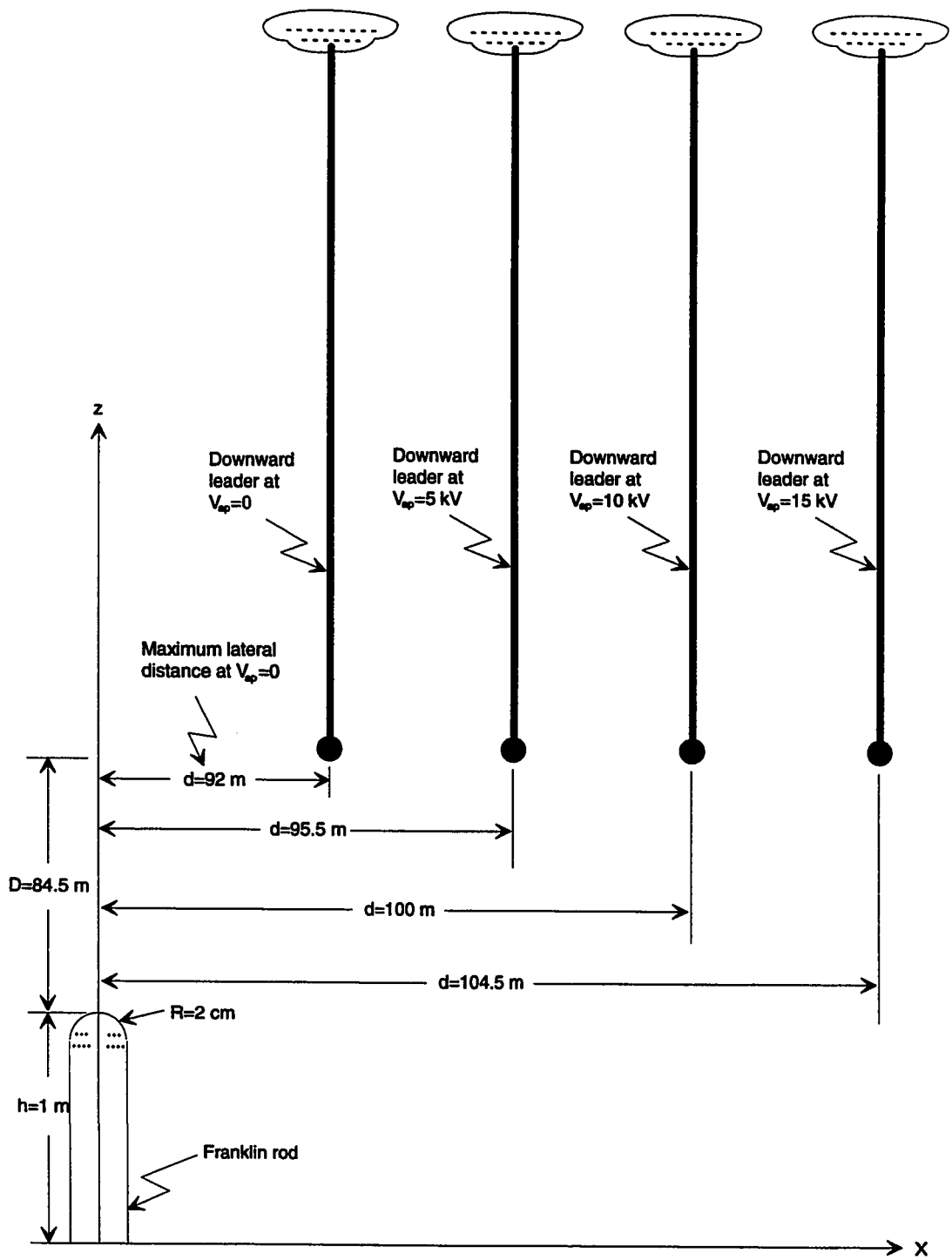

Fig. 5.11 Increase of the downward lateral-distance due to the pulse voltage applied to the rod.

lateral distance becmes 8 m. Further increase in the applied pulse voltage to 15 kV results in a maximum lateral distance increase of 12.5 m. This increase in the lateral distance will reflect itself on the increase of the protection radius of the lightning rod. The output results of these cases are shown in Appendix-B.

5.2 Virtual Increase in Rod Height Due to Pulse Voltage Applied

As discussed in section 5.1 at constant leader current, satisfaction of streamer onset condition at larger leader heights calls for either an increase of the pulse voltage applied of the rod or an increase of the rod height at constant rod radius and leader current. This means that energizing the rod by a pulse voltage is as if the rod is elongated in length. Such elongation is denoted as a virtual (or fictitious) increase h' in rod height due to the applied pulse voltage, Fig. 5.12. This virtual increase h' is simply the increase in height of the downward leader for energized rod above that for non-energized (classical) rod:

$$h' = D_{\text{energized rod}} - D_{\text{classical rod}} \qquad (5.1)$$

where D is the height of the downward above the lightning rod .

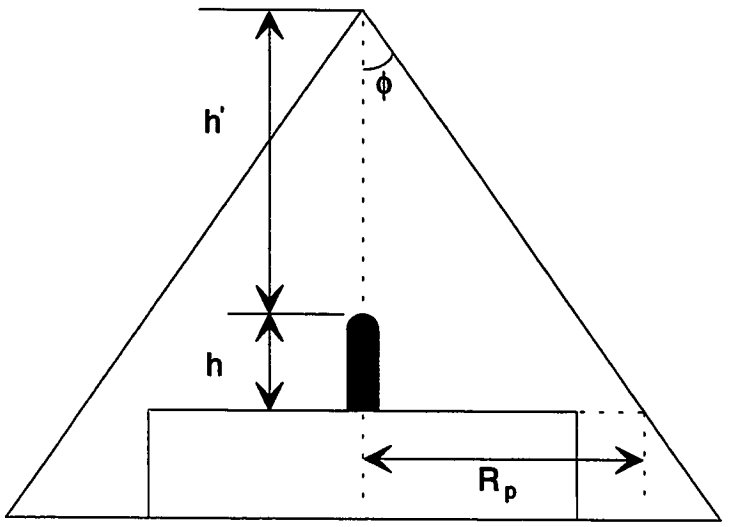

Fig. 5.12 Electrogeometrical model of energized Franklin rod.

Then, the virtual rod height due to the applied pulse voltage is expressed as:

$$h_v = h + h' \tag{5.2}$$

In Figs. 5.13-5.15, the virtual increase in rod height due to the applied voltage has been calculated from Figs. 5.7-5.9 for rod height h=1 m, different lateral distances (50 m, 150 m and 250 m) and different voltages applied (2.5 kV, 5 kV, 10 kV and 15 kV) to the rod. For the same value of the applied pulse voltage, the leader electric field at the rod tip depends heavily on the spacing between the leader and the rod at low leader currents. This will result in low virtual increase in the rod height for small leader current. On the other hand, the virtual increase in the rod height h' increases sharply with the increase of the applied pulse voltage, Figs. 5.13-5.15. This is simply explained by the fact that the increase of the pulse voltage applied to the rod increases the electric field at the tip of the rod and eventually will result in a faster development of the upward streamer. For the same value of the leader current and the applied pulse voltage, the virtual increase in the rod height h' also increases with the lateral distance. This increase in the lateral distance reduces the effect of leader electric-field on streamer development. However, the electric field due to the applied pulse voltage become dominating in streamer development. According, the virtual increase in rod height due to the effect of electric field of the applied pulse voltage will be larger for higher lateral distances.

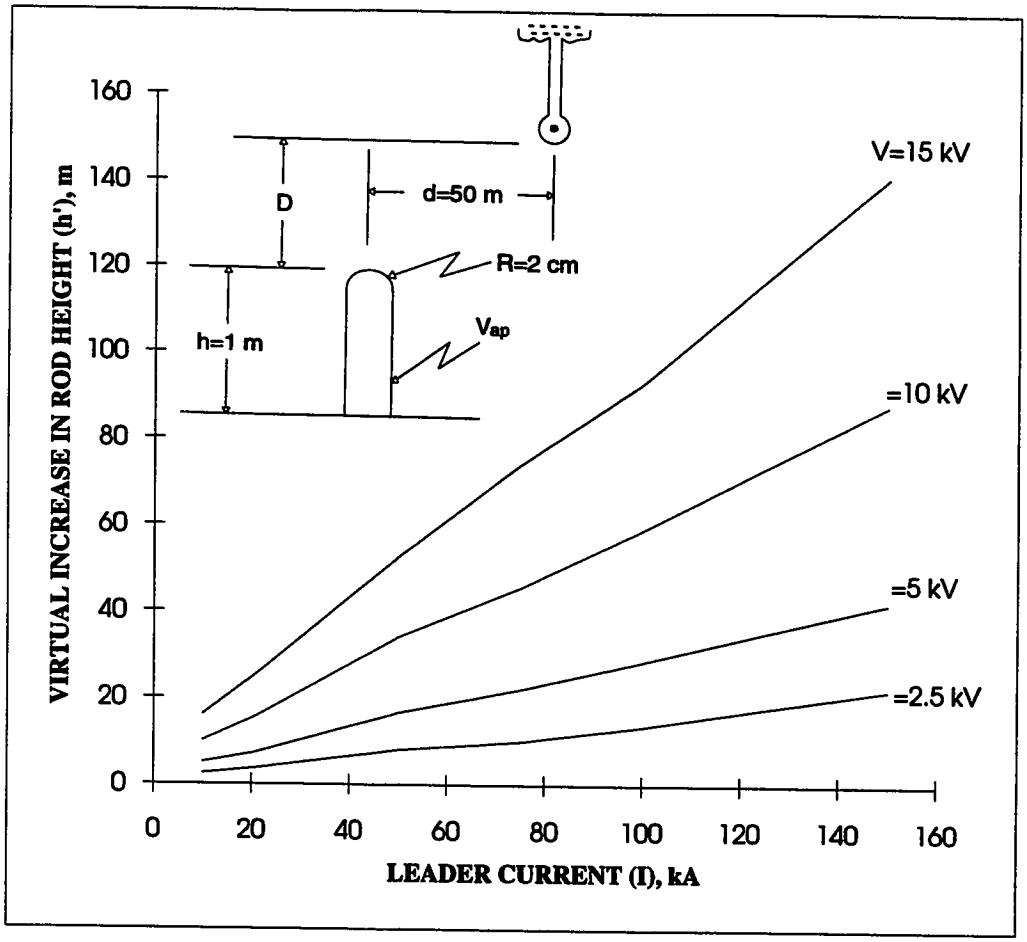

Fig. 5.13 Virtual increase in rod height versus leader current for different values of the applied pulse voltage (d=50 m and h=1 m).

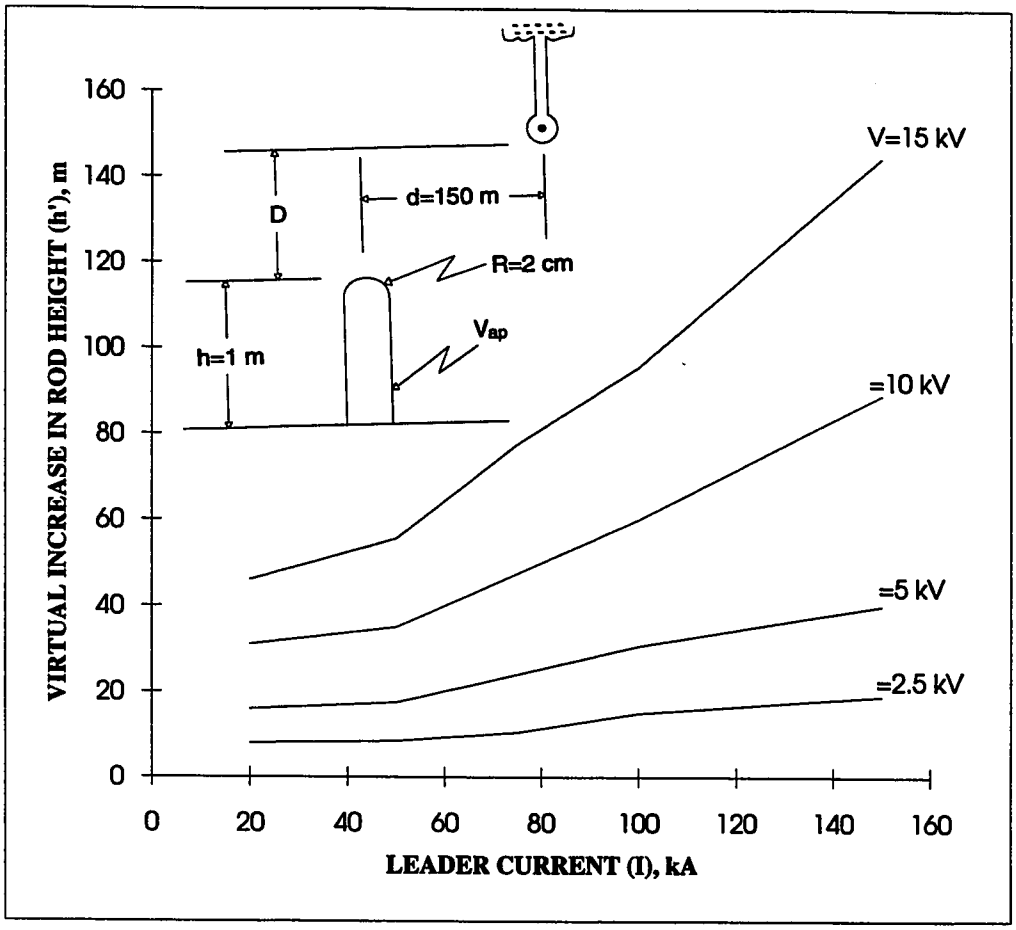

Fig. 5.14 Virtual increase in rod height versus leader current for different values of the applied pulse voltage (d=150 m and h=1 m).

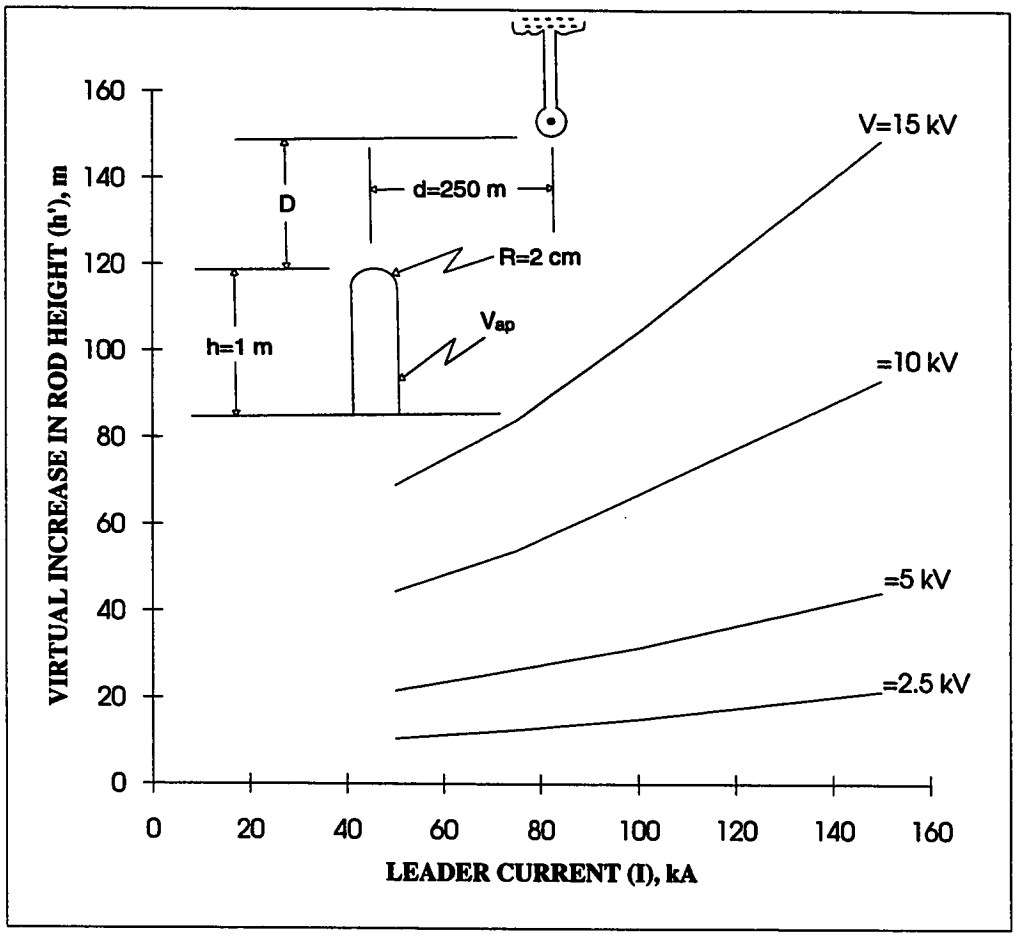

Fig. 5.15 Virtual increase in rod height versus leader current for different values of the applied pulse voltage (d=250 m and h=1 m).

5.3 Radius of Protection Around Energized Franklin Rod

The radii of protection R_p, Fig. 5.12, is obtained according to the electrogeometrical model [7,8,16,18], applied to a vertical rod. The radius of protection is given by the formula:

$$R_p = (h + h') \cdot \tan\phi \qquad (5.3)$$

where ϕ is the cone protection angle, Fig. 5.12.

Different values has been suggested for the cone protection angle ϕ such as 60° and 45° [5,7,18,40]. Helita [5,7] adopted 60° for the angle ϕ based on the French standard (NF C17-100, February 1987). As the results of this study will be compared with those obtained by Helita [7], the angle ϕ is considered 60° in the present work.

The radius of protection versus the leader current for constant values of rod height (h=1 m) and rod radius (R=2 cm) is shown in Figs. 5.16-5.18. These figures present the values of the radius of protection for different values of the applied voltage and lateral distances. The radius of protection increases sharply with the increase of the leader current and applied voltage. For the same value of the leader current and applied voltage, the increase in the radius of protection increases with the lateral

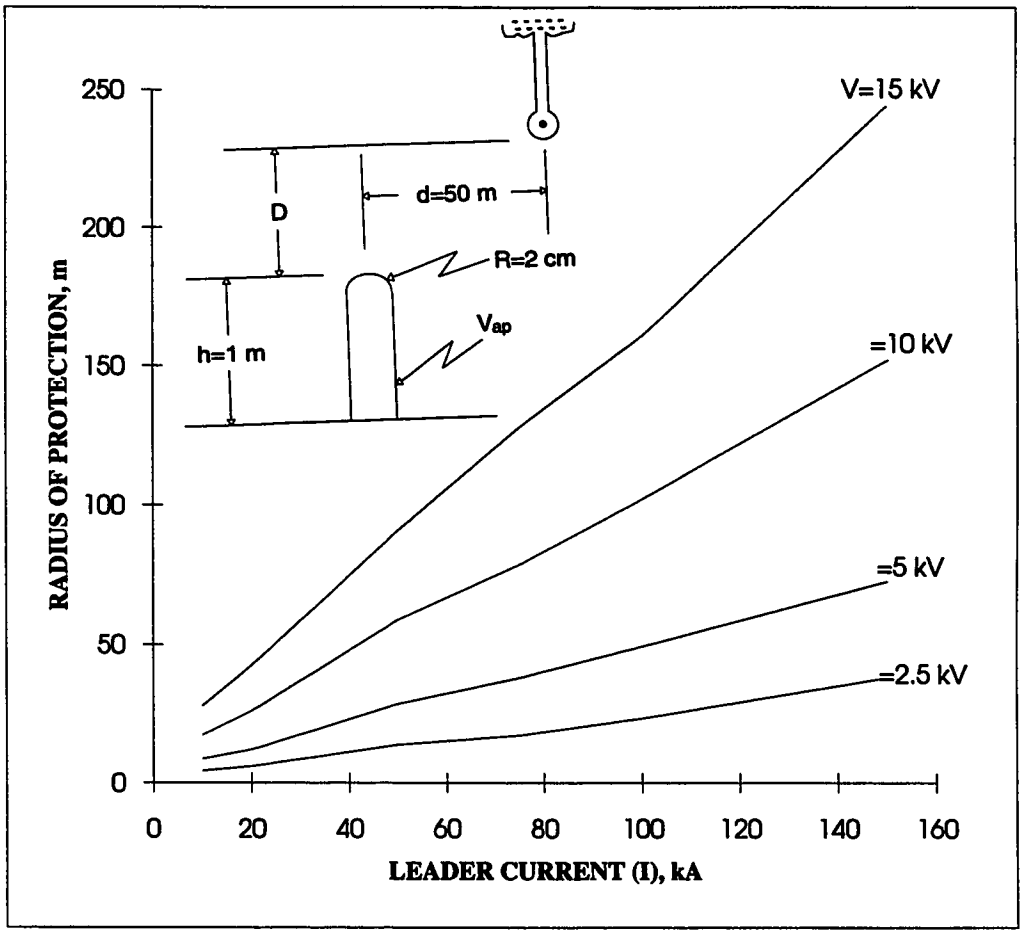

Fig. 5.16 Radius of protection versus leader current for different values of the applied pulse voltage (d=50 m and h=1 m).

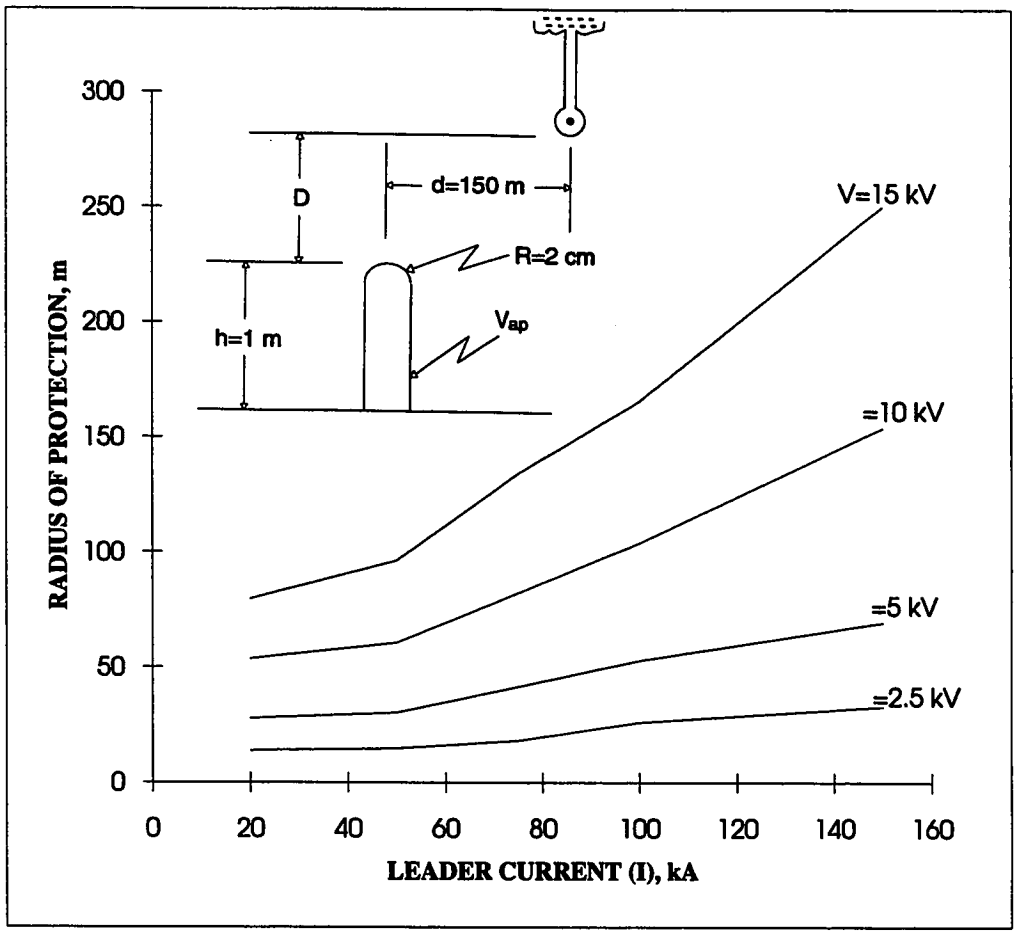

Fig. 5.17 Radius of protection versus leader current for different values of the applied pulse voltage (d=150 m and h=1 m).

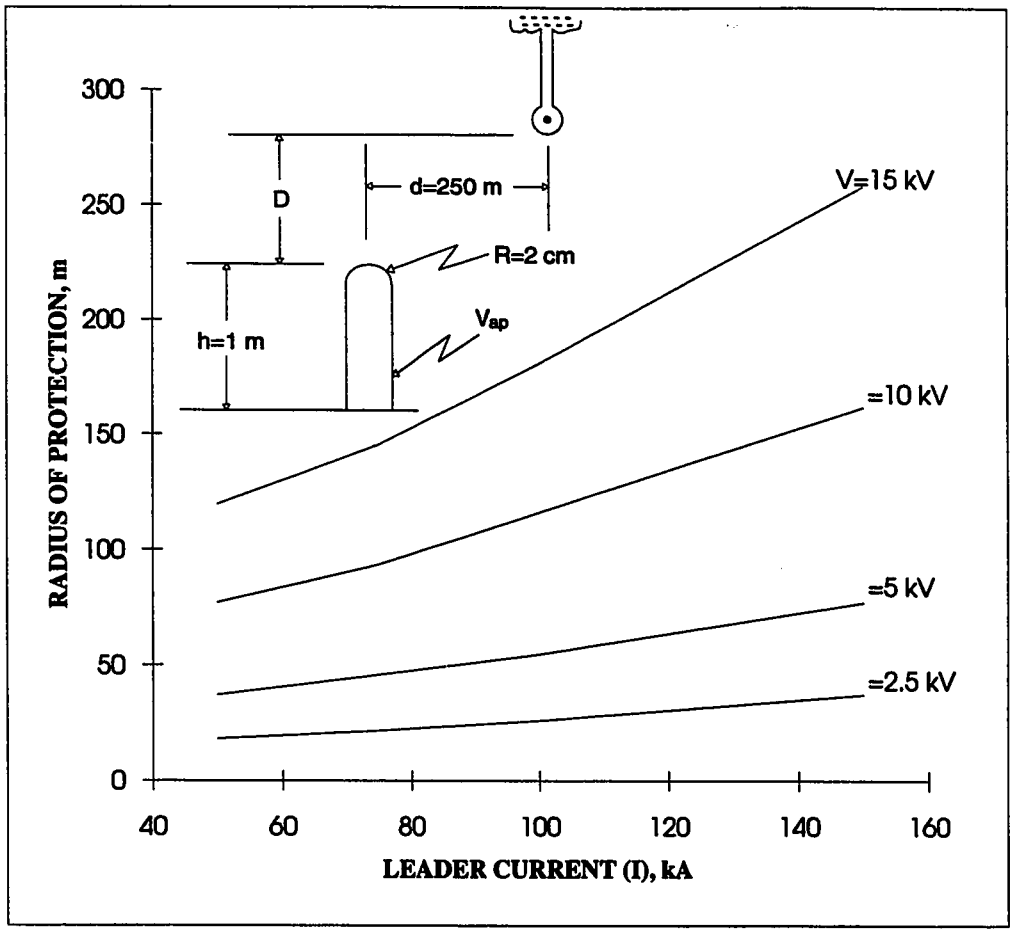

Fig. 5.18 Radius of protection versus leader current for different values of the applied pulse voltage (d=250 m and h=1 m).

distance. This is because at low values of lateral distance, the contribution of the downward leader in enhancing the electric field at the rod tip is significant with respect to the field enhancement due to the applied pulse voltage.

Figure 5.19 presents the minimum radius of protection versus the applied voltage for different lateral distances. If the lateral distances are 150 m and 250 m, then the minimum leader current that could trigger upward streamers at the tip of the Franklin rod is 20 kA and 50 kA, respectively. If the current of the downward leader is less than these values, then the upward-streamer onset condition will not be fulfilled.

5.4 Comparison with Published Data

In analogy with Fig. 5.11, Fig. 5.20 shows the increase in leader height due to the applied pulse voltage at the lowest leader current (I=10 kA) where the rod height and rod radius are kept constants at 1 m and 2 cm, respectively. At first, the maximum lateral distance when there is no applied pulse voltage is defined and found 92 m at leader height of 84.5 m. Then, on applying 5 kV to the rod for the same lateral distance (92 m) the virtual increase in the rod height h' is 9 m. For 10 kV applied pulse voltage the increase in the virtual height h' reachs 17.5 m. Further increase in the applied pulse voltage to 15 kV brings the virtual increase in rod height h' to 26 m. The output results of these cases are shown in

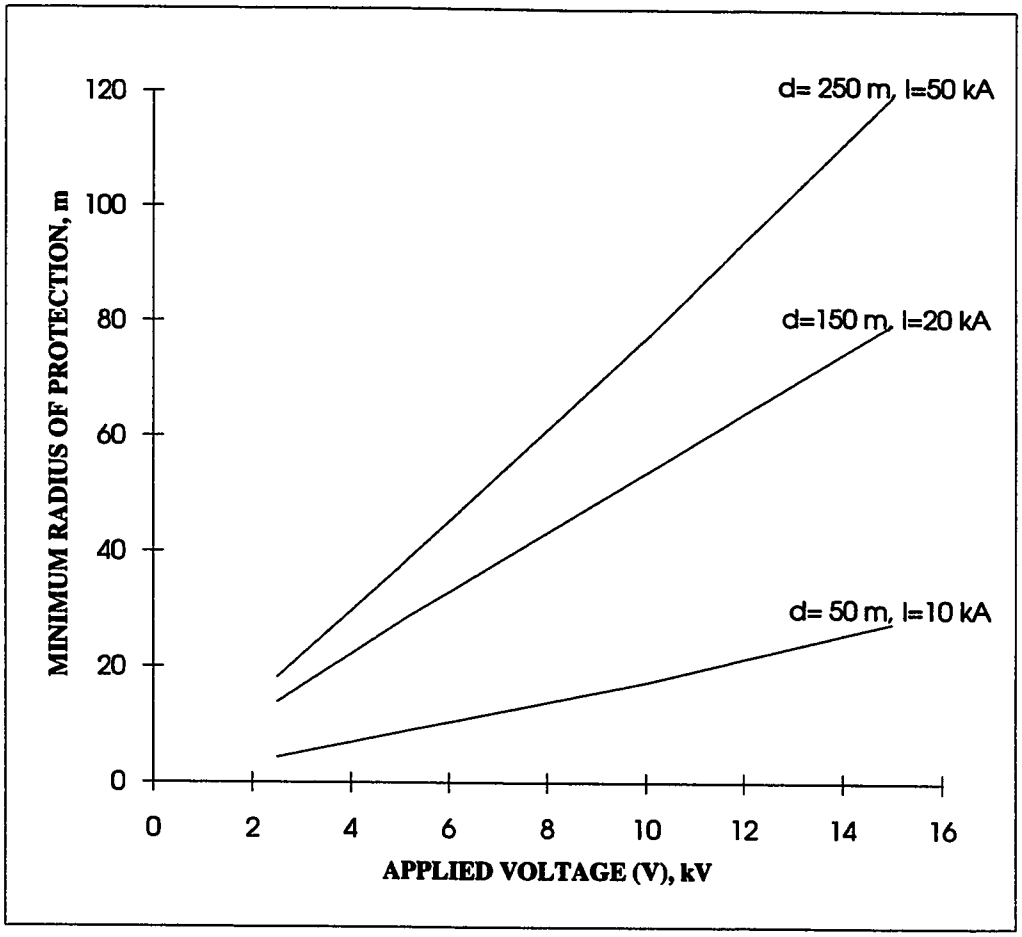

Fig. 5.19 Minimum radius of protection versus magnitude of pulse voltage applied to the rod for different lateral distances.

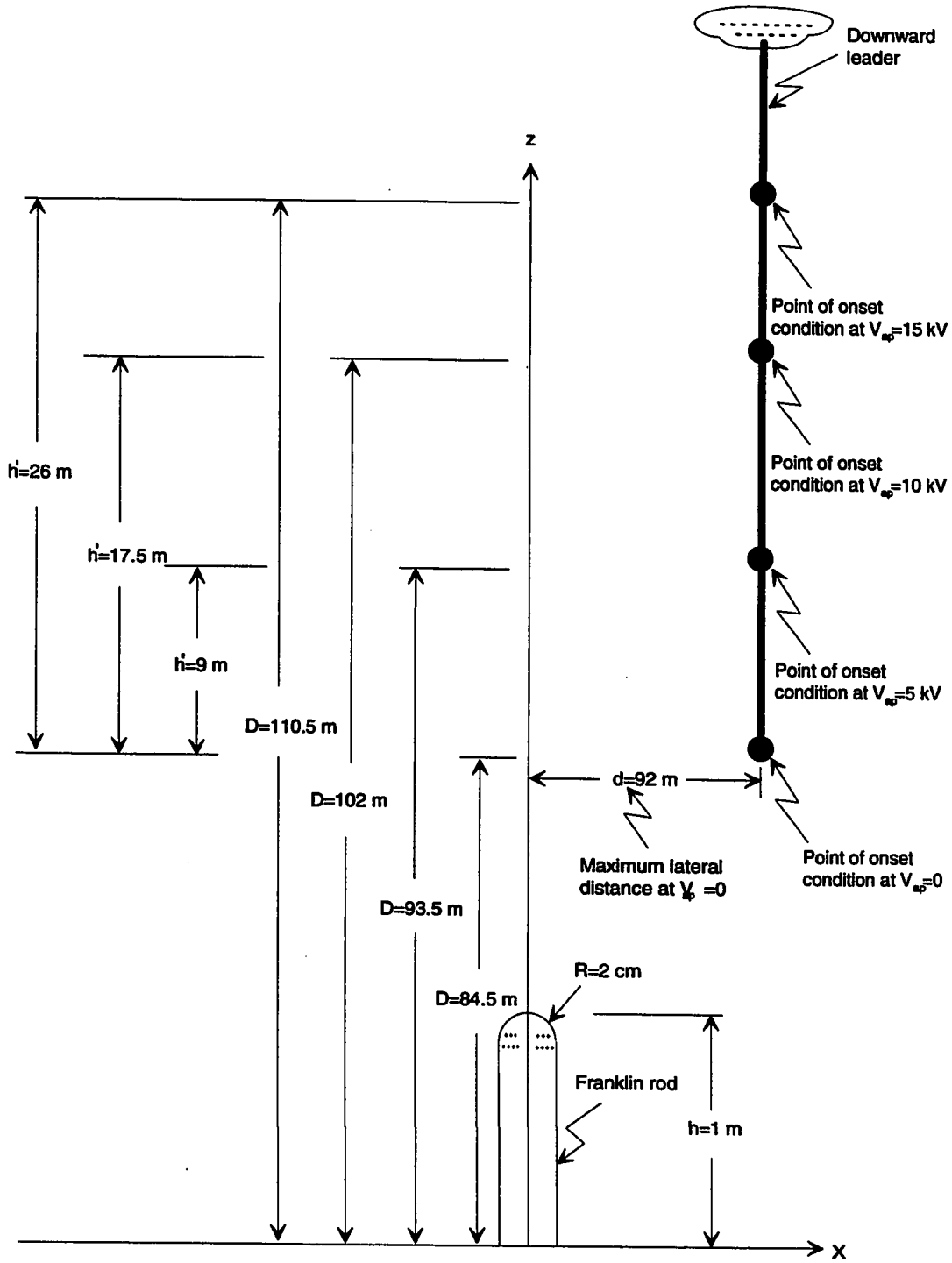

Fig. 5.20 Virtual increase in rod height due to the pulse voltage applied to the rod.

Appendix-B. Subsequently, the radius of protection can be calculated using equation 5.3 for different applied voltages as follows:

$$R_{P5kV} = (1+9)\cdot\tan(60)$$
$$=17.5 \text{ m}$$

$$R_{P10kV} = (1+17.5)\cdot\tan(60)$$
$$=32.0 \text{ m}$$

$$R_{P15kV} = (1+26)\cdot\tan(60)$$
$$=46.8 \text{ m}$$

The results reported by Helita in France [7] for different values of rod height and various types of their product are shown in Fig. 5.21. The rod height is limited to 1 m in present analysis due to the huge number of simulation fictitious charges needed in modeling the rod. This is why Helita data, Fig. 5.21, has been extrapolated to rod height h=1 m, Fig. 5.22.

The increase in the radius of protection due to the rod energization as calculated by the present analysis and reported by Helita is shown in Table 5.1a&b. It is not the intent of this analysis to compare the two results because Helita parameters of the pulse voltage applied to Franklin rod are unknown. Moreover, the rod investigated in the present analysis is hemispherically-capped which is different from those manufactured by

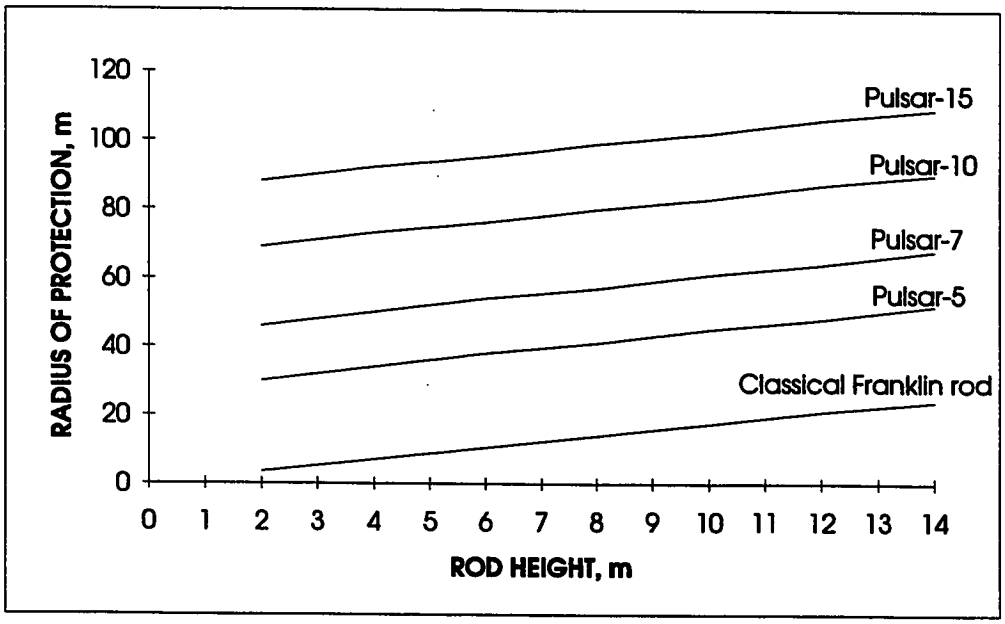

Fig. 5.21 Radius of protection versus rod height for various types of Helita product.

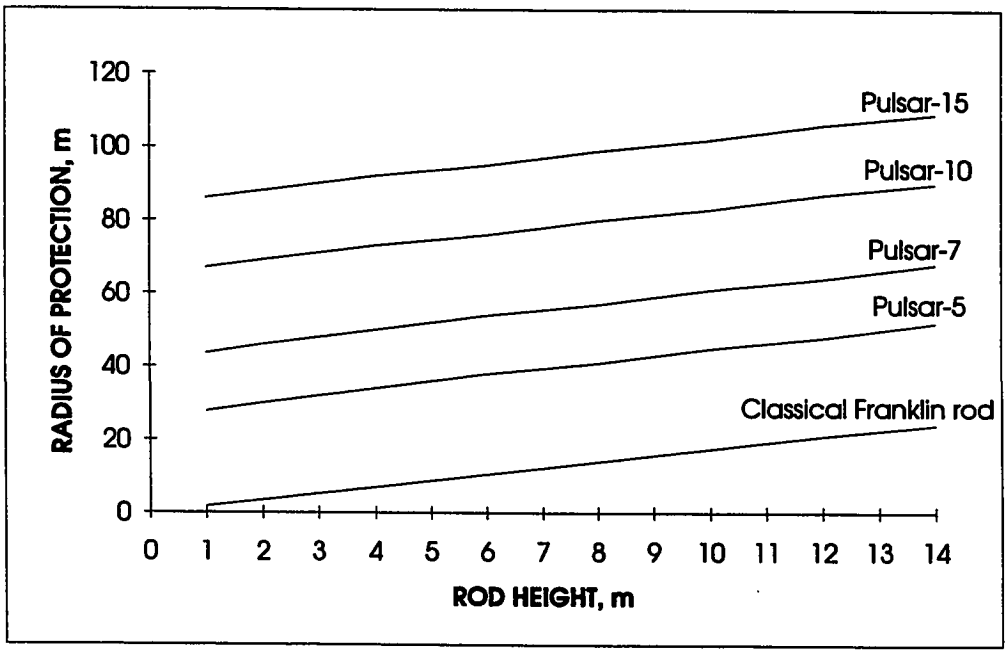

Fig. 5.22 Radius of protection versus rod height for various types of Helita product after being extrapolated to h=1 m.

Helita, Fig. 2.8. The purpose of the analysis is to assess the effect of the applied pulse voltage on the radius of protection. However, there is a good correlation between the present results and those of Helita values, Table 5.1a&b. Accordingly, one could conclude that the pulse voltage applied to the Franklin rod will cause a significant increase in the radius of protection.

		Helita values for different type their products			
Type	Franklin rod	Pulsar-5	Pulsar-7	Pulsar-10	Pulsar-15
Radius of protection (m)	1.732	27.7	43.6	67	86

Table 5.1 a) Reported radius of protection for various types of Helita product.

		Present values		
Applied voltage	Franklin rod	$V_{ap} = 5$ kV	$V_{ap} = 10$ kV	$V_{ap} = 15$ kV
Radius of protection (m)	1.732	17.5	32.0	46.8

Table 5.1 b) Present values of the radius of protection.

CHAPTER 6

CONCLUSIONS AND SUGGESTIONS FOR FUTURE WORK

With a better understanding the phenomenon of lightning, several attempts have been made to improve the classical Franklin rod. Researchers in this regard followed two approaches. The first approach is to protect the structure from being struck by the lightning stroke. This approach was achieved by using Faraday cage and Spline Ball Ionizer. The other approach is to develop a methodology to attract the lightning stroke toward the lightning rod and provide a safe path to dissipate the lightning stroke energy. This approach was also achieved by using the following methods namely; laser-triggered ionizer, radioactived ionizer and energized Franklin rod.

Energized Franklin rod has been designed and manufactured by Helita in France. High voltage experiments have been performed to confirm an increase in the protection efficiency of an energized Franklin rod compared with the classical Franklin rod. They argued that a voltage pulse applied to the lightning rod will enhance the corona discharge at the tip of the rod and eventually will result in faster launching of the upward streamer which will result in a more efficient lightning rod.

6.1 Conclusions

On the basis of the analysis presented in this thesis, the following conclusions may be drawn:

1- A method is developed for calculating the electric field in the vicinity of an energized Franklin rod at the time when a negative downward leader is approaching the rod. The charge simulation technique was used for field computation. The accuracy of the calculated electric field values in the vicinity of Franklin rod was checked against previous reported values. It was found that the present calculated values agreed satisfactorily with those reported before.

2- The onset criterion of the positive corona at the tip of the energized Franklin rod is formulated. The criterion was checked against a widely-used empirical formula. There was a good match between the present calculated onset-field values and those obtained by the formula.

3- It was found that the rod parameters (radius and height) have a significant effect on the onset condition of the upward streamers:

a) Decreasing the rod radius triggers the upward streamers at a higher leader height with a subsequent increase of the radius of protection. However, the decrease of the rod radius is limited

by the ampacity of the rod to carry safely the current of the downward leader.

b) Increasing the rod height triggers the upward streamers at a considerable higher leader height with a subsequent increase of the radius of protection. However, the height of the lightning rod should not be too long to prevent side and ascending strokes and to withstand the mechanical stresses due to the wind.

4- The onset of the upward streamers are influenced by the features of the downward leader (leader height and current and the lateral distance measured from the rod axis):

a) The upward streamer is triggered at a higher leader height for larger leader current. Consequently, the radius of protection is calculated based on the smallest leader current.

b) The leader height at the onset of the upward streamers decreases with the increase of the lateral distance. Further increase of the lateral distance above the maximum value results in losing the rod effectiveness in lightning protection.

5- The effect of the pulse voltage applied to the Franklin rod was studied. It has been found that the upward streamers are triggered from the energized rod at a leader height higher than that of the

classical rod. This represents an increase in the radius of protection. The higher the amplitude of the pulse voltage applied to the rod the better is the performance of the rod.

6- Energizing the rod by a pulse voltage appears as if the rod is elongated in length and denoted as "virtual" increase in the rod height. The radius of protection is computed based on the virtual rod height.

7- The increase in the radius of protection due to the pulse voltage applied to the rod at the lowest leader current (I=10 kA) is calculated. Although Helita parameters of the pulse voltage are unknown, there is a good correlation between the present values of the radius of protection and those reported by Helita.

6.2 Suggestions for Future Work

For future work pertinent to the thesis the following directions of research are recommended:

1- Modeling of the downward leader model is to be improved to account for the leader branches.

2- Different geometries of the rod tip are to be investigated instead of hemispherically-capped tip. The protection efficiency, of course, depends on the geometry of the rod tip. Rods of multiple sharp points as shown in Fig. 2.4 call also for investigation..

3- Extension of the present study for other shapes of the pulse voltage applied to the Franklin rod instead of a step-pulse voltage.

APPENDIX-A

COMPUTER PROGRAM FOR CALCULATING THE ONSET CONDITION OF THE UPWARD STREAMER

```
PARAMETER (M=195)
IMPLICIT DOUBLE PRECISION(A-H,O-Z)
DIMENSION XP(M),YP(M)
DIMENSION ZP(M),XT(M),YT(M),ZT(M),QTP(M)
DIMENSION ER(M),P(M,M),QP(M)
COMMON /COM5/ EXX(550),EYY(550),EZZ(550)
COMMON /COM1/ P,QP
COMMON /COM2/ X(M),Y(M),Z(M),RR(M),XPT,YPT,ZPT,QPC,XPL,YPL,ZPL
+,QLC,PI,EPS,XTR,YTR,ZTR
COMMON /COM3/ QR(M)
COMMON /COM4/ AREA(550),XIO(M),ZIO(M),NM,XION(M),ZION(M)
OPEN (UNIT = 10,FILE ='NEW2.DAT',STATUS='OLD')
OPEN (UNIT = 20,FILE ='prol0.OUT',STATUS='OLD')
READ(10,*)ZR,RM,N1,N2,F1,F2,F3,F4

PI=3.141593
EPS=1.0/(36.0*PI)*1.0E-9
SN=0

STEP11=2*ZR/((N1+1)*(N1+2))
RF=F1*RM
RC=F2*RF
C=RF-RC
ZS=ZR

DO 10 I=1,N1
 ZS=ZS-STEP11*I
 IF(ZS.LT.0)STOP
 RR(4*I-3)=RC
 RR(4*I-2)=RC
 RR(4*I-1)=RC
 RR(4*I)=RC

 X(4*I-3)=C
 X(4*I-2)=0.0
 X(4*I-1)=(-C)
 X(4*I)=0.0

 Y(4*I-3)=0.0
 Y(4*I-2)=C
```

```
      Y(4*I-1)=0.0
      Y(4*I)=(-C)

      Z(4*I-3)=ZS
      Z(4*I-2)=ZS
      Z(4*I-1)=ZS
      Z(4*I)=ZS

      XP(4*I-3)=RM
      XP(4*I-2)=0.0
      XP(4*I-1)=(-RM)
      XP(4*I)=0.0

      YP(4*I-3)=0.0
      YP(4*I-2)=RM
      YP(4*I-1)=0.0
      YP(4*I)=(-RM)

      ZP(4*I-3)=ZS
      ZP(4*I-2)=ZS
      ZP(4*I-1)=ZS
      ZP(4*I)=ZS

      AN=COS(PI/4.0)
      XT(4*I-3)=RM*AN
      XT(4*I-2)=(-RM*AN)
      XT(4*I-1)=(-RM*AN)
      XT(4*I)=RM*AN

      YT(4*I-3)=RM*AN
      YT(4*I-2)=RM*AN
      YT(4*I-1)=(-RM*AN)
      YT(4*I)=(-RM*AN)

      ZT(4*I-3)=ZS
      ZT(4*I-2)=ZS
      ZT(4*I-1)=ZS
      ZT(4*I)=ZS

   10 CONTINUE

      STEP2=RM/(N2*1.0+1.0)
      STEPL=0.0
      DO 20 I=N1+1,N1+N2
       STEPL=STEPL+STEP2
       ZS=ZR+STEPL
       RT=SQRT(RM**2-STEPL**2)
       RF=F3*RT
       RC=F4*RF
       C=RF-RC
       RR(4*I-3)=RC
       RR(4*I-2)=RC
```

```
      RR(4*I-1)=RC
      RR(4*I)=RC

      X(4*I-3)=C
      X(4*I-2)=0.0
      X(4*I-1)=(-C)
      X(4*I)=0.0

      Y(4*I-3)=0.0
      Y(4*I-2)=C
      Y(4*I-1)=0.0
      Y(4*I)=(-C)

      Z(4*I-3)=ZS
      Z(4*I-2)=ZS
      Z(4*I-1)=ZS
      Z(4*I)=ZS

      XP(4*I-3)=RT
      XP(4*I-2)=0.0
      XP(4*I-1)=(-RT)
      XP(4*I)=0.0

      YP(4*I-3)=0.0
      YP(4*I-2)=RT
      YP(4*I-1)=0.0
      YP(4*I)=(-RT)

      ZP(4*I-3)=ZS
      ZP(4*I-2)=ZS
      ZP(4*I-1)=ZS
      ZP(4*I)=ZS

      AN=COS(PI/4.0)
      XT(4*I-3)=RT*AN
      XT(4*I-2)=(-RT*AN)
      XT(4*I-1)=(-RT*AN)
      XT(4*I)=RT*AN

      YT(4*I-3)=RT*AN
      YT(4*I-2)=RT*AN
      YT(4*I-1)=(-RT*AN)
      YT(4*I)=(-RT*AN)

      ZT(4*I-3)=ZS
      ZT(4*I-2)=ZS
      ZT(4*I-1)=ZS
      ZT(4*I)=ZS

   20 CONTINUE

C-------- COORDINATE OF THE POINT CHARGE AT THE ROD ----------------
```

```
      XTR=0.0
      YTR=0.0
      ZTR=ZR
      XP((N1+N2)*4+1)=0.0
      YP((N1+N2)*4+1)=0.0
      ZP((N1+N2)*4+1)=ZR+RM
      XT((N1+N2)*4+1)=0.0
      YT((N1+N2)*4+1)=0.0
      ZT((N1+N2)*4+1)=ZR+RM

      READ(10,*)RTL,ZTT
      ZL=ZTT+0.5
      XPT=RTL
      YPT=0.0
      ZPT=ZTT

      XPL=RTL
      YPL=0.0
      ZPL=ZL


      READ(10,*)QRR,CURR,H
      QPC=CURR/150.0/(4.0*PI*EPS)
      QLC=0.9*CURR/(15.0*H)/(4.0*PI*EPS)


      NM=(N1+N2)*4+1

      DO 100 I=1,NM

       DO 110 J=1,NM-1
        RP=SQRT((XP(I)-X(J))**2+(YP(I)-Y(J))**2)
        ALF1=SQRT((RP+RR(J))**2+(ZP(I)-Z(J))**2)
        ALF2=SQRT((RP+RR(J))**2+(ZP(I)+Z(J))**2)
        C1=2.0*SQRT(RP*RR(J))/ALF1
        C2=2.0*SQRT(RP*RR(J))/ALF2
        CALL ELINK(C1,EK1)
        CALL ELINK(C2,EK2)
         P(I,J)=2.0/PI*(EK1/ALF1-EK2/ALF2)
110   CONTINUE


       DPR=SQRT((XP(I)-XTR)**2+(YP(I)-YTR)**2+(ZP(I)-ZTR)**2)
       DIR=SQRT((XP(I)-XTR)**2+(YP(I)-YTR)**2+(ZP(I)+ZTR)**2)
       P(I,(N1+N2)*4+1)=(1.0/DPR-1.0/DIR)

       DP=SQRT((XP(I)-XPT)**2+(YP(I)-YPT)**2+(ZP(I)-ZPT)**2)
       DI=SQRT((XP(I)-XPT)**2+(YP(I)-YPT)**2+(ZP(I)+ZPT)**2)
       QT=QPC*(1.0/DP-1.0/DI)

       DLC=SQRT((XP(I)-XPL)**2+(YP(I)-YPL)**2+(ZP(I)-ZPL)**2)
```

```
      DLI=SQRT((XP(I)-XPL)**2+(YP(I)-YPL)**2+(ZP(I)+ZPL)**2)
      QL=QLC*LOG((ZP(I)+ZPL+DLI)/(ZPL-ZP(I)+DLC))

      QP(I)=QRR-QT-QL
  100 CONTINUE

      CALL NGAUSS(NM)

      EMAX=0.0

      DO 200 I=1,NM

      DP=SQRT((XT(I)-XPT)**2+(YT(I)-YPT)**2+(ZT(I)-ZPT)**2)
      DI=SQRT((XT(I)-XPT)**2+(YT(I)-YPT)**2+(ZT(I)+ZPT)**2)
      QT=QPC*(1.0/DP-1.0/DI)

      DLC=SQRT((XT(I)-XPL)**2+(YT(I)-YPL)**2+(ZT(I)-ZPL)**2)
      DLI=SQRT((XT(I)-XPL)**2+(YT(I)-YPL)**2+(ZT(I)+ZPL)**2)
      QL=QLC*LOG((ZT(I)+ZPL+DLI)/(ZPL-ZT(I)+DLC))
      QTP(I)=QT+QL
      DO 210 J=1,NM-1
       RP=SQRT((XT(I)-X(J))**2+(YT(I)-Y(J))**2)
       ALF1=SQRT((RP+RR(J))**2+(ZT(I)-Z(J))**2)
       ALF2=SQRT((RP+RR(J))**2+(ZT(I)+Z(J))**2)
       C1=2.0*SQRT(RP*RR(J))/ALF1
       C2=2.0*SQRT(RP*RR(J))/ALF2
       CALL ELINK(C1,EK1)
       CALL ELINK(C2,EK2)
       P(I,J)=(2.0/PI)*(EK1/ALF1-EK2/ALF2)
       QTP(I)=QTP(I)+QR(J)*P(I,J)
  210  CONTINUE

      DPR=SQRT((XT(I)-XTR)**2+(YT(I)-YTR)**2+(ZT(I)-ZTR)**2)
      DIR=SQRT((XT(I)-XTR)**2+(YT(I)-YTR)**2+(ZT(I)+ZTR)**2)
      PT=(1.0/DPR-1.0/DIR)
      QTP(I)=QTP(I)+QR((N1+N2)*4+1)*PT

       ER(I)=QRR-QTP(I)
       IF(ABS(ER(I)).GT.EMAX) EMAX=ABS(ER(I))

  200 CONTINUE


      WRITE(20,*)
      WRITE(20,*)
      WRITE(20,*)'OUTPUT REPORT FOR THE CASE WHEN THE SYSTEM PARAMETERS
     +ARE FIXED AS:'
      WRITE(20,*)
      WRITE(20,9)'ROD HEIGHT=',ZR,'m'
      WRITE(20,9)'ROD RADIUS=',RM,'m'
      WRITE(20,9)'ROD VOLTAGE=',QRR/1000.0,'kV'
      WRITE(20,9)'LATERAL DISTANCE BETWEEN FRANKLIN ROD & DOWNWARD LEADE
```

```
  +R=',RTL,'m'
   WRITE(20,9)'DOWNWARD LEADER HEIGHT=',ZPT,'m'
   WRITE(20,9)'DOWNWARD LEADER CURRENT=',CURR,'kA'
   WRITE(20,*)
   WRITE(20,*)
9  FORMAT(2X,A,F9.3,2X,A)
22  FORMAT(4X,A,E16.8)
23  FORMAT(4X,A)

   IF(QRR.NE.0.0)EMAX=EMAX/QRR*100.0
   IF(QRR.EQ.0.0)DISS=SQRT((ZTT-ZR-RM)**2+RTL**2)
   IF(QRR.EQ.0.0)VREF=ABS(QPC)/(4.0*PI*EPS)*1.0/DISS
   IF(QRR.EQ.0.0)EMAX=ABS(EMAX)/VREF*100.0
   WRITE(20,56)EMAX
56  FORMAT('THE MAX. PERCENT ERROR IN ROD SURFACE POTENTIAL=',F8.4)
   WRITE(20,*)
   WRITE(20,*)
   WRITE(20,*)
   WRITE(20,*)'THE ELECTRIC FIELD AROUND THE TIP:'
   WRITE(20,*)
   WRITE(20,44)
   WRITE(20,32)
   WRITE(20,*)'==================================================
  +==================='

   DO 500 I=1,181,10
    TH=(I-1)*PI/180.0
    XE=RM*COS(TH)
    YE=0.0
    ZE=ZR+RM*SIN(TH)
    CALL FIELD(NM,XE,YE,ZE,EX,EY,EZ,E)
    THE=I-1
    FD=ATAN(EZ/EX)*180/PI

    IF(THE.EQ.0)WRITE(20,77)THE,FD,EX,EY,EZ,E
    IF(THE.EQ.30.)WRITE(20,77)THE,FD,EX,EY,EZ,E
    IF(THE.EQ.60.)WRITE(20,77)THE,FD,EX,EY,EZ,E
    IF(THE.EQ.90.)WRITE(20,77)THE,FD,EX,EY,EZ,E
500 CONTINUE

77  FORMAT(F11.4,8X,F11.4,16X,E11.4,8X,E11.4,8X,E11.4,6X,E11.4,/)
44  FORMAT(3X,'  TH   ',7X,'ATAN(EZ/EX)',12X,'X COMP.',11X,
  +'Y COMP.',11X,'Z COMP.',11X,'TOT. E',/)
32  FORMAT(3X,' (DEGREE) ',4X,' (DEGREE)  ',16X,'  (m)  ',17X,
  +'  (m)  ',14X,'  (m)  ',16X,' (V/m) ')
    WRITE(20,*)'==================================================
  +==================='
    WRITE(20,*)
    WRITE(20,*)

   L=1
   YE=0.0
```

```
      READ(10,*)DLD,FF
      STEP=DLD/(FF*1.0)
      XZ=-STEP
      XZN=-STEP
      DO 222 J=1,165,10
       TH=(J-1)*PI/180.0
787   DO 111 I=1,FF
       XZ=XZ+STEP
       ZE=ZR+RM+XZ*COS(TH)
       XE=XZ*SIN(TH)
       CALL FIELD(NM,XE,YE,ZE,EX,EY,EZ,E)
       E=E/100.0
       CALL ATTION(E,FION,ATT,AV)
       IF(I.EQ.1.AND.J.EQ.1)WRITE(20,*)'ELECTRIC FIELD, IONIZATION AND
     +ATTACHMENT COEFFICIENT AT ROD TIP:'
       IF(I.EQ.1.AND.J.EQ.1)WRITE(20,*)
       IF(I.EQ.1.AND.J.EQ.1)WRITE(20,25)E
       IF(I.EQ.1.AND.J.EQ.1)WRITE(20,59)FION,ATT
       IF(I.EQ.1.AND.J.EQ.1)WRITE(20,*)
       IF(I.EQ.1.AND.J.EQ.1)WRITE(20,589)AV
       IF(I.EQ.1.AND.J.EQ.1)WRITE(20,*)
       IF(I.EQ.1.AND.ATT.GE.FION)WRITE(20,*)'ATT. GREATER THAN ION.'
       IF(I.EQ.1.AND.ATT.GE.FION)XZ=XZ/2.0
       IF(I.EQ.1.AND.ATT.GE.FION)GOTO 787
       IF(ABS(AV).LT..01*FION)GOTO 55
111   CONTINUE
      WRITE(20,*)'WARNING AV NOT LESS THAN .1 AT TH=',J-1
      STOP
55     IF(ZE.LT.ZR.AND.XE.LT.RM)GOTO 987
      IF(SQRT((ZE-ZR)**2+XE**2).LE.RM)GOTO 987
      TH2=-TH
898   DO 444 IN=1,FF
       XZN=XZN+STEP
       ZEN=ZR+RM+XZN*COS(TH2)
       XEN=XZN*SIN(TH2)
       CALL FIELD(NM,XEN,YE,ZEN,EXN,EYN,EZN,EN)
       EN=EN/100.0
       CALL ATTION(EN,FIONN,ATTN,AVN)
       IF(IN.EQ.1.AND.ATTN.GE.FIONN)WRITE(20,*)'ATT. GT ION.'
       IF(IN.EQ.1.AND.ATTN.GE.FIONN)XZN=XZN/2.0
       IF(IN.EQ.1.AND.ATTN.GE.FIONN)GOTO 898

       IF(ABS(AVN).LT..01*FIONN)GOTO 666
444   CONTINUE
      WRITE(20,*)'WARNING AV NOT LESS THAN .1 AT TH2=',J-1
      STOP
666   ZIO(L)=ZE
      XIO(L)=XE
      ZION(L)=ZEN
      XION(L)=XEN
      IF(J-1.EQ.0)WRITE(20,*)
      IF(J-1.EQ.0)WRITE(20,*)'IONIZATION-ZONE BOUNDARY ABOVE THE ROD TI
```

```
  +P:'
   IF(J-1.EQ.0)WRITE(20,*)
   IF(J-1.EQ.0)WRITE(20,59)FION,ATT
   IF(J-1.EQ.0)WRITE(20,*)
   IF(J-1.EQ.0)WRITE(20,589)AV
59  FORMAT(6X,'IONIZATION COEFF.=',F10.5,2X,'(1/m)',4X,'ATTACHMENT CO
  +EFF.=',F10.5,' (1/m)')
589 FORMAT(6X,'IONIZATION COEFF.-ATTACHMENT COEFF.=',E12.5,' (1/m)
  +',/)
   IF(J-1.EQ.0)WRITE(20,25)E
25  FORMAT(6X,'ELECTRIC FIELD=',E12.5,1X,' V/cm',/)
   IF(J-1.EQ.0)WRITE(20,26)ZIO(L),XIO(L)
26  FORMAT(6X,'POINT COORDINATES',' Z=',F10.6,'     X=',F10.6,/)
   IF(J-1.EQ.0)GOTO 91
91   L=L+1
222 CONTINUE
987 WRITE(20,*)

C SEGMENTS IN THE IONIZATION ZONE.

   L=L-1
   NAA=1
   DO 35 I=2,L
    ROS=XIO(I)-XION(I)
    RIONX=XIO(I)-ROS/2.0
    YST=0.0
    STH=ROS/(2*.006)+2
    NTH=91/STH
    IF(NTH.GT.10)NTH=NTH
    IF(NTH.LE.10)NTH=10
    DO 79 J=10,91,NTH
     THS=J*PI/180.0
     THS2=(J-10)*PI/180.0
     STEPY=ROS/(2.0)*SIN(THS)-YST
     YST=ROS/(2.0)*SIN(THS)
     XSTT=RIONX+ROS/(2.0)*COS(THS2)
     NXY=((XSTT-RIONX)*2.0/0.006)+1
     STEPX=(XSTT-RIONX)*2.0/(NXY*1.0)
     DO 97 KC=1,NXY
      XST=XSTT-(KC-1)*STEPX
      CRIT1=SQRT(XST**2+YST**2+(ZIO(I)-ZR)**2)
      IF(ZIO(I).LT.ZR+RM.AND.ZIO(I).GT.ZR.AND.CRIT1.LT.RM)GOTO 97
      CRIT2=SQRT(XST**2+YST**2)
      IF(ZIO(I).LT.ZR.AND.CRIT2.LT.RM)GOTO 97
      ZE=ZIO(I)
      XE=XST
      YE=YST
      CALL FIELD(NM,XE,YE,ZE,EX,EY,EZ,E)
      EXX(NAA)=EX
      EYY(NAA)=EY
      EZZ(NAA)=EZ
      NAA=NAA+1
```

```
      if(naa.ge.550)WRITE(20,*)'NO. OF AREAS MORE THAN 550'
      if(naa.ge.550)goto 454
 97   CONTINUE
 79   CONTINUE
 35  CONTINUE
454  WRITE(20,*)

C        NO OF PHOTOELECTRONS THAT WILL BE CREATED IN EACH DETERMINED
C        SUBVOLUME

    WRITE(20,*)
    WRITE(20,*)
    WRITE(20,*)'GROWTH OF PRIMARY AVALANCHE SIZE:'
    WRITE(20,*)
    WRITE(20,445)
    WRITE(20,437)
    WRITE(20,447)
445  FORMAT('STEP',3X,'APPL. FIELD',3X,'SPACE CHARGE FIELD',7X,
   +'TOT. FIELD',7X,'Z-COORD.',9X,'AVALANCHE')
437  FORMAT('        ',6X,'          ',13X,'                ',16X,
   +'        ',8X,'          ',24X,'   SIZE    ')
447  FORMAT('        ',6X,'  (V/cm)  ',13X,'    (V/cm)    ',16X,
   +' (V/cm)  ',8X,'   (m)   ',11X,'  (IONS)   ')
19   FORMAT(A)
    WRITE(20,19)'==================================================
   +=================='
    TAW=0.0
    READ(10,*)NOA,NINT
    TL=ZIO(1)-(ZR+RM)
    DO 37 K=1,NOA
     ESC=0.0
     ZL=TL*K/(NOA*1.0)
     NINT=NINT+15
     STEPI=ZL/(NINT*1.0)
     SUM2=0.0
     DO 38 NN=1,NINT
      ZE=ZIO(1)-(NN-1)*STEPI
      ZC=ZE
      XE=0.0
      YE=0.0
      CALL FIELD(NM,XE,YE,ZE,EX,EY,EZ,E)
      IF(NN.GT.1.0)ESC=1.6E-19*(EXP(SUM2)-1.0)/(4.0*PI*EPS*ZSC**2)
      EZT=EZ-ESC
      ET=SQRT(EZT**2+EX**2+EY**2)/100.0
      IF(EZT.LT.0.0)WRITE(20,*)'SPACE CHARGE FIELD GT APPLIED FIELD'
      IF(EZT.LT.0.0)STOP
      CALL ATTION(ET,FION,ATT,AV)
      ZSC=1.0/(FION*100.0)
      SUM2=SUM2+STEPI*AV*100.0
      IF(K.EQ.NOA)CALL EMOBS(ET,EMOB)
      IF(K.EQ.NOA)TAW=TAW+STEPI/(EMOB*ET*100.0)
      IF(K.EQ.NOA.AND.NN.EQ.NINT)CALL RADIUSPA(ET,TAW,RPA)
```

```
38  CONTINUE
    EIONS=EXP(SUM2)
    AVPR=EIONS
    IF(K.EQ.1)WRITE(20,99)K,E/100.0,ESC/100.0,ET,ZE,EIONS
    IF(K.EQ.10)WRITE(20,99)K,E/100.0,ESC/100.0,ET,ZE,EIONS
    IF(K.EQ.20)WRITE(20,99)K,E/100.0,ESC/100.0,ET,ZE,EIONS
    IF(K.EQ.30)WRITE(20,99)K,E/100.0,ESC/100.0,ET,ZE,EIONS
    IF(K.EQ.40)WRITE(20,99)K,E/100.0,ESC/100.0,ET,ZE,EIONS
    IF(K.EQ.50)WRITE(20,99)K,E/100.0,ESC/100.0,ET,ZE,EIONS
99  FORMAT(I3,9X,E10.4,18X,E10.4,18X,E10.4,9X,F8.6,14X,E8.3,/)
    CALL FAREA(EIONS,L,ZR,RM,ZC,ZSC,NAA)
37  CONTINUE

    WRITE(20,19)'==================================================
   +==================='

C   CALCULATING THE SECONDARY AVALANCHES SIZE

    DELTAL=.00004
    SAVALA=0.0
    NAA=1
    DO 65 I=2,L
     ROS=XIO(I)-XION(I)
     RIONX=XIO(I)-ROS/2.0
     YST=0.0
     STH=ROS/(2*.006)+2
     NTH=91/STH
     IF(NTH.GT.10)NTH=NTH
     IF(NTH.LE.10)NTH=10
     DO 799 J=10,91,NTH
      THS=J*PI/180.0
      THS2=(J-10)*PI/180.0
      YST=ROS/(2.0)*SIN(THS)
      XSTT=RIONX+ROS/(2.0)*COS(THS2)
      NXY=((XSTT-RIONX)*2.0/0.006)+1
      STEPX=(XSTT-RIONX)*2.0/(NXY*1.0)
      DO 66 KC=1,NXY
       XST=XSTT-(KC-1)*STEPX
       CRIT1=SQRT(XST**2+YST**2+(ZIO(I)-ZR)**2)
       IF(ZIO(I).LT.ZR+RM.AND.ZIO(I).GT.ZR.AND.CRIT1.LT.RM)GOTO 66
       CRIT2=SQRT(XST**2+YST**2)
       IF(ZIO(I).LT.ZR.AND.CRIT2.LT.RM)GOTO 66
       ZE=ZIO(I)
       XE=XST
       YE=YST
       SUM4=0.0
       ESC=0.0
       ESSC=0.0
       DO 67 MS=1,300
        IF(MS.GT.1)DELTAL=1.0/(9.0*FION*100.0)
        CALL FIELD(NM,XE,YE,ZE,EX,EY,EZ,E)
        SCP=SQRT((ZE-(ZR+RM+RPA))**2+XE**2+YE**2)
```

```
      ESC=1.6E-19*(AVPR-1.0)/(4.0*PI*EPS*SCP**2)
      EXSC=XE/SCP*ESC
      EYSC=YE/SCP*ESC
      EZSC=(ZE-(ZR+RM+RPA))/SCP*ESC
      IF(MS.GT.1)ESSC=1.6E-19*(EXP(SUM4)-1.0)/(4.0*PI*EPS*SSC**2)
      IF(ET/760.0.LT.25)ESSC=0.0
      EXSSC=-ESSC*(EX+EXSC)/ET
      EYSSC=-ESSC*(EY+EYSC)/ET
      EZSSC=-ESSC*(EZ+EZSC)/ET
      ET=SQRT((EX+EXSC+EXSSC)**2+(EY+EYSC+EYSSC)**2+
     +(EZ+EZSC+EZSSC)**2)
      ETT=ET/100.0
      CALL ATTION(ETT,FION,ATT,AV)
      SSC=1.0/(FION*100.0)
      SUM4=SUM4+AV*DELTAL*100.0
      XE=XE-DELTAL*(EX+EXSC+EXSSC)/ET
      YE=YE-DELTAL*(EY+EYSC+EYSSC)/ET
      ZE=ZE-DELTAL*(EZ+EZSC+EZSSC)/ET
      SCPP=SQRT((ZE-(ZR+RM+RPA))**2+XE**2+YE**2)
      IF(SCPP.LE.RPA)GOTO 123
      DROD=SQRT((ZE-ZR)**2+XE**2+YE**2)
      IF(DROD.LE.RM.AND.ZE.LE.ZR+RM.AND.ZE.GE.ZR)GOTO 123

      XXYY=SQRT(XE**2+YE**2)
      IF(XXYY.LE.RM.AND.ZE.LE.ZR)GOTO 123
 67   CONTINUE
      WRITE(20,*)'THERE IS AN ERROR IN THE SECONDARY AVALANCHE CALC.'
      STOP
123   SION=EXP(SUM4)
      SAVALA=SAVALA+AREA(NAA)*SION
      NAA=NAA+1
 66   CONTINUE
 799  CONTINUE
 65   CONTINUE
      WRITE(20,*)
      WRITE(20,*)
      WRITE(20,479)'PRIMARY  AVALANCHE SIZE=',AVPR,'IONS'
      WRITE(20,*)
      WRITE(20,479)'SECONDARY AVALANCHE SIZE=',2.0*SAVALA,'IONS'
      WRITE(20,*)
      WRITE(20,479)'PRIMARY AVALANCHE GROWTH TIME=',TAW,'SECONDS'
      WRITE(20,*)
479   FORMAT(2X,A,E13.5,2X,A)
      WRITE(20,*)'END OF OUTPUT REPORT'
      CLOSE (10 , STATUS='KEEP')
      CLOSE (20 , STATUS='KEEP')
      END

C                SUBROUTINE THAT CALCULATING THE COMPETE ELLIPTICAL
C                INTEGRAL OF FIRST KIND.

      SUBROUTINE ELINK(Z,ELINK1)
```

```
      IMPLICIT DOUBLE PRECISION(A-H,O-Z)
      P=1-Z*Z
      IF(P.EQ.0)GO TO 1
      ELINK1=1.38629436+P*(.096663443+P*(.035900924+P*(.037425637
     ++.014511962*P)))-DLOG(P)*(.5+P*(.12498594+P*(.068802486+P*
     +*(.033283553+.0044178701*P))))
      RETURN
    1 ELINK1 =DEXP(88.0D0)
      RETURN
      END

C                 SUBROUTINE THAT CALCULATING THE COMPETE ELLIPTICAL
C                 INTEGRAL OF SECOND KIND.

      SUBROUTINE ELINE(Z,ELINE1)
      IMPLICIT DOUBLE PRECISION(A-H,O-Z)
      P=1-Z*Z
      IF(P.EQ.0)GO TO 1
      ELINE1=1.+P*(.44325141+P*(.062606012+P*(.047573836+
     +.017365065*P)))-DLOG(P)*P*(.24998368+P*(.0920018+P*(
     +.04069675+.0052644964*P)))
      RETURN
    1 ELINE1 =1
      RETURN
      END

C                 SUBROUTINE THAT FINDING THE INVERSE OF A MATRIX.

      SUBROUTINE NGAUSS(N)
      PARAMETER (M=195)
      IMPLICIT DOUBLE PRECISION(A-H,O-Z)
      COMMON /COM1/ P(M,M),QP(M)
      COMMON /COM3/ QR(M)
      DO 4 K=1,N-1
       DO 3 I=K+1,N
        XMULT=P(I,K)/P(K,K)
        DO 2 J=K+1,N
         P(I,J)=P(I,J)-XMULT*P(K,J)
    2   CONTINUE
        P(I,K)=XMULT
        QP(I)=QP(I)-XMULT*QP(K)
    3   CONTINUE
    4 CONTINUE
      QR(N)=QP(N)/P(N,N)
      DO 6 I=N-1,1,-1
       SUM=QP(I)
       DO 5 J=I+1,N
        SUM=SUM-P(I,J)*QR(J)
    5   CONTINUE
        QR(I)=SUM/P(I,I)
    6 CONTINUE
      RETURN
```

```
      END

C               SUBROUTINE THAT CALCULATING THE ELECTRIC FIELD AT ANY POINT
C               (x,y,z)

      SUBROUTINE FIELD(NM,XE,YE,ZE,EX,EY,EZ,E)
      PARAMETER (M=195)
      IMPLICIT DOUBLE PRECISION(A-H,O-Z)
      COMMON /COM2/ X(M),Y(M),Z(M),RR(M),XPT,YPT,ZPT,QPC,XPL,YPL,ZPL
     +,QLC,PI,EPS,XTR,YTR,ZTR
      COMMON /COM3/ QR(M)
C THE ELECTRIC FIELD CAUSED BY POINT CHARGE
      DPC=SQRT((XE-XPT)**2+(YE-YPT)**2+(ZE-ZPT)**2)
      DPI=SQRT((XE-XPT)**2+(YE-YPT)**2+(ZE+ZPT)**2)
      EXP=QPC*(XE-XPT)*(1.0/DPC**3-1.0/DPI**3)
      EYP=QPC*(YE-YPT)*(1.0/DPC**3-1.0/DPI**3)
      EZP=QPC*((ZE-ZPT)/DPC**3-(ZE+ZPT)/DPI**3)

C THE ELECTRIC FIELD CAUSED BY SIME-INFINITE LINE CHARGES
      DLC=SQRT((XE-XPL)**2+(YE-YPL)**2+(ZE-ZPL)**2)
      DLI=SQRT((XE-XPL)**2+(YE-YPL)**2+(ZE+ZPL)**2)
      EXL=QLC*(XE-XPL)*(1.0/(DLC*(ZPL-ZE+DLC))-1.0/(DLI*
     +(ZPL+ZE+DLI)))
      EYL=QLC*(YE-YPL)*(1.0/(DLC*(ZPL-ZE+DLC))-1.0/(DLI*
     +(ZPL+ZE+DLI)))
      EZL=-QLC*((1.0+(ZE+ZPL)/DLI)/(ZPL+ZE+DLI)+(1.0+
     +(ZPL-ZE)/DLC)/(ZPL-ZE+DLC))

C THE ELECTRIC FIELD CAUSED BY POINT CHARGE ON THE ROD
      DTC=SQRT((XE-XTR)**2+(YE-YTR)**2+(ZE-ZTR)**2)
      DTI=SQRT((XE-XTR)**2+(YE-YTR)**2+(ZE+ZTR)**2)
      EXR=QR(NM)*(XE-XTR)*(1.0/DTC**3-1.0/DTI**3)
      EYR=QR(NM)*(YE-YTR)*(1.0/DTC**3-1.0/DTI**3)
      EZR=QR(NM)*((ZE-ZTR)/DTC**3-(ZE+ZTR)/DTI**3)

      EX=EXP+EXL+EXR
      EY=EYP+EYL+EYR
      EZ=EZP+EZL+EZR

C THE ELECTRIC FIELD CAUSED BY RINGS CHARGES
      DO 410 J=1,NM-1
       RP=SQRT((XE-X(J))**2+(YE-Y(J))**2)
       ALF1=SQRT((RP+RR(J))**2+(ZE-Z(J))**2)
       ALF2=SQRT((RP+RR(J))**2+(ZE+Z(J))**2)
       BTA1=SQRT((RP-RR(J))**2+(ZE-Z(J))**2)
       BTA2=SQRT((RP-RR(J))**2+(ZE+Z(J))**2)
       C1=2.0*SQRT(RP*RR(J))/ALF1
       C2=2.0*SQRT(RP*RR(J))/ALF2
       CALL ELINK(C1,EK1)
       CALL ELINK(C2,EK2)
       CALL ELINE(C1,EE1)
       CALL ELINE(C2,EE2)
```

```
      ERX=-QR(J)*1.0/(PI*RP)*(((RR(J)**2-RP**2+(ZE-Z(J))
     +**2)*EE1-BTA1**2*EK1)/(ALF1*BTA1**2)-((RR(J)**2-RP**2+(ZE+Z(J))
     +**2)*EE2-BTA2**2*EK2)/(ALF2*BTA2**2))*(XE-X(J))/RP
      ERY=-QR(J)*1.0/(PI*RP)*(((RR(J)**2-RP**2+(ZE-Z(J))
     +**2)*EE1-BTA1**2*EK1)/(ALF1*BTA1**2)-((RR(J)**2-RP**2+(ZE+Z(J))
     +**2)*EE2-BTA2**2*EK2)/(ALF2*BTA2**2))*(YE-Y(J))/RP
      ERZ=-QR(J)*2.0/PI*(((Z(J)-ZE)*EE1)/(ALF1*BTA1**2)+
     +((Z(J)+ZE)*EE2)/(ALF2*BTA2**2))
      EX=EX+ERX
      EY=EY+ERY
      EZ=EZ+ERZ
410   CONTINUE
      E=SQRT(EX**2+EY**2+EZ**2)
      RETURN
      END

C                SUBROUTINE THAT CALCULATING THE IONIZATION α AND THE
C                ATTACHMENT η COEFFICIENTS

      SUBROUTINE ATTION(E,FION,ATT,AV)
      IMPLICIT DOUBLE PRECISION(A-H,O-Z)
      ATT=(.01298-0.541E-3*(E/760.0)+0.87E-5*(E/760.0)**2)*760.0
      IF(E/760.0.LT.25.0)THEN
       AV=0.0
      ELSEIF(E/760.0.GE.25.0.AND.E/760.0.LE.60.0)THEN
       FION=(4.7786*EXP(-221.0*760.0/E))*760.0
       AV=FION-ATT
      ELSEIF(E/760.0.GT.60.0)THEN
       FION=(9.682*EXP(-264.2*760.0/E))*760.0
       AV=FION-ATT
      ELSE
       WRITE(20,*)E/760.0,'     IONIZATION IS NOT IN THE RANGE'
      ENDIF
44    RETURN
      END

C                SUBROUTINE THAT CALCULATING THE COEFFICIENT OF APSORBTION μ

      SUBROUTINE ABSORPTION(E,AMU)
       IMPLICIT DOUBLE PRECISION(A-H,O-Z)
       E=E/100.0
       EAB=E/1000.0
       IF(EAB.GE.19.0.AND.EAB.LE.190.0)THEN
        AMU=100.0*EXP(-31.568+6.785*LOG(EAB))
       ELSEIF(EAB.GT.190.0)THEN
        AMU=100.0*EXP(-11.743+2.78*LOG(EAB))
       ELSE
       ENDIF
      RETURN
      END

C                SUBROUTINE THAT CALCULATING  THE AVALANCHE TIP RADIUS.
```

```
      SUBROUTINE RADIUSPA(E,TAW,RPA)
       IMPLICIT DOUBLE PRECISION(A-H,O-Z)
       CALL EMOBS(E,EMOB)
       ERA=E/1000.0
       BK=1.37E-23
       ECHA=1.6E-19
       IF(ERA.LT.0.532)TR=12.267+3.16*LOG(ERA)
       IF(ERA.GE.0.532)TR=20.632+14.29*LOG(ERA)
       TG=298.0
       DE=EMOB*(BK/ECHA)*TR*TG
       RPA=SQRT(6.0*DE*TAW)
      RETURN
      END

C                SUBROUTINE THAT CALCULATING  THE ELECTRONS MOBILITY.

      SUBROUTINE EMOBS(E,EMOB)
      IMPLICIT DOUBLE PRECISION(A-H,O-Z)
       EMO=E/1000.0
       IF(EMO.LE.76.0)EVELOC=1.217E4*EMO**0.715
       IF(EMO.GT.76.0)EVELOC=1.837E4*EMO**0.62
       EMOB=EVELOC/(E*100.0)
      RETURN
      END

C                SUBROUTINE THAT CALCULATING  THE NUMBER OF PHOTOELECTRONS
C                CREATED IN EACH SEGMENT.

      SUBROUTINE FAREA(EIONS,L,ZR,RM,ZC,ZSC,NAA)
      PARAMETER (M=195)
      IMPLICIT DOUBLE PRECISION(A-H,O-Z)
      COMMON /COM4/ AREA(550),XIO(M),ZIO(M),NM,XION(M),ZION(M)
      COMMON /COM2/ X(M),Y(M),Z(M),RR(M),XPT,YPT,ZPT,QPC,XPL,YPL,ZPL
     +,QLC,PI,EPS,XTR,YTR,ZTR
      COMMON /COM3/ QR(M)
      COMMON /COM5/ EXX(550),EYY(550),EZZ(550)
      THETA=ACOS(RM/(ZC-ZR))
      ZTAN=ZR+RM*COS(THETA)
      XTAN=RM*SIN(THETA)
      NAA=1
      DO 35 I=2,L
       DRO=ABS(ZIO(I-1)-ZIO(I))
       ROS=XIO(I)-XION(I)
       RIONX=XIO(I)-ROS/2.0
       YST=0.0
       STH=ROS/(2*.006)+2
       NTH=91/STH
       IF(NTH.GT.10)NTH=NTH
       IF(NTH.LE.10)NTH=10
       DO 57 J=10,91,NTH
        THS=J*PI/180.0
```

```
      THS2=(J-10)*PI/180.0
      STEPY=ROS/(2.0)*SIN(THS)-YST
      YST=ROS/(2.0)*SIN(THS)
      XSTT=RIONX+ROS/(2.0)*COS(THS2)
      NXY=((XSTT-RIONX)*2.0/0.006)+1
      STEPX=(XSTT-RIONX)*2.0/(NXY*1.0)
      DO 67 KC=1,NXY
       XST=XSTT-(KC-1)*STEPX
       XFT=(XTAN/(ZTAN-ZC))*ZIO(I)-XTAN*ZC/(ZTAN-ZC)
       TANG=SQRT(XST**2+YST**2)
       IF(ZIO(I).LT.ZR+RM.AND.TANG.LT.XFT)GOTO 67
       CRIT1=SQRT(XST**2+YST**2+(ZIO(I)-ZR)**2)
       IF(ZIO(I).LT.ZR+RM.AND.ZIO(I).GT.ZR.AND.CRIT1.LT.RM)GOTO 67
       CRIT2=SQRT(XST**2+YST**2)
       IF(ZIO(I).LT.ZR.AND.CRIT2.LT.RM)GOTO 67
       RO1=SQRT((ZIO(I)-ZC)**2+XST**2+YST**2)
       PAREA=STEPX*STEPY
       TAREA=4.0*PI*RO1**2
       F1F2=2.46*EXP(-696.92*RO1)+28.3*EXP(-3002*RO1)+528.0*
     +EXP(-30590.0*RO1)
       SCP=SQRT((ZIO(I)-(ZC+ZSC))**2+XST**2+YST**2)
       ESC=1.6E-19*(EIONS-1.0)/(4.0*PI*EPS*SCP**2)
       EXSC=XST/SCP*ESC
       EYSC=YST/SCP*ESC
       EZSC=(ZIO(I)-(ZC+ZCP))/SCP*ESC
       ET=SQRT((EXX(NAA)+EXSC)**2+(EZZ(NAA)+EZSC)**2+
     +(EYY(NAA)+EYSC)**2)
       CALL ABSORPTION(ET,AMU)
       AREA(NAA)=AREA(NAA)+EIONS*PAREA/TAREA*F1F2*AMU*
     +EXP(-AMU*RO1)*DRO
       NAA=NAA+1
 67    CONTINUE
 57    CONTINUE
 35   CONTINUE
      RETURN
      END

C***********************************************************************
```

APPENDIX - B

SAMPLES OF THE PROGRAM OUTPUT

CASE 1

OUTPUT REPORT FOR THE CASE WHEN THE SYSTEM PARAMETERS ARE FIXED AS:

ROD HEIGHT= 1.000 m
ROD RADIUS= .020 m
ROD VOLTAGE= .000 kV
LATERAL DISTANCE BETWEEN FRANKLIN ROD & DOWNWARD LEADER= 92.000 m
DOWNWARD LEADER HEIGHT= 84.500 m
DOWNWARD LEADER CURRENT= -10.000 kA

THE MAX. PERCENT ERROR IN ROD SURFACE POTENTIAL= .6523

THE ELECTRIC FIELD AROUND THE TIP:

TH (DEGREE)	ATAN(EZ/EX) (DEGREE)	X COMP. (m)	Y COMP. (m)	Z COMP. (m)	TOT. E (V/m)
.0000	-.8414	.2854E+07	-.7801E-10	-.4191E+05	.2854E+07
30.0000	27.8461	.3225E+07	-.5025E-09	.1704E+07	.3648E+07
60.0000	56.5886	.2332E+07	-.1523E-08	.3536E+07	.4235E+07
90.0000	-89.8589	-.1108E+05	-.7233E-08	.4497E+07	.4497E+07

ELECTRIC FIELD, IONIZATION AND ATTACHMENT COEFFICIENT AT ROD TIP:

ELECTRIC FIELD= .44969E+05 V/cm

IONIZATION COEFF.= 86.69738 (1/m) ATTACHMENT COEFF.= 8.68542 (1/m)

IONIZATION COEFF.-ATTACHMENT COEFF.= .78012E+02 (1/m)

IONIZATION-ZONE BOUNDARY ABOVE THE ROD TIP:

IONIZATION COEFF.= 3.50633 (1/m) ATTACHMENT COEFF.= 3.47653 (1/m)

IONIZATION COEFF.-ATTACHMENT COEFF.= .29805E-01 (1/m)

ELECTRIC FIELD= .24192E+05 V/cm

POINT COORDINATES Z= 1.026907 X= .000000

GROWTH OF PRIMARY AVALANCHE SIZE:

STEP	APPL. FIELD (V/cm)	SPACE CHARGE FIELD (V/cm)	TOT. FIELD (V/cm)	Z-COORD. (m)	AVALANCHE SIZE (IONS)
1	.2444E+05	.4041E-08	.2444E+05	1.026772	.100E+01
10	.2689E+05	.1677E-05	.2689E+05	1.025533	.124E+01
20	.3014E+05	.5313E-04	.3014E+05	1.024153	.298E+01
30	.3409E+05	.2252E-02	.3409E+05	1.022771	.242E+02
40	.3892E+05	.5762E+00	.3892E+05	1.021390	.178E+04
50	.4493E+05	.2749E+04	.4218E+05	1.020009	.434E+07

PRIMARY AVALANCHE SIZE= .43384E+07 IONS

SECONDARY AVALANCHE SIZE= .46668E+07 IONS

PRIMARY AVALANCHE GROWTH TIME= .47691E-07 SECONDS

END OF OUTPUT REPORT

CASE 2

OUTPUT REPORT FOR THE CASE WHEN THE SYSTEM PARAMETERS ARE FIXED AS:

ROD HEIGHT= 1.000 m
ROD RADIUS= .020 m
ROD VOLTAGE= 5.000 kV
LATERAL DISTANCE BETWEEN FRANKLIN ROD & DOWNWARD LEADER= 95.500 m

DOWNWARD LEADER HEIGHT= 84.500 m
DOWNWARD LEADER CURRENT= -10.000 kA

THE MAX. PERCENT ERROR IN ROD SURFACE POTENTIAL= .5212

THE ELECTRIC FIELD AROUND THE TIP:

TH (DEGREE)	ATAN(EZ/EX) (DEGREE)	X COMP. (m)	Y COMP. (m)	Z COMP. (m)	TOT. E (V/m)
.0000	-.8415	.2870E+07	-.7595E-10	-.4215E+05	.2870E+07
30.0000	27.8394	.3241E+07	-.4792E-09	.1711E+07	.3665E+07
60.0000	56.5769	.2343E+07	-.2267E-08	.3550E+07	.4254E+07
90.0000	-89.8672	-.1047E+05	-.1659E-07	.4516E+07	.4516E+07

ELECTRIC FIELD, IONIZATION AND ATTACHMENT COEFFICIENT AT ROD TIP:

ELECTRIC FIELD= .45163E+05 V/cm

IONIZATION COEFF.= 88.10107 (1/m) ATTACHMENT COEFF.= 8.78073 (1/m)

IONIZATION COEFF.-ATTACHMENT COEFF.= .79320E+02 (1/m)

IONIZATION-ZONE BOUNDARY ABOVE THE ROD TIP:

IONIZATION COEFF.= 3.50062 (1/m) ATTACHMENT COEFF.= 3.47646 (1/m)

IONIZATION COEFF.-ATTACHMENT COEFF.= .24163E-01 (1/m)

ELECTRIC FIELD= .24186E+05 V/cm

POINT COORDINATES Z= 1.026960 X= .000000

GROWTH OF PRIMARY AVALANCHE SIZE:

STEP	APPL. FIELD (V/cm)	SPACE CHARGE FIELD (V/cm)	TOT. FIELD. (V/cm)	Z-COORD. (m)	AVALANCHE SIZE (IONS)
1	.2443E+05	.3924E-08	.2443E+05	1.026825	.100E+01
10	.2690E+05	.1705E-05	.2690E+05	1.025576	.124E+01

20	.3018E+05	.5511E-04	.3018E+05	1.024185	.302E+01
30	.3416E+05	.2431E-02	.3416E+05	1.022793	.256E+02
40	.3905E+05	.6834E+00	.3905E+05	1.021401	.206E+04
50	.4512E+05	.3312E+04	.4181E+05	1.020009	.559E+07

PRIMARY AVALANCHE SIZE= .55868E+07 IONS

SECONDARY AVALANCHE SIZE= .80647E+07 IONS

PRIMARY AVALANCHE GROWTH TIME= .48016E-07 SECONDS

END OF OUTPUT REPORT

CASE 3

OUTPUT REPORT FOR THE CASE WHEN THE SYSTEM PARAMETERS ARE FIXED AS:

ROD HEIGHT= 1.000 m
ROD RADIUS= .020 m
ROD VOLTAGE= 10.000 kV
LATERAL DISTANCE BETWEEN FRANKLIN ROD & DOWNWARD LEADER= 100.000 m
DOWNWARD LEADER HEIGHT= 84.500 m
DOWNWARD LEADER CURRENT= -10.000 kA

THE MAX. PERCENT ERROR IN ROD SURFACE POTENTIAL= .2654

THE ELECTRIC FIELD AROUND THE TIP:

TH (DEGREE)	ATAN(EZ/EX) (DEGREE)	X COMP. (m)	Y COMP. (m)	Z COMP. (m)	TOT. E (V/m)
.0000	-.8416	.2861E+07	-.9193E-10	-.4203E+05	.2862E+07
30.0000	27.8326	.3228E+07	-.8877E-09	.1704E+07	.3651E+07
60.0000	56.5653	.2334E+07	-.1845E-08	.3534E+07	.4235E+07
90.0000	-89.8761	-.9725E+04	-.1259E-07	.4497E+07	.4497E+07

ELECTRIC FIELD, IONIZATION AND ATTACHMENT COEFFICIENT AT ROD TIP:

ELECTRIC FIELD= .44971E+05 V/cm

IONIZATION COEFF.= 86.71154 (1/m) ATTACHMENT COEFF.= 8.68638 (1/m)

IONIZATION COEFF.-ATTACHMENT COEFF.= .78025E+02 (1/m)

IONIZATION-ZONE BOUNDARY ABOVE THE ROD TIP:

IONIZATION COEFF.= 3.47919 (1/m) ATTACHMENT COEFF.= 3.47619 (1/m)

IONIZATION COEFF.-ATTACHMENT COEFF.= .30052E-02 (1/m)

ELECTRIC FIELD= .24165E+05 V/cm

POINT COORDINATES Z= 1.026907 X= .000000

GROWTH OF PRIMARY AVALANCHE SIZE:

STEP	APPL. FIELD (V/cm)	SPACE CHARGE FIELD (V/cm)	TOT. FIELD (V/cm)	Z-COORD. (m)	AVALANCHE SIZE (IONS)
1	.2441E+05	.3249E-08	.2441E+05	1.026772	.100E+01
10	.2687E+05	.1620E-05	.2687E+05	1.025533	.124E+01
20	.3012E+05	.5190E-04	.3012E+05	1.024153	.295E+01
30	.3407E+05	.2201E-02	.3407E+05	1.022771	.238E+02
40	.3892E+05	.5611E+00	.3892E+05	1.021390	.173E+04
50	.4493E+05	.2710E+04	.4222E+05	1.020009	.425E+07

PRIMARY AVALANCHE SIZE= .42459E+07 IONS

SECONDARY AVALANCHE SIZE= .44957E+07 IONS

PRIMARY AVALANCHE GROWTH TIME= .47711E-07 SECONDS

END OF OUTPUT REPORT

CASE 4

OUTPUT REPORT FOR THE CASE WHEN THE SYSTEM PARAMETERS ARE FIXED AS:

ROD HEIGHT= 1.000 m
ROD RADIUS= .020 m
ROD VOLTAGE= 15.000 kV
LATERAL DISTANCE BETWEEN FRANKLIN ROD & DOWNWARD LEADER= 104.500 m
DOWNWARD LEADER HEIGHT= 84.500 m
DOWNWARD LEADER CURRENT= -10.000 kA

THE MAX. PERCENT ERROR IN ROD SURFACE POTENTIAL= .1811

THE ELECTRIC FIELD AROUND THE TIP:

TH (DEGREE)	ATAN(EZ/EX) (DEGREE)	X COMP. (m)	Y COMP. (m)	Z COMP. (m)	TOT. E (V/m)
.0000	-.8418	.2863E+07	-.1074E-09	-.4207E+05	.2863E+07
30.0000	27.8258	.3228E+07	-.1491E-08	.1704E+07	.3650E+07
60.0000	56.5536	.2333E+07	-.1223E-08	.3531E+07	.4232E+07
90.0000	-89.8849	-.9029E+04	-.1298E-07	.4494E+07	.4494E+07

ELECTRIC FIELD, IONIZATION AND ATTACHMENT COEFFICIENT AT ROD TIP:

ELECTRIC FIELD= .44941E+05 V/cm

IONIZATION COEFF.= 86.49458 (1/m) ATTACHMENT COEFF.= 8.67166 (1/m)

IONIZATION COEFF.-ATTACHMENT COEFF.= .77823E+02 (1/m)

IONIZATION-ZONE BOUNDARY ABOVE THE ROD TIP:

IONIZATION COEFF.= 3.49707 (1/m) ATTACHMENT COEFF.= 3.47641 (1/m)

IONIZATION COEFF.-ATTACHMENT COEFF.= .20662E-01 (1/m)

ELECTRIC FIELD= .24182E+05 V/cm

POINT COORDINATES Z= 1.026880 X= .000000

GROWTH OF PRIMARY AVALANCHE SIZE:

STEP	APPL. FIELD (V/cm)	SPACE CHARGE FIELD (V/cm)	TOT. FIELD (V/cm)	Z-COORD. (m)	AVALANCHE SIZE (IONS)
1	.2443E+05	.3753E-08	.2443E+05	1.026746	.100E+01
10	.2688E+05	.1649E-05	.2688E+05	1.025512	.124E+01
20	.3013E+05	.5227E-04	.3013E+05	1.024137	.295E+01
30	.3407E+05	.2195E-02	.3407E+05	1.022761	.237E+02
40	.3891E+05	.5477E+00	.3891E+05	1.021385	.170E+04
50	.4490E+05	.2602E+04	.4229E+05	1.020009	.402E+07

PRIMARY AVALANCHE SIZE= .40213E+07 IONS

SECONDARY AVALANCHE SIZE= .40772E+07 IONS

PRIMARY AVALANCHE GROWTH TIME= .47518E-07 SECONDS

END OF OUTPUT REPORT

CASE 5

OUTPUT REPORT FOR THE CASE WHEN THE SYSTEM PARAMETERS ARE FIXED AS:

ROD HEIGHT= 1.000 m
ROD RADIUS= .020 m
ROD VOLTAGE= 5.000 kV
LATERAL DISTANCE BETWEEN FRANKLIN ROD & DOWNWARD LEADER= 92.000 m
DOWNWARD LEADER HEIGHT= 93.500 m
DOWNWARD LEADER CURRENT= -10.000 kA

THE MAX. PERCENT ERROR IN ROD SURFACE POTENTIAL= .5184

THE ELECTRIC FIELD AROUND THE TIP:

TH (DEGREE)	ATAN(EZ/EX) (DEGREE)	X COMP. (m)	Y COMP. (m)	Z COMP. (m)	TOT. E (V/m)
.0000	-.8423	.2858E+07	-.9910E-10	-.4203E+05	.2859E+07

30.0000	27.8387	.3228E+07	-.1827E-09	.1705E+07	.3650E+07
60.0000	56.5790	.2334E+07	-.1977E-08	.3537E+07	.4237E+07
90.0000	-89.8778	-.9593E+04	-.1313E-07	.4499E+07	.4499E+07

ELECTRIC FIELD, IONIZATION AND ATTACHMENT COEFFICIENT AT ROD TIP:

ELECTRIC FIELD= .44987E+05 V/cm

IONIZATION COEFF.= 86.82874 (1/m) ATTACHMENT COEFF.= 8.69433 (1/m)

IONIZATION COEFF.-ATTACHMENT COEFF.= .78134E+02 (1/m)

IONIZATION-ZONE BOUNDARY ABOVE THE ROD TIP:

IONIZATION COEFF.= 3.50207 (1/m) ATTACHMENT COEFF.= 3.47647 (1/m)

IONIZATION COEFF.-ATTACHMENT COEFF.= .25597E-01 (1/m)

ELECTRIC FIELD= .24187E+05 V/cm

POINT COORDINATES Z= 1.026907 X= .000000

GROWTH OF PRIMARY AVALANCHE SIZE:

STEP	APPL. FIELD (V/cm)	SPACE CHARGE FIELD (V/cm)	TOT. FIELD (V/cm)	Z-COORD. (m)	AVALANCHE SIZE (IONS)
1	.2443E+05	.3918E-08	.2443E+05	1.026772	.100E+01
10	.2689E+05	.1671E-05	.2689E+05	1.025533	.124E+01
20	.3014E+05	.5311E-04	.3014E+05	1.024153	.297E+01
30	.3409E+05	.2257E-02	.3409E+05	1.022771	.242E+02
40	.3894E+05	.5808E+00	.3893E+05	1.021390	.179E+04
50	.4494E+05	.2779E+04	.4216E+05	1.020009	.440E+07

PRIMARY AVALANCHE SIZE= .43962E+07 IONS

SECONDARY AVALANCHE SIZE= .49117E+07 IONS

PRIMARY AVALANCHE GROWTH TIME= .47689E-07 SECONDS

END OF OUTPUT REPORT

CASE 6

OUTPUT REPORT FOR THE CASE WHEN THE SYSTEM PARAMETERS ARE FIXED AS:

ROD HEIGHT= 1.000 m
ROD RADIUS= .020 m
ROD VOLTAGE= 10.000 kV
LATERAL DISTANCE BETWEEN FRANKLIN ROD & DOWNWARD LEADER= 92.000 m
DOWNWARD LEADER HEIGHT= 102.000 m
DOWNWARD LEADER CURRENT= -10.000 kA

THE MAX. PERCENT ERROR IN ROD SURFACE POTENTIAL= .2650

THE ELECTRIC FIELD AROUND THE TIP:

TH (DEGREE)	ATAN(EZ/EX) (DEGREE)	X COMP. (m)	Y COMP. (m)	Z COMP. (m)	TOT. E (V/m)
.0000	-.8431	.2864E+07	-.9988E-10	-.4215E+05	.2864E+07
30.0000	27.8314	.3231E+07	-.7276E-09	.1706E+07	.3654E+07
60.0000	56.5688	.2336E+07	-.7714E-09	.3539E+07	.4240E+07
90.0000	-89.8941	-.8320E+04	-.2991E-08	.4502E+07	.4502E+07

ELECTRIC FIELD, IONIZATION AND ATTACHMENT COEFFICIENT AT ROD TIP:

ELECTRIC FIELD= .45019E+05 V/cm

IONIZATION COEFF.= 87.06335 (1/m) ATTACHMENT COEFF.= 8.71025 (1/m)

IONIZATION COEFF.-ATTACHMENT COEFF.= .78353E+02 (1/m)

IONIZATION-ZONE BOUNDARY ABOVE THE ROD TIP:

IONIZATION COEFF.= 3.50555 (1/m) ATTACHMENT COEFF.= 3.47652 (1/m)

IONIZATION COEFF.-ATTACHMENT COEFF.= .29028E-01 (1/m)

ELECTRIC FIELD= .24191E+05 V/cm

POINT COORDINATES Z= 1.026907 X= .000000

GROWTH OF PRIMARY AVALANCHE SIZE:

STEP	APPL. FIELD (V/cm)	SPACE CHARGE FIELD (V/cm)	TOT. FIELD (V/cm)	Z-COORD. (m)	AVALANCHE SIZE (IONS)
1	.2443E+05	.4026E-08	.2443E+05	1.026772	.100E+01
10	.2689E+05	.1684E-05	.2689E+05	1.025533	.124E+01
20	.3015E+05	.5359E-04	.3015E+05	1.024153	.298E+01
30	.3411E+05	.2289E-02	.3411E+05	1.022771	.245E+02
40	.3896E+05	.5959E+00	.3896E+05	1.021390	.183E+04
50	.4498E+05	.2852E+04	.4212E+05	1.020009	.454E+07

PRIMARY AVALANCHE SIZE= .45436E+07 IONS

SECONDARY AVALANCHE SIZE= .51173E+07 IONS

PRIMARY AVALANCHE GROWTH TIME= .47677E-07 SECONDS

END OF OUTPUT REPORT

CASE 7

OUTPUT REPORT FOR THE CASE WHEN THE SYSTEM PARAMETERS ARE FIXED AS:

ROD HEIGHT= 1.000 m
ROD RADIUS= .020 m
ROD VOLTAGE= 15.000 kV
LATERAL DISTANCE BETWEEN FRANKLIN ROD & DOWNWARD LEADER= 92.000 m
DOWNWARD LEADER HEIGHT= 110.500 m
DOWNWARD LEADER CURRENT= -10.000 kA

THE MAX. PERCENT ERROR IN ROD SURFACE POTENTIAL= .1809

THE ELECTRIC FIELD AROUND THE TIP:

TH (DEGREE)	ATAN(EZ/EX) (DEGREE)	X COMP. (m)	Y COMP. (m)	Z COMP. (m)	TOT. E (V/m)
.0000	-.8437	.2869E+07	-.5062E-10	-.4224E+05	.2869E+07
30.0000	27.8242	.3234E+07	.6813E-09	.1707E+07	.3657E+07
60.0000	56.5583	.2337E+07	-.1269E-08	.3539E+07	.4241E+07
90.0000	-89.9085	-.7190E+04	-.9563E-08	.4503E+07	.4503E+07

ELECTRIC FIELD, IONIZATION AND ATTACHMENT COEFFICIENT AT ROD TIP:

ELECTRIC FIELD= .45034E+05 V/cm

IONIZATION COEFF.= 87.17051 (1/m) ATTACHMENT COEFF.= 8.71753 (1/m)

IONIZATION COEFF.-ATTACHMENT COEFF.= .78453E+02 (1/m)

IONIZATION-ZONE BOUNDARY ABOVE THE ROD TIP:

IONIZATION COEFF.= 3.49945 (1/m) ATTACHMENT COEFF.= 3.47644 (1/m)

IONIZATION COEFF.-ATTACHMENT COEFF.= .23011E-01 (1/m)

ELECTRIC FIELD= .24185E+05 V/cm

POINT COORDINATES Z= 1.026907 X= .000000

GROWTH OF PRIMARY AVALANCHE SIZE:

STEP	APPL. FIELD (V/cm)	SPACE CHARGE FIELD (V/cm)	TOT. FIELD (V/cm)	Z-COORD. (m)	AVALANCHE SIZE (IONS)
1	.2443E+05	.3848E-08	.2443E+05	1.026772	.100E+01
10	.2689E+05	.1674E-05	.2689E+05	1.025533	.124E+01
20	.3015E+05	.5345E-04	.3015E+05	1.024153	.298E+01
30	.3411E+05	.2288E-02	.3411E+05	1.022771	.244E+02
40	.3897E+05	.5981E+00	.3897E+05	1.021390	.183E+04

50	.4499E+05	.2873E+04	.4212E+05	1.020009	.458E+07

PRIMARY AVALANCHE SIZE= .45822E+07 IONS

SECONDARY AVALANCHE SIZE= .51687E+07 IONS

PRIMARY AVALANCHE GROWTH TIME= .47677E-07 SECONDS

END OF OUTPUT REPORT

NOMENCLATURE

$V(t)$	:	Lightning overvoltage wave.
V_L	:	Peak of lightning overvoltage wave.
ψ_1, ψ_2	:	Constants related to the lightning overvoltage wave.
N_e	:	Number of electrons produced by the avalanche.
z_1	:	Z-coordinate of the starting point p_1 of the initiatory (primary) avalanche.
z_2	:	Z-coordinate of the end point p_2 of the initiatory (primary) avalanche.
α	:	Coefficient of ionization by electron collision.
η	:	Coefficient of electron attachment.
E_{sc}	:	Space-charge field produced by the positive ions left behind the avalanche.
e	:	Electron charge ($= 1.6 \times 10^{-19}$ C).
ε	:	Permittivity of air ($= \frac{1}{36\pi} \times 10^{-9}$ F / m).
R_{av}	:	Radius of the head of the initiatory avalanche.
D_e	:	Electron diffusion coefficient (m^2/s).
τ	:	Avalanche transit time (s).
E_{psc}	:	Electric field caused by the positive ions left behind the primary avalanche.
r_s	:	Radial distance from the simulation point charge.
N_{+1}	:	Size of the initiatory (primary) avalanche.

h	:	Lightning rod height.
q_j	:	The jth simulation charge.
$P_{i,j}$	:	Potential coefficient calculated at the ith boundary point due to the jth simulation charge.
Φ_i	:	Potential at the ith boundary point.
$[V_{ap}]$	:	$n \times 1$ matrix of the applied voltage at the boundary points.
$[P]$	:	$n \times n$ matrix of the potential coefficients.
$[q]$	:	$n \times 1$ matrix of the simulation charges.
$[\bar{f}]$	:	$n \times n$ matrix of the electric field coefficients.
L	:	Downward leader length.
q_ℓ	:	Semi-infinite line charge per unit length.
Q_t	:	Downward leader tip charge.
N_Z	:	Number of the Z-levels of the simulation ring charges for the rod.
M	:	Number of the simulation ring charges in each Z-level.
Q_{r_n}	:	Value of the nth simulation ring charge in the rod.
Q_p	:	Value of the simulation point charge in the rod.
P_{r_n}	:	Potential coefficient of the nth simulation ring charge in the rod.
P_p	:	Potential coefficient of the simulation point charge in the rod.
P_t	:	Potential coefficient of the simulation point charge at the tip of the downward leader.
P_ℓ	:	Potential coefficient of the simulation semi-infinite line charge of the downward leader.

$V_{ap}(t)$: Instantaneous value of pulse voltage applied to the lightning rod.

r_{j_n} : Radius of the nth simulation ring charge.

V_{ch} : Potential at the check points on the rod.

$\bar{f}_{r_n}$: Electric field coefficient of the nth simulation ring charge.

$\bar{f}_p$: Electric field coefficient of the simulation point charge in the rod.

$\bar{f}_t$: Electric field coefficient of the simulation point charge at the tip of the downward leader.

$\bar{f}_\ell$: Electric field coefficient of the simulation semi-infinite line charge of the downward leader.

$\bar{E}_{dl}$: Electric field due to the downward leader charge.

$\bar{E}_{to}$: Electric field due to the downward leader charge and the pulse voltage applied to the Franklin rod.

$\bar{E}_{ap}$: Electric field due to the pulse voltage applied to the Franklin rod.

H : The height of the cloud above the ground plane.

I : Peak current of the first lightning stroke.

n_{ph} : Emitted photons from growing avalanche.

f_2 : Ratio between the number of excited states and the number of ionizing events.

f_1 : Probability of ionization.

ρ_s : Distance from the head of the primary avalanche to the segment.

μ : Coefficient of photon absorption.

ℓ_1 : The coordinate of the segment from which the successor avalanche starts its growth.

ℓ_2 : The coordinate of the end point at which the successor avalanche terminates its growth.

ℓ : The distance measured along the direction of growth of successor avalanche.

$\overline{E}_{ssc}$: The field resulting from the positive space charge of the successor avalanche.

$N_{segment}$: The number of the positive ions produced by each segment.

N_{+2} : The total number of positive ions produce by all successor avalanches of the second genetation.

K : The total number of segments in the ionization-zone as whole.

ρ_r : The distance from the head of the primary avalanche to any point on the ring periphery.

r_r : The ring radius.

Δr : The ring thickness.

ℓ'_1 : The coordinate at any point of the ring periphery from which the successor avalanche starts its growth.

ℓ'_2 : The coordinate of the end point at which the successor avalanche terminates its growth.

ℓ' : The distance measured along the direction of growth of successor avalanche from the ring.

K_r : The total number of rings in the ionization-zone.

p : The atmospheric pressure in torr (= 760 torr).

k_e	:	Electron mobility.
v_e	:	Electron velocity.
J	:	The rate of flow of charge from the high density to the low density.
∇n	:	The concentration gradient in three dimensional space.
K_{bol}	:	The Boltzmann's constant (1.37×10^{-23} W·sec/K).
T_e	:	The electron temperature in K°.
T_g	:	The gas temperature (= 298 K° at N.T.P.).
D	:	The height of the downward leader.
h'	:	The virtual increase in the rod height.
h_v	:	The virtual rod height.
R_p	:	Radius of protection.
ϕ	:	The cone protection angle.

REFERENCES

[1] R. Golde, Lightning, Academic Press, London, 1977.

[2] R. Carpenter, "A New Look at Lightning Protection for Power Transmission & Distribution Systems", Proc. of the 2nd Middle East Electricity Conference, Dubai, UAE, 1994.

[3] K. Nakamura, T. Suzuki, C. Yamabe and K. Horii., "Laser-Triggered Spark Gap Without the Irradiation of Surface of Electrodes Using UV Lasers", Japan Institute of Electric Engineer, Vol. 111, No. 9, pp. 588-591, Sept. 1991.

[4] T. Shindo, Y. Aihara, M. Miki and T. Suzuki, "Model Experiments of Laser-Triggered Lightning", IEEE Transactions on Power Delivery, Vol. 8, No. 1, pp. 311-317, Jan. 1993.

[5] N. Floret, "Efficiency Assessment of Early Streamer Emission Air-Terminals", 2nd Middle East Power System Conference, MEPCON-92 Assiut Univ., Egypt, pp. 359-362, 1992.

[6] G. Berger, "Determination of the Inception Electric Field of the Lightning Upward Leader", 8th International Symposium on High Voltage Engineering, Yokohama, Japan, Paper No. 70.02, 1993.

[7] Helita Catalog in Lightning Protection, June 1992.

[8] M. Abdel-Salam, M. El-Mohandes, G. Berger and B. Senouci, "Onset Criterion of Upward Streamers From a Franklin Rod", Journal of Electrostatics, Vol. 24, pp. 45-59, 1989.

[9] H. Singer, H, Steinbigler and P. Weiss, "A Charge Simulation Method for the Calculation of the High Voltage Fields", IEEE Trans. Power Appar. Syst., PAS-93, pp. 1660-1668, 1974.

[10] M. Abdel-Salam and E. Abdel-Aziz, "A new charge-simulation-based method for analysis of monopolar Poissnian fields", Journal of Physics D: Applied Physics, No. 27, pp. 807-817, 1994.

[11] S. Sato and W. Zaengl, "Effective 3-Dimensional Electric Field Calculation by Surface Charge Simulation Method," IEE Proc., Vol.133, Pt.A,No.2,pp.77-83, March 1986.

[12] A. Yializis, E. Kuffel, and P. Alexander, "An Optimized Charge Simulation Method For the Calculation of High Voltage Fields," IEEE Trans. Power App. Syst., Vol. PAS-97, pp. 2434-2440, 1978.

[13] M. D. R. Beasley et al, "Comparative Study of Three Methods for Computing Electric Fields," IEE Proc., Vol.126, No.1,pp.126-134, Jan. 1979.

[14] E. Kuffel and W.S. Zaengl, High-Voltage Engineering Fundamentals, Pergamon Press, Oxford, 1984.

[15] L. Wahlin, Atmospheric Electrostatics, John Wiley & Sons Inc., New York, 1986.

[16] T. Horvath, Computation of Lightning Protection, John Wiley & Sons Inc., New York, 1991.

[17] M. Khalifa, High-Voltage Engineering Theory and Practice, Marcel Dekker Inc., New York, NY, 1990.

[18] J. Chalmers, Atmospheric Electricity, Pergamon Press Ltd., 1967.

[19] B. Schonland, The Lightning discharge, Handbuch der Physik, (ed. S. Flugge), 1956.

[20] N. Kitagawa, M. Koyabashi, "Distribution of negative charge in the cloud taking part in a flash to ground," Pap. Met. Geophys., Vol.9, pp. 99-105, 1958.

[21] E. Pierce, "Electrostatic field-charges due to lightning discharges," Quart. J. R. Met. Soc., Vol.81, pp. 211-239, 1955.

[22] H. Norinder, E. Knudsen, "Lightning discharge paths photographed in daylight and analyzed by simultaneous variations of magnetic field components," Ark. Geofys., Vol.3, pp.375-476, 1961.

[23] Vo-Viet-Dan, "New evaluation of lightning protection effect of Franklin rod," Fifth International Symposium on High Voltage Engineering, Braunschweig, Germany, Paper No.83.07, 1987.

[24] M. Frydenloud, "Franklin Lightning Protection Still the Only Credible System", EC&M, pp. 162+1, November 1989.

[25] D. Mackerras, M. Darveveniza and A. Liew, "Standard and Non-standard Lightning Protection Methods", Journal of Electrical and Electronic Engineering, Vol. 7, No. 2, pp. 133-140, June 1987.

[26] E. Nasser, Fundamentals of Gaseous Ionization and Plasma Electronics, Wiley-Interscience, New York, NY, 1970.

[27] M. Khalifa, R. Radwan, A. Zeitoun and A. Abdel-Fattah, "Computation of corona current and its effect on traveling surges,

Part1-Case of positive lightning surges", IEEE Trans. Power Appar. Syst., Vol. PAS-80, No. 8, pp. 1816-1825, Nov. 1970.

[28] M. Abdel-Salam and Z. Al-Hamouz and A. Mufti, "Adaptive Finite-Element Ballooning Analysis of Monopolar Ionized Field," Submitted for publicatio in Journal of Physics D: Applied Physics, 1994.

[29] Z. Luo and N. Demerdash, " A Finite-Element Ballooning Model for 2D Eddy Current Open Boundary Problems For Aerospace Applications," IEEE Trans. Magn, Vol. 28, No. 5, 1992.

[30] D. Cristescu, G. Dragan, C. Gary, R. Garabedian, B. Hutzler, B.Popa and R. Enche, "New Aspects of the Physics of Lightning Impact in the Laboratory", Fifth International Symposium on High Voltage Engineering, Braunschweig, Germany, Paper No.81.01, 1987.

[31] P. Thum, A. Liew and C. Wong, "Computer Simulation of the Initial Stages of the Lightning Protection Mechanism", IEEE Trans. Power Appar. Syst., Vol. PAS-101, No. 11, pp. 4370-4377, Nov. 1982.

[32] S. Berger, "Onset or breakdown voltage reduction by electrode surface roughness in air and SF6," IEEE Trans. Power App. Syst., Vol. PAS-95, No. 4, pp. 1073-1079, July/August 1976.

[33] M. Sarma, W. Janischewskyi, "DC Corona on Smooth Conductors in Air", Proc. IEE, Vol. 116, No. 1, pp. 161-166, Jan. 1969.

[34] E. Nasser and M. Abou-Seada, "Calculation of Streamer Thresholds Using Digital Techniques", Gas Discharges Conference, London, pp. 534-538, 1972.

[35] S. C. Brown, Basic Data of Plasma Physics, M.I.T. Press, Cambridge, MA, 1967.

[36] L.B. Loeb, Electrical Coronas, The University of California Perss, California, 1965.

[37] G.W.Penney and G.T.Hammert, "Photoionization measurement in air, oxygen and nitrogen, J. Appl. Phys., 41, pp.572-577, 1970.

[38] A.E. Uber and G.W.Penney, "Photoionization as the secondary mechanism in a Townsend breakdown in air", Proc. IEEE Ind. Appl. Soc. Annual Meeting, pp.1214-1218, 1982.

[39] M. Abdel-Salam and N.L. Allen, "Inception of corona and rate of rise of voltage in diverging electric field", IEE Proc., Vol. 137, Pt. A, No. 4, pp. 217-220, July. 1990.

[40] M. Uman, Understanding Lightning, Bek Technical Publications Inc., Pennsylvania, 1971.